To the Graduate Council:

I am submitting herewith a thesis written by **Abhijeet A. Godbole** entitled **"Study of UV Curable Rubber-Toughened Epoxy Systems"**. I have examined the final **electronic** copy of this thesis for form and content and recommend that it be accepted in partial fulfillment of the requirements for the degree of Master of Science, with a major in Polymer Engineering.

Dr. Kevin Kit, Major Professor

_____

We have read this thesis
and recommend its acceptance:

Dr. Jack Fellers, Graduate Committee Member

_____

Dr. Roberto Benson, Graduate Committee Member

_____

Accepted for the Council:

Dr. Anne Mayhew

_____

Interim Vice Provost and
Dean of The Graduate Studies

(Original signatures are on file in the Graduate Admissions and Records Office)

Study of UV Curable Rubber-Toughened Epoxy Systems

A Thesis

Presented for the

Master of Science

Degree

University of Tennessee, Knoxville

Abhijeet A. Godbole

May 2002

ACKNOWLEDGEMENTS

I would like to thank Dr. Kevin Kit, my graduate advisor, for his constant encouragement, support and guidance throughout the course of this project. I would also like to thank Dr. Jack Fellers for his help and valuable suggestions in the light scattering experiments and analysis. Thanks also go to Dr. Roberto Benson for his helpful comments on the FTIR analysis.

I would like to thank Dr. Steven McKnight and Dr. James Sands from the Army Research Labs for their financial support for this project.

I would like to mention all my friends here in Knoxville, who helped me enjoy my time here in the most memorable way. A special acknowledgement goes to all my friends back home and here for their continued support and encouragement during the course of this work.

ABSTRACT

Rubber-toughened epoxy resins are used extensively in various structural applications. Current thermal curing processes limit the possible structural designs and require higher inputs in terms of pressure, temperature and time. UV and electron beam curing offers almost instantaneous curing of even complex structural shapes using minimal inputs. Various formulations were quenched from single phase at high temperatures to various temperatures below the corresponding cloud point temperatures, before being allowed to cool to room temperature. These quenched formulations were then cured using UV and thermal energy. The cured material toughness increases with decreasing particle size by over 150%. The rate of cooling affects the particle size achieved during phase separation. Particle size decreases with faster cooling rates. Particle size of rapidly cooled samples changes with time at room temperature. This is thought to be due to Ostwald ripening in which densely populated small-sized particles coalesce together forming small number of large-sized particles. This phenomenon is predicted to reduce the intended shelf life of the B-stage resin.

Triaryl sulphonium hexafluoroantimonate (TASHFA) cured two phase and three component samples were partly uncured even after curing under UV radiation for 15 minutes. Additional thermal curing step in a conventional oven resulted in complete cure. FT-IR studies of the samples confirmed the presence of unreacted epoxide rings in the UV cured samples. Additional short-time thermal curing step, without any additional peroxide catalyst, was found to be sufficient for complete cure. DMA results showed that

some amount of rubber remains dissolved in the epoxy matrix. This dissolved rubber contributes to the observed shift of $30^{o}C$ in the epoxy tan δ peak for the fastest cooled sample. The amount of the particulate rubber, dispersed in the matrix, reduced with an increase in the cooling rate.

TABLE OF CONTENTS

CHAPTER **PAGE**

LIST OF TABLES

TABLE **PAGE**

LIST OF FIGURES

FIGURE **PAGE**

FIGURE **PAGE**

FIGURE **PAGE**

FIGURE **PAGE**

CHAPTER 1- INTRODUCTION

Epoxy resins constitute one of the major classes of industrial thermosetting resins. They are mostly used in structural (structural adhesives) and electronic (micro-encapsulation) applications. Epoxies are very well suited for electronic encapsulation owing to their good electrical resistance. Use of epoxy resins in chemical storage tanks is justified by their exceptional chemical solvent resistance. Owing to their very high thermal stability, they are used in rocket tips. Structural applications (FRPs) like airplane bodies and ship's hulls require exceptional mechanical properties (toughness in particular) and chemical and thermal resistance. In all, epoxy resins find use in some of the most important specialized industrial applications.

This class of thermosetting resins contains the epoxide rings, which break open during the curing reaction. Depending on the nature of the main chain, these resins can be either aliphatic or aromatic. Amine or carboxylic acid terminated hardeners are most effective for cure. Though these cured structures have good electrical, thermal and chemical resistance they are very brittle. Some of the structural components in aerospace and shipbuilding industry are often subjected to harsh environments demanding good toughness.

Toughness of epoxy resins can be improved be the incorporation of liquid oligomers or thermoplastic resins. This liquid oligomer should be able to phase separate from the homogeneous solution during the curing reaction. Enhanced toughness is possible only due to a finer dispersion of the oligomers (size range: 1-5 micron) in the epoxy matrix. During failure, the propagating crack tip encounters resistance from large

number of small oligomers particles, effectively absorbing much of the energy. For this purpose, the oligomer should be initially semi-compatible with the epoxy resin. If the oligomer is too compatible with the resin, the ultimate properties are similar to a random copolymer and not much improvement in toughness is achieved. On the other hand, if the oligomer is totally incompatible, there is a tendency to phase separate completely before initiation of curing, usually leading to very large particle sizes and no improvement in toughness at all. Carboxyl or amine terminated butadiene-acrylonitrile rubbers (CTBN or ATBN) are often used for this purpose. Commonly used curing agents include amine containing multi-functional compounds like piperidine and di-amino di-phenyl sulphone (DDS). Carboxylic acid containing multi-functional compounds can also be used; but they are less reactive and less efficient for curing.

The most common and traditional method of initiating the curing reaction is by supplying thermal energy to the system. The above-mentioned curing agents react with the epoxy, gradually building up the molecular weight and increasing the system viscosity. Subsequent reactions bring about the complete cross-linking. Curing reaction results in an increase in the system viscosity and eventually a state of vitrification or gelation. Build-up of viscosity often reduces diffusional mobility of the reacting molecules. It is of utmost importance to ensure complete phase separation in the desired size distribution before gelation sets in. Any further rubber-phase particle size changes are impossible after gelation of the epoxy matrix. Thermal curing, though easy and cheap, requires very high inputs like high cure temperatures, high cure times and high cure pressures in Resin Transfer Molding and Compression Molding techniques. This process demands robust and higher-investment equipment. Necessary cure cycles, as high as 3-4

hours, limit industrial productivity. The curing reaction is adversely affected (slowed down) by the presence of oxygen. Often, the waste produced is very high. All these disadvantages make thermal curing of epoxies very costly.

An alternative curing mechanism uses other energy sources like electron beams (e-beam) or ultra-violet (UV) radiation. Correspondingly, the nature of the curing agent is different. Multifunctional cationic initiators like aryl sulphonium salts dissociate producing cations. These reactive cations induce cationic polymerization of the epoxy resins in the presence of UV or e-beam. The advantages of this process are obvious. Cationic curing can occur at much lower temperatures, even close to room temperature (lower thermal input). The curing is very fast (shorter cure cycles) and can be localized (less machinery investment). Also, the curing, once initiated by UV radiation, can proceed in absence of further UV radiation. Thus the UV radiation input energy is required only for initiating the ionic species for initiation. There is no need for robust machinery and higher pressures. The curing reaction is not affected and slowed down by the presence of oxygen. The waste is almost non-existent. In addition, due to the absence of specific equipment requirements, the process can be used to cure any intricate shapes, which are otherwise impossible to make using thermal curing.

Since e-beam and UV catalyzed curing is very rapid, the thermodynamics and kinetics of the phase separation should allow the formation of sufficiently small-sized particles of the dispersed oligomer phase before gelation occurs. For this purpose, the oligomer and UV or e-beam curing agent should be properly chosen. UV curing compounds usually have an optimum absorption range of frequency at which their absorption is maximum, resulting in rapid curing. *We think that the development of this*

phase-separated structure is affected by the thermal processing (quenching) of the homogeneous solution, ultimately affecting the final mechanical properties of the cured structure. Studies on optimum system components and the relationship between the thermal processing conditions on particle size and ultimately, the mechanical properties form the main objective of this work.

Sometimes, reactive multifunctional dimethacrylates are added in the system to produce inter-penetrating networks of the cured epoxies and dimethacrylates. The method of phase separation in most cases is the entropically induced phase separation due to the curing of thermoset network. In the present study, the separation of rubber phase as discrete particles of proper sizes is achieved by externally stimulated thermal change before the initiation of curing reaction. In other words, the formulation containing the epoxy, dimethacrylates, rubber and the photoinitiator is cooled from a homogeneous single phase (at higher temperatures) to room temperature at varying rates to achieve various particle sizes of the dispersed rubber phase. Once the desired particle size is achieved, there is a need to lock the generated morphology. This is done by the UV-irradiated initiation of the curing of epoxy and dimethacrylates. The toughness of these samples is related to the particle sizes achieved.

The idea is to bring about the phase separation by thermal energy i.e. cooling the system in melt at a proper rate to produce the desired particle size, then cure the epoxy matrix by either UV or e-beam curing to lock the morphology generated and then cure the dimethacrylates to result in covalently bonded interpenetrating network (IPN) with the epoxy matrix. Such strong adhesion forces (covalent bonds) at the interface improve stress transfer and ultimately toughness.

The prediction of the two major phases, dispersed rubber and the epoxy-dimethacrylates matrix phase, would enable the choice of proper volume fractions of all the components to be mixed. This would then allow the formation of the desired stable rubber particle size necessary for the desired toughness values for individual applications. The main parameters for the complete definition of such a system are the individual weight fractions of the seven components, dimethacrylates composition (δ), the matrix composition (β), the monoepoxide composition (γ), and the branching coefficient (α). The limiting branching coefficient in our case is 0.577 as the epoxy is tetrafunctional.

CHAPTER 2- LITERATURE SURVEY

2.1 General:

Epoxy resins are extensively used in industry due to their superior chemical and thermal resistance properties. However, unmodified epoxy resins are often very brittle after cure. In order to enhance their toughness, reactive liquid rubbers like carboxyl-terminated butadiene-acrylonitrile (CTBN) are often added to the uncured epoxies. Enhanced toughness comes from the resistance offered to the crack propagation by fine rubber particles that phase separate during the epoxy cure [1-3]. The toughness and other mechanical and thermal properties of these cured epoxies strongly depend on the rubber phase morphology and its volume fraction [3-5].

The factors contributing towards the end morphology, in turn, are the precure compatibility between resin and rubber, the curing agent used and the curing conditions [3]. Ideally, the rubber should not be too compatible with the epoxy so as to resist phase separation; but the rubber should be compatible enough to enhance the adhesion with epoxy resin in its final particulate form. The curing agent and the curing conditions should allow sufficient time for the rubber to phase separate, as the epoxy cure proceeds. In addition, the morphology generated should be thermodynamically stable. The ultimate properties of the cured system are thus dependent on the kinetic, thermodynamic and morphological aspects of rubber phase separation.

In the analysis done by Lee et al [6], the epoxy system considered is a diglycidyl ether of bisphenol A (DGEBA). The reactive liquid rubber is a carboxyl-terminated butadiene-acrylonitrile (CTBN) with varying acrylonitrile contents and with molecular weights around 3500 g/mol. Curing amines used are diamino diphenyl sulphone (DDS)

and boron trifluoromonoethylamine (BF_3MEA) as catalyst. The rubber volume fraction was varied from 0% to about 30 %.

Optical microscopy (OM) and transmission electron microscopy (TEM) were used for characterization. OsO_4 was used as a staining agent for SEM. The various aspects of toughening in the above-mentioned system are given below.

2.2 Study of Morphology:

Acrylonitrile groups of the CTBN rubber are compatible with the epoxy matrix [7]. This may lead to a homogeneous single-phase solution even at room temperature. Consequently, no phase separation occurred with the 26 % acrylonitrile content CTBN, when piperidine was used as the curing agent. However, the same system phase separated when the curing agent was changed to DDS and BF_3MEA. This is due to the phase separation induced by the curing agent [7] upon its addition. During curing, the already separated minute particles undergo growth and new particles also phase separate.

According to Rowe et al. [5], higher acrylonitrile content in the rubber results in smaller observed particle size. This is attributed to the higher compatibility, with the epoxy, due to the higher acrylonitrile content of the rubber. This, in fact, suppresses the phase separation.

A study of actual measured (experimental) compositions of the dispersed and the matrix phases, as against the theoretically calculated values from density data showed large variations [8]. In some cases, the actual volume fraction of epoxy matrix (from the analysis of TEM photomicrographs) was found to be much lower that the experimental values. This indicated that some fraction of the epoxy resin is trapped inside the

precipitated rubber particles, dilating them. Similarly, the actual volume fraction of the rubber particles is less that the initial volume before epoxy curing. This indicates that some rubber remains dissolved and does not precipitate out. Both these facts lead to changes in the modulli of rubber and epoxy resin. Such corrected values of rubber and matrix modulli have to be used in toughness calculations of the cured resins.

2.3. Thermodynamic Description:

Unlike low molecular weight materials, polymers are mostly thermodynamically incompatible with each other, owing to their high molecular weight. In the current system, the molecular weights of the uncured epoxy resin and the CTBN rubber are about 390 and 3900 g/mol, respectively. The uncured systems show Upper Critical Solution Temperatures (UCSTs) for various molecular weights of rubber [9,10]. Data from Verchere et al. [11] shows a very high sensitivity of the location of the miscibility gap (maximum in the UCST curves) with respect to molecular weight of the epoxy resin. The higher the molecular weight of epoxy, the higher is the UCST.

Now, the Gibbs's free energy per unit volume, for the mixing of epoxy and CTBN rubber is given by

$$\Delta G = RT\,[(\phi_E / V_E)\ln\phi_E + (\phi_R / V_R)\ln\phi_R] + \chi\,\phi_E\,\phi_R$$

where

R is the gas constant, T is the absolute temperature, ϕ_E and ϕ_R are the volume fractions of epoxy and rubber respectively and V_E and V_R are the molar volumes of epoxy and rubber respectively.

Since, as mentioned above, $V_E << V_R$, (about 10%), hence, apart from the composition dependence, small changes in epoxy molecular weights produces large relative changes in the free energy of mixing. Depending on the nature of the change in epoxy molecular weight, the value of ΔG will either increase or decrease (for all other parameters remaining constant), with either assisting or resisting thermodynamic miscibility of the unreactive system.

A corresponding ΔG equation for reactive systems (curing reaction) is as given below:

$$\Delta G = (RT / V_{E0}) [(\phi_E / Z_E) \ln \phi_E + (\phi_R / Z_R) \ln \phi_R] + \chi \phi_E \phi_R$$

where

V_{E0}: initial molar volume of the epoxy-amine hardener pre-cured adduct and

$Z_E = V_E / V_{E0}$, $Z_R = V_R / V_{E0}$

Verchere et al. [11] further show that the increase in the value of Z_E during cure produces large changes in the Gibbs's free energy of mixing, driving the phase separation.

Phase diagram for such system gives the binodal and spinodal decomposition curves for the reactive system. A critical rubber volume fraction can be defined using such phase diagrams. Actual phase separation can occur via two possible mechanisms; nucleation and growth or spinodal decomposition or a combination of both. For the first mechanism, the rubber must be able to generate centers of nucleation (precipitate out into

small particles or start growing on the preexisting external nuclei of impurity particles like the curing agent). Subsequent phase separation results into the growth of these nucleated particles, resulting into increase in their radii. This mechanism results into the generation of small number of large size particles upon the completion of phase separation. Spinodal decomposition, on the other hand, is the spontaneous precipitation of the minor phase at a certain conversion or extent of the curing reaction. This process leads to a spontaneous generation of periodic worm-like domains of rubber. Subsequent growth occurs via coalescence of the phase-separated rubber phase. The coalescence process leads to coarsening of the particle surfaces with diffused or extended boundaries. Both these morphologies show up distinctly in the TEM micrographs. However, a detailed thermodynamic analysis of the kinetics, followed by morphology analysis for conformation should be the proper route.

2.4. Kinetics:

One important kinetic parameter in this respect is the ratio, K, of the rates of phase separation and polymerization. Very high K values indicate that the particles are being generated at a faster rate than the crosslinking reaction. This allows sufficient time for the dissolved rubber to diffuse to the generated nuclei, leading to nucleation-growth mechanism dominating the phase separation. A value of K tending to zero indicates that the matrix hardens at a rate higher that the particle generation rate, resulting in the sudden precipitation of rubber particles (at large number of sites, when a particular extent of crosslinking has occurred. The subsequent growth of these particles, by particle coalescence, has to compete with the rapidly hardening matrix.

The nucleation rate depends strongly on the surface energy between the two phases. Since the current system has very low surface tension values [12,13], the nucleation rates are very high. Hence, if the polymerization rates are not so high, phase separation occurs predominantly by the nucleation-growth mechanism. Spinodal decomposition of the rubber phase is likely to occur in systems in which the resins are cured rapidly or if the entire system is quenched from the reaction temperature. This is because in such systems, nucleation and growth is suppressed due to lower available time for phase separation.

2.5. Toughened Systems:

Various toughening agents have been tried for thermally cured epoxy resins with varying results. These include rubbers or elastomers, either as discrete particles or reacted with the epoxy [14-19], epoxy functionalized flexibilizers [20], engineering thermoplastics [21-24], and amine or hydroxy-terminated thermoplastics oligomers [25-28]. But very few results exist for UV-cured epoxies. Garg and Mai [30] discuss the various toughening mechanisms for cross-linked epoxies. Pearson and Yee [31] study the effect of type of CTBN rubber, the dispersion quality, and the rubber particle size on the particle toughness. According to them, these factors in various combinations induce various toughness mechanisms in the above systems. McGarry [32] studied the failure envelopes in rubber-toughened epoxies. The critical particle size required for toughening is smaller for ductile matrices like PVC than that for brittle matrices like epoxies [33]. In case of brittle polymers, the craze termination must be effectively carried out by the rubber particles themselves, which means larger particle sizes of the dispersed phase are

necessary. Also, the adhesion between the matrix and rubber must be strong enough to prevent crack formation from the crazing stage.

2.6. Toughening Mechanisms:

Glassy polymers deform by one of the two mechanisms, shear processes or cavitation processes (See Figure 1) [34, 45]. Shear processes include diffuse shear yielding and localized shear band formations and occur without the loss of intermolecular cohesion in the polymer with very little change in the density. Cavitation processes include crazing, void formation and fracture and is a result of the local loss of intermolecular cohesion. These two mechanisms may be coexistent and may interact in the overall fracture process of the material [34].

Shear yielding consists of a distortion of shape without a significant change in its volume. In metals, shear yielding occurs along specific slip planes due to dislocation glide. Slip occurs on planes of maximum resolved shear stress in case of highly crystalline polymers. In the case of amorphous polymers, due to absence of well-defined structure, the large strain deformations require higher stresses and results in the shear stresses getting localized in some selected areas of higher concentration of either the small amount of crystallites (if present) or any inclusions. In some polymers, diffused shear yielding occurs throughout the stressed region while localized yielding occurs in other polymers. This localized yielding is concentrated in well-defined shear microbands. According to Argon [34], the localized stored elastic energy is relieved by the formation of a pair of molecular kinks in adjacent chains, increasing the shear strain. Shear microbands occur in areas of high inhomogeneities of strain due to internal flaws or stress

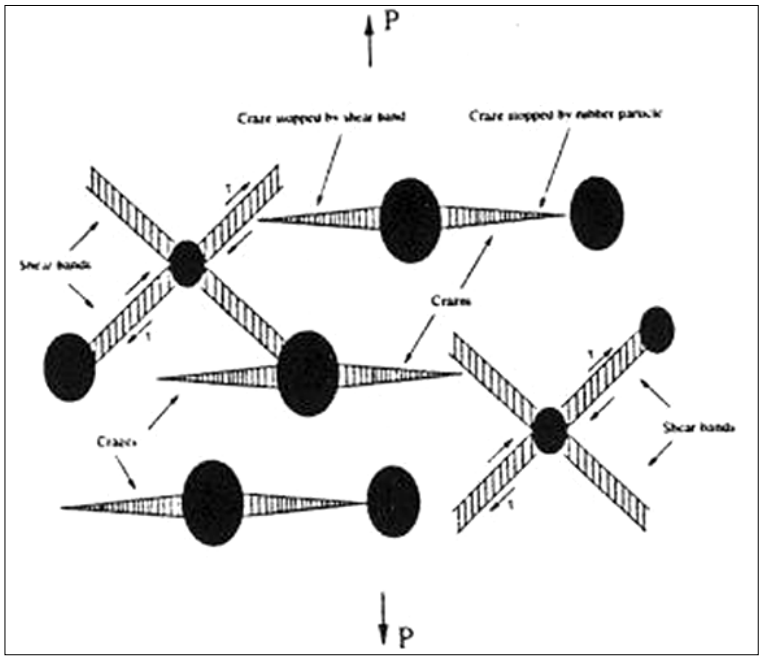

Fig. 1: Schematic of combined crazing/ shear banding mechanism. [45]

concentrations. Beyond the yield point, the shear band areas offer lesser resistance to deformation than the surrounding material. This further increases the strain strain inhomogeneities, which in turn further reduces the shear resistance of the material within the shear bands. This whole process leads to the softening of the material at the tip of the shear bands, leading to the propagation of the band along a plane of maximum resolved shear stress [33, 34].

In the other mechanism, under the application of stress, a polymer may develop small voids in a plane perpendicular to the applied stress, initiating a crack. But these small cracks stabilize due to the formation of oriented fibrils of the polymer spanning the gap and preventing the crack from widening. This combined interpenetrating network of voids and polymer fibrils is known as a craze.

In order to understand the actual toughening mechanisms in epoxy-rubber systems, an understanding of the stress fields around the rubber particles is necessary. In

most cases, a triaxial stress state exists at the crack tip [34]. This triaxial stress field ahead of the rubber particle leads to the two important deformation processes. One is the initiation and growth of multiple localized shear-yield deformation in the matrix. The stress concentration points around the rubber particles act as the initiation points for the matrix plastic shear deformation. Due to the presence of a large number of rubber particles, large amount of energy is dissipated due to this process. Shear deformation generally initiates at one particle and terminates at the other particle [34]. The other deformation process is the cavitation of rubber particles. Cavitation produces dilation. Due to uneven cooling of the cured system, stresses are generated within the particles. Along with these stresses, dilation causes failure and void formation either inside the particles or at the rubber-epoxy matrix. Void growth consumes the remaining energy. In addition, voids also enhance the shear yielding of the matrix, which lowers the stress required for shear yielding and enhances the matrix plastic shear deformation [33]. However, such cavitation and the corresponding relief of plane-strain constraint will occur only when the matrix is able to deform plastically to a substantial extent. Under stress, these crazes relax and extend, breaking the fibrils and coalescing the voids, ultimately leading to the formation of a crack that fractures the specimen.

There has been considerable debate on whether matrix shear yielding can occur at all in thermosets. While studying the fracture mechanisms of the thermoset resins containing 1,2-dihydroxybenzocyclobutene and meleimide functional groups, Sue et al. [35] clearly observed crazing even though the resins were highly crosslinked (having a high crosslink density). Jang et al. [36] studied the fracture toughness of interpenetrating networks of a brittle thermoset resin and a tough thermoplastic. The thermoset resin was

prepared from the monomethyl ester of 5-norbornene-2, 3-dicarboxylic acid, 4, 4'-methylenedianiline and 3, 3', 4, 4'-benzophenonetetracarboxylic acid. Two different thermoplastics were used as the dispersed toughening agents. In one case, the mechanism of fracture was found to be a combination of shear yielding and crazing. In the other case, no shear yielding or crazing was observed. In this case, the diffuse shear yielding was seen clearly. But in both cases, the shear yielding observed was diffuse and localized. This was attributed to the limited ability of the highly crosslinked thermoset matrix to yield plastically. An altogether different toughening mechanism was proposed by Argon et al. [34].

However, Kinloch et al. [37] argue that due to restricted segment mobility in highly crosslinked thermoset matrices, shear yielding of the matrix cannot occur. In a study on epoxy-CTBN systems cured with 4,4'-diaminodiphenylsulfone, Pearson and Yee [38] found out that the crosslink density plays a major role in deciding the final fracture toughness of the cured system. According to their findings, the fracture energy, G_{Ic}, increased marginally for unmodified systems and significantly (almost 40 times in one case) for CTBN toughened systems. Finch et al. [39] performed similar work using the same system but using piperidine as the curing agent. In this study as well, the molecular weight between crosslinks or the crosslink density affected the fracture toughness significantly. From the work of Kinloch et al. [40], it is seen that plastic shear yielding in the matrix is the main source of impact energy dissipation. Such plastic deformation caused by the interaction of the stress field ahead of the crack tip and the rubber particles is seen to be greater in case of the matrix of rubber-toughened thermosets than unmodified thermosets.

Thus there is an on-going debate on whether the ductility of the matrix or the cavitation inside the rubber particles is the major source of energy dissipation in case of rubber-toughened thermosets.

2.7. UV curing of epoxy resins:

Cationic photocrosslinking of epoxy resins is based on the ring-opening polymerization of the epoxide ring, leading to the formation of a reactive ether link in the structure. Crivello [29] discusses various photo-curing agents for epoxies. According to him, amongst the studied salts, diaryliodonium, triarylsulfonium and ferrocenium salts are the most effective in UV curing the epoxy resins. But the ones that are commercially important are the onium salts like diaryliodonium, triarylsulfonium and ferrocenium salts. Diaryliodonium and triarylsulfonium salts are highly photosensitive in the UV region. They are very stable in the absence of light. Also, their structure can be easily modified to achieve specific desirable UV absorption characteristics.

The general mechanism by which aryl salts polymerize epoxies is a result of the formation of Bronstead acid. Absorption of UV light results in the hemolytic and heterolytic cleavage of the C-S bond. Both these resulting cationic species react further to form strong protonic acids, which in turn initiate and propagate the cationic polymerization of epoxies. Once the protonic acids are generated, further polymerization reactions can occur in the absence of light. Since the organic cation is the main light absorbing species, a variety of cationic photoinitiators can be generated by property choosing the onium salts which operate at a range of UV radiation frequencies. The strongest known acid is the SbF_6 acid. The onium salt first photolyses to form a

Bronstead acid by the mechanism as given below. The photoinitiator, TASHFA, breaks homolytically into two cations as follows:

$$X^-Ar_3S^+\text{-}S\text{-}S^+Ar_3X^- \longrightarrow 2(Ar_3S^+X^-) + S^{-2}$$

$$Ar_3S^+X^- \longleftrightarrow Ar_2S^{\cdot+} + Ar^{\cdot} + X^-$$

$$Ar_2S^{\cdot+} + R\text{-}H \longrightarrow Ar_2S^+\text{-}H + R^{\cdot}$$

$$Ar_2S^+\text{-}H \longrightarrow Ar_2S + H^+X^-$$

Here,

Ar	Aryl group
X^-	SbF_6^-
R-H	Donor for hydrogen abstraction

The bronstead acid formed then polymerizes the epoxy cationically by opening the epoxide ring. Termination occurs by either the reaction of the growing cationic chain end with a nucleophile or basic impurities or corresponding reactive sites of the epoxy molecule [41]. The free radicals generated in this photolyses reaction initiate the free radical polymerization of the dimethacrylates, leading to the formation of interpenetrating network with the epoxy network (See Figure 2 for cured epoxy ladder-like structure).

$$H^+X^- + M \longrightarrow HM^+X^-$$

$$HM^+X^- + nM \longrightarrow H(M)_{n-1}M^+X^-$$

where,

M	Epoxy monomer

The UV crosslinking of the methacrylates is well known and would not be covered here.

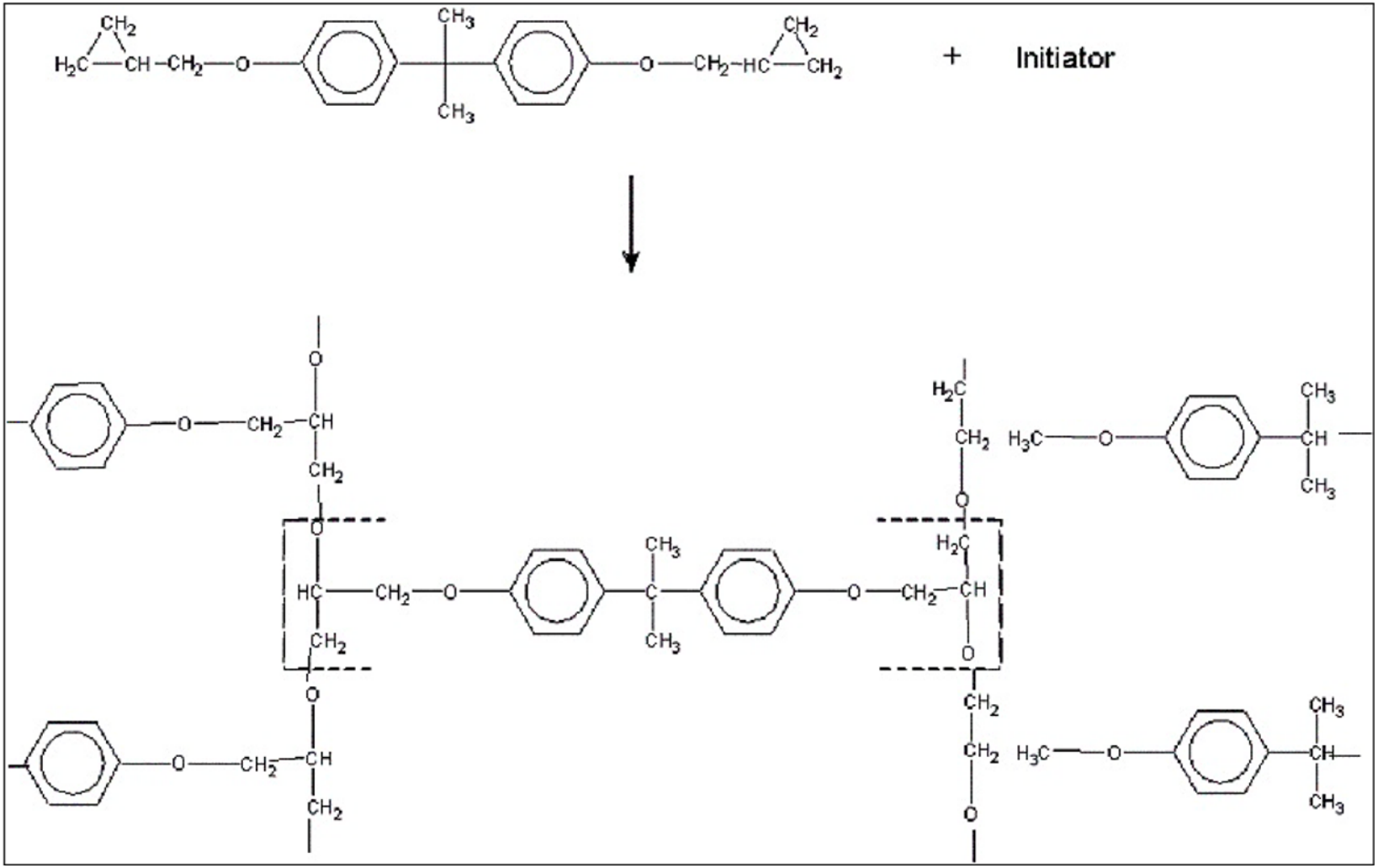

Fig. 2: Ladder-like post curing network structure of epoxy resins

CHAPTER 3- EXPERIMENTAL DETAILS

3.1. Materials System:

Diglycidyl ether of bis-phenol A (DGEBA) was used due to its suitability for structural adhesives applications. Epon-828 (Courtesy: Shell Chemical Company) with epoxy molecular weight of 380 g/mol was used due to its lower viscosity, which aids mixing and dispersion of rubber in it. Its refractive index was 1.573 and its specific gravity was 1.16. This epoxy is tetrafunctional after the opening of the oxirane rings. Ring opening was carried out by the use of cationic photoinitiator triaryl sulphonium hexafluoroantimonate (TASHFA) (Courtesy: Dow Chemicals Company/ Union Carbide). Carboxyl-terminated butadiene acrylonitrile copolymers (HYCAR CTBN 1300X8, X13, X31 and CTB X162) (Courtesy: BFGoodrich Chemical Company) were used as the reactive toughening oligomers. They had the same molecular weight of 3900 and an average functionality of 1.9. The acrylonitrile content was different in each of them. Their refractive indices were in the range 1.56-1.6 and their specific gravities were in the range 0.924-0.96. It was used in varying proportions to give 4 different compositions containing 5%, 10%, 15% and 20% by volume of rubber for each elastomer. Experiments were limited to 20 % by volume rubber because of the phenomenon of phase inversion in these systems beyond this composition [33] (Table 1 and Figure 3 for chemicals used).

Dimethacrylates used included the highly viscous fully methacrylated diglycidyl ether of bisphenol A (bisGMA) (Sartomer CN 151) and the low viscosity 1, 6 hexanediol methacrylate (HDDMA) (Sartomer SR 239). Their molecular weights were 254 g/mol

Table 1: Chemicals Used and their general properties

Chemical Category	Trade Name	Manufacturer	Mol. Wt. (g / mol.)	Important Property
Diglycidyl ether of bisphenol-A (DGEBA)	Epon 828	Shell Chem. Co.	390	Epoxy Eq. Wt.: 185-192
1, 6 hexanediol dimethacrylate (HDDMA)	SR 239	Sartomer Co.	254	Viscosity: 8 cp @25 ^{o}C
Bis-methacrylated DGEBA (bis-GMA)	CN 151	Sartomer Co.	552	Viscosity: 1380 cp @70 ^{o}C
Carboxyl terminated butadiene-acrylonitrile Elastomer (CTBN)	**HYCAR Grade** CTB 2000X162 CTBN 1300X31 CTBN 1300X8 CTBN 1300X13	BF Goodrich Chemicals	 4200 3800 3550 3150	**Acrylonitrile / Tg (^{o}C)** 0 mol% / -77 10 mol% / -66 18 mol% / -52 26 mol% / -39
Triaryl sulfonium hexafluoroantimonate (TASHFA) cationic photoinitiator	Cyracure	Dow Chemical Company	847	UV absorption: 280-380 nm

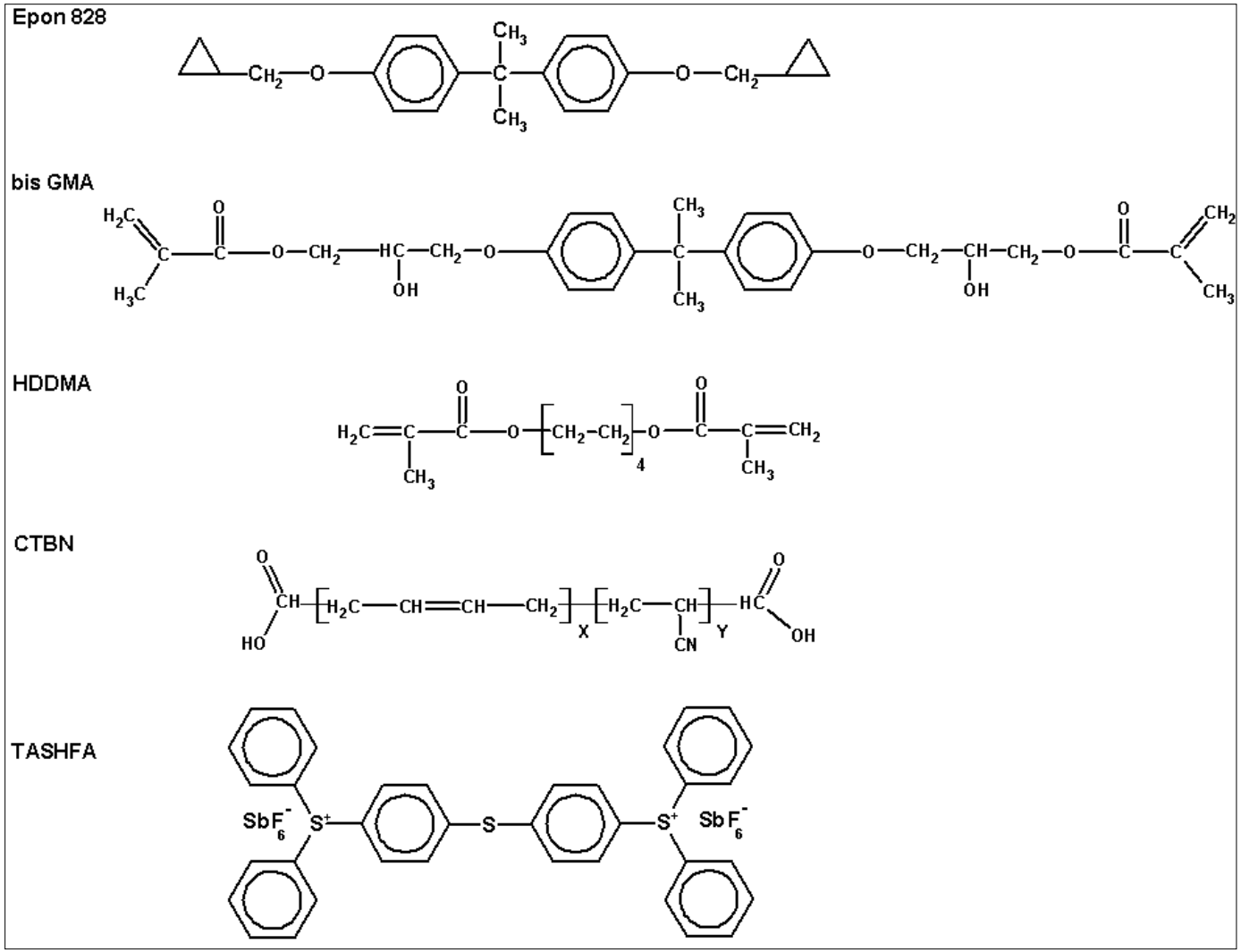

Fig. 3: Structures of the chemical components used

and 552 g/mol respectively. Varying proportions of them could be used to give the desired viscosity suitable for mixing. The internal ration of HDDMA: bisGMA of 1:1 by weight, for all formulations, was found to give suitable viscosity matching with that of the Epon-828/CTBNX31 dispersions (See figures 2 and 3).

As mentioned above, the cationic initiators used were triaryl sulphonium hexafluorophosphate (TASHFP) (Sartomer) and triaryl sulphonium hexafluoroantimonate (TASHFA) (Courtesy: Dow Chemical Company). Both, TASHFP and TASHFA had an optimum UV absorption in the 280-380 nm wavelength range. Hence, 365 nm was the chosen wavelength of the UV used. The UV source had a power of 275 watt/inch.

Stable dispersions of the Epon-828, CTBNX31 and TASHFA were prepared by homogenizing at 40^{o}C for 4 hrs in dark, amber colored glass bottles. TASHFA quantities used in the formulation were 3 % by weight of Epon-828 taken. From trial runs on the mixtures taken in Petri dishes, the exposure time required for complete cure was found to be 15 mins. Izod impact specimens were cured in situ. Thinner samples (1.5 mm thickness) were used instead of the standard ASTM specified dimensions to avoid an incomplete or non-uniform UV cure of the specimen with respect to thickness.

3.2. Techniques used for measurements and analysis:

The following characterization techniques were used for a complete analysis of the systems used:

3.2.1 Optical Microscopy:

A Nikon polarizing microscope with a MTI digital camera was used for carrying out the optical microscopy experiments. Optical microscopy was performed on catalyst-free

dispersions to know the phase separation temperature and to study the effect of different cooling rates on the ultimate particle size in the phase separated rubber phase. For this purpose, a small drop of the mixture of epoxy and rubber, without the catalyst, was deposited on a glass slide. Five-minute cure epoxy adhesive was applied along the perimeter of a cover slip and the cover slip was gently placed on top of the glass slide, enclosing the dispersion drop. Care was taken to avoid the entrapment of air bubbles in the specimen. The glass slide was heated in a Mettler hot stage with temperature control to within +/- 0.1^{o}C accuracy. The samples were maintained at a temperature slightly above the expected phase dissolution temperature for an hour for complete dissolution of the rubber phase and to ensure uniform temperature throughout the mass. The samples were cooled to 30^{o}C at different rates. The dissolution and precipitation processes were recorded on videotape. Images were captured and digitized using standard software (Scion Image). Particle size measurement was carried out using standard software (Scion Image).

To begin with, 5 10, 15, and 20 volume % of each CTBN was dispersed in Epon 828 to form different formulations. Epon 828 was heated in an air-convection oven at 60^{o}C to reduce its viscosity and facilitate the dispersion of rubber in it. Slides were prepared for optical microscopy using the technique described above.

The same slides were then used for Small Angle Laser Light Scattering measurements. The 15-volume % CTBN dispersed epoxy system was chosen for further experimentation.

In the next set of experiments, slides were prepared for the formulations containing the dimethacrylates. OM was done on only the 15-volume % CTBN case,

which proved to be the most consistent and repeatable (as will be supported later with the help of SALS data).

3.2.2 Small Angle Laser Light Scattering (SALS):

SALS was used for comparing with respect to the particle size measurements from optical microscopy. A He-Ne laser (red) at 628.8 nm was used with polarized laser output. A collimator was used to reduce and concentrate the laser beam diameter. The sample was mounted in the holder. The screen distance from the sample was adjusted so as to allow maximum intensity of scattered light to fall on the screen, yet not high enough to *blind* the camera. The distance of the camera from the screen was adjusted so as to give scattering pattern big enough to fit the video window on the computer. A black, fluffy textured beam stop (5 mm diameter circular disc) was fixed on the screen to stop the transmitted light beam from being captured by the camera. This procedure helped to prevent camera-blinding and also ensured an error-free analysis during the step of finding the pattern image center. Blank slide pattern was captured before every sample run for normalization to remove stray light effect. A Matlab code (developed by Dr. Kit) was used to average the intensity with respect to the radius of the scattering pattern and to calculate this average intensity and the scattering angle. Calculated data was plotted for samples cooled at various rates to relate qualitatively and quantitatively the particle size relation with the cooling rate. Analysis suggested by Effler et al. [42] [27] was used to calculate the particle size. As a result, the log of the intensity data was fitted to a sixth powered polynomial in the quantity q^2 where,

$$\mathbf{q = \{4*\pi / \lambda\} * \{ \sin (\theta/2) \}}$$

The radius of the chain is related to the coefficients of the zeroth and first order terms of the polynomial by the relation

$$\mathbf{R = sqrt\ \{6*(-B_1 / B_0)\}}$$

where B_1, B_0 are the first and the zeroth order coefficients of the sixth-order polynomial. Guinier plot analysis was also tried on the same set of data for comparison purpose. But the method suggested by Effler et al. [42] gave better data comparison with the OM results. Hence, the analysis suggested by Effler et al. [42] was thought to be sufficient for comparison purpose.

3.2.3 Fourier Transform Infrared Spectroscopy (FT-IR):

A Bio-Rad FT-IR spectroscope was used to access the extent of photo crosslinking reaction of the epoxy resin and the dimethacrylates. Films of Epon828-dimethacrylates (100 phr; d=0.5)-CTBN X31 (15 vol. %) were cured with UV. In the other case, a similar film was additionally cured thermally in an oven at 150 ^{o}C for 3 hours after the UV curing step. ATR mode scans were taken at intervals of 5 cm^{-1}. 1024 scans were taken for each step.

3.2.4 Impact Testing (IT):

Impact Testing was carried out on a Tinius Olsen model 92T Izod Impact Tester. A final formulation of 2:1:1 of Epon828: bisGMA:HDDMA by volume was maintained. The final formulation consisted of 85-volume% of the above mixture and 15-volume% of CTBNX31. Specimens were cut from a 10cm x 10 cm x 1.5mm film cured in an aluminum mold pre-coated with a silicone mold release agent. Formulations were poured

in the mold, the mold kept in a controlled-temperature oven at 120^{o}C for 30 minutes for temperature equilibration and the mold transferred to another chamber maintained at 80, 70, 60, 50, and 20 ^{o}C (in the last case, the mold was taken out of the oven maintained at 120 ^{o}C and kept in open air at room temperature) respectively. The range of quench rates was from *3-5 ^{o}C/min*. All these temperatures were below the cloud temperature for the Epon828-dimethacrylates-CTBNX31 system. This step hopefully dispersed the rubber phase in the desired size range and distribution. After this quench, the mold was placed in open atmosphere for natural cooling to room temperature followed by UV cure for 15 mins. For complete cure, the UV irradiated, partly uncured sheet was maintained at high temperature of 150 ^{o}C for 3 hours. As proved by the FT-IR data, this step ensured the complete curing of the formulations. Specimens were cut into 55mm x 11mm x 1.5mm sized strips with a sharp razor. Care was taken to keep the cutting speed low to prevent the formation of crazes or whitening in the specimens.

Impact testing was carried out according to ASTM D256. Un-notched specimens were used because the specimens were thin. Impact energies were recorded in kJ/m^2.

3.2.5 Dynamic Mechanical Analysis (DMA):

DMA was used to study the effect of the dispersed rubber phase on the change in storage and loss modulus of the epoxy. Since there is supposed to be adhesion between the epoxy and rubber phases, the tan δ peaks are expected to shift by a small amount accordingly. Also, the composite modulus of the system is expected to drop slightly. The resultant toughness values are analyzed from the combined IT and DMA results.

A Rheometrics Scientifics DMTA V system was used for DMA testing. The same specimens, which were used for IT, were used for DMA as well. The tests were carried out in a three-point bending mode. Temperature was ramped from -150^{o}C to +200^{o}C at 2.5 ^{o}C/min. The tan δ peaks were analyzed critically to understand the extent of adhesion between the dimethacrylates in matrix phase and the CTBN in the dispersed particles.

3.2.6 Scanning Electron Microscopy (SEM):

SEM was used to study the morphology of the three-component cured systems. Izod impact specimens were prepared by irradiating the three-component mixture (with TASHFP added) with UV radiation of 365 nm wavelength for varying times. The Aluminum molds were half filled to give specimen of near-standard ASTM dimensions. The cured specimen were fractured in the Izod impact testing and a thin cross-section of the fractured surface was observed under the SEM. Specimen were sputtered with gold to prevent charge accumulation on the section surface. In low concentration specimens, a 10 weight % CrO_3 solution was used to preferentially etch out the rubber phase for better contrast. CrO_3, being a strong oxidizing agent, preferentially reacts with the CTBN double bonds changing its color.

CHAPTER 4- RESULTS AND DISCUSSION

4.1 Optical Microscopy:

The first thing to do was to understand the phase separation behavior of the CTB/CTBN from Epon828 (cloud point data). This data enabled the correct determination of the exact temperature at which the CTB/CTBN phase starts precipitating from the Epon828-CTB/CTBN solution while cooling from a homogeneous one-phase solution. Knowledge of the cloud point curves helped in determining the starting temperature of the solution from where the solution has to be quenched. In this case, the cloud point experiments were carried in a loop. The solution was first heated to monitor the dissolution temperature of the CTB/CTBN phase at a constant heating rate. The solution was maintained at a temperature 30^{o}C above the dissolution temperature for 45 minutes, sufficient for temperature equilibration after which it was quenched.

Table 2 shows the cloud point temperatures for the epon 828-CTB and epon 828-CTBN systems for 5, 10, 15 and 20-volume % CTB/CTBN respectively. It is seen that for a particular volume content of CTBN (X8, X31 and X13) higher the acrylonitrile content, lower are the cloud point temperatures observed. Also, for a particular acrylonitrile content (particular CTBN chosen), the higher the CTBN volume fraction, the lower is the observed cloud point temperature. Both these observations are attributed to the enhanced compatibility as a result of the increased content of acrylonitrile groups. Compatibility is also enhanced to a small extent by the presence of polar carboxylic acid end groups in the CTBN, which may be forming hydrogen bonds with the ether –O- links of the Epon828. Better compatibility reduces the thermal energy input (lower

Table 2: Cloud point temperatures for various Epon 828 / CTBN compositions.

System	Acrylonitrile (mol %)	CTB/CTBN content (volume %)	Cloud Point (^{o}C)
Epon828 / CTB 2000X162	0% Acrylonitrile	5	158
Epon828 / CTB 2000X162		10	150
Epon828 / CTB 2000X162		15	145
Epon828 / CTB 2000X162		20	130
Epon828 / CTBN 1300X31	10% Acrylonitrile	5	110
Epon828 / CTBN 1300X31		10	95
Epon828 / CTBN 1300X31		15	80
Epon828 / CTBN 1300X31		20	65
Epon828 / CTBN 1300X8	18% Acrylonitrile	5	150
Epon828 / CTBN 1300X8		10	140
Epon828 / CTBN 1300X8		15	135
Epon828 / CTBN 1300X8		20	115
Epon828 / CTBN 1300X13	26% Acrylonitrile	5	95
Epon828 / CTBN 1300X13		10	80
Epon828 / CTBN 1300X13		15	70
Epon828 / CTBN 1300X13		20	60

temperature) necessary to dissolve the added volume fraction of CTBN in the epon 828 matrix and hence, the observed lower cloud point temperatures.

In case of CTBX162 (0 mol % acrylonitrile), the polar carboxylic acid groups, forming hydrogen bonds with the –O- groups of the Epon828, result in the observed small decrease in the cloud point temperatures with an increase in the CTB volume fraction from 5 to 20%. Since this hydrogen bonding effect is limited, the amount of cloud point decrease is low.

Optical micrographs of 10, 15 and 20-volume% CTBN X31 are presented in figures 4-6. In each case, the formulations are cooled from well above their cloud points (180^{o}C) to 30^{o}C at different cooling rates. In figure 4, for the 10-volume% CTBN X31, the average particle size remains constant at 2.1+/-0.105 micron, irrespective of the quenching rate. The resulting particle size distribution is unimodal. In figure 5, for the 15-volume% CTBN X31, the average particle size reduces from 3.7+/-0.185 micron for 0.3^{o}C/min to 2.5+/-0.125 micron for 2.5^{o}C/min quench rate. The resulting particle size distribution is unimodal for higher quench rates and bimodal for lower quench rates. In figure 6, for the 20-volume% CTBN X31, the average particle size reduces from 3.8+/-0.190 micron for 0.3^{o}C/min to 2.1+/-0.105 micron for 2.5^{o}C/min quench rate. The resulting particle size distribution is unimodal for higher quench rates and bimodal for lower quench rates. In all cases, the particle size of the dispersed CTBNX31 reduces with increasing quench rate. Higher quench rate does not provide sufficient time for the dispersed CTBNX31 droplets to grow into larger sizes by merging with adjoining droplets. As mentioned earlier in chapter 2 (Section on Kinetics), a higher quench rate induces phase separation by spinodal decomposition, which generally results in a

a

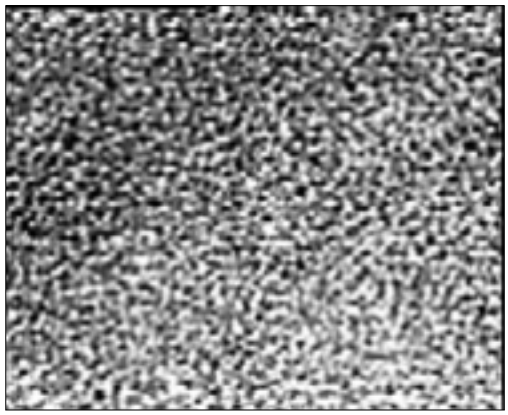

b

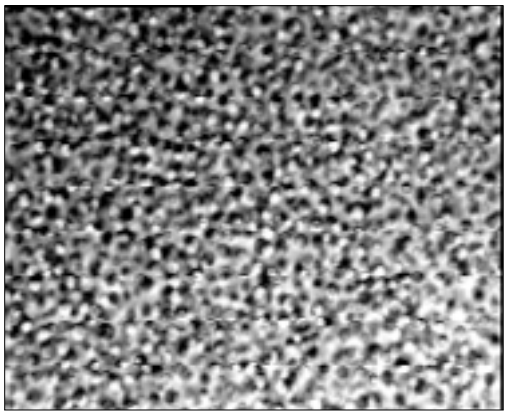

c

20 μm

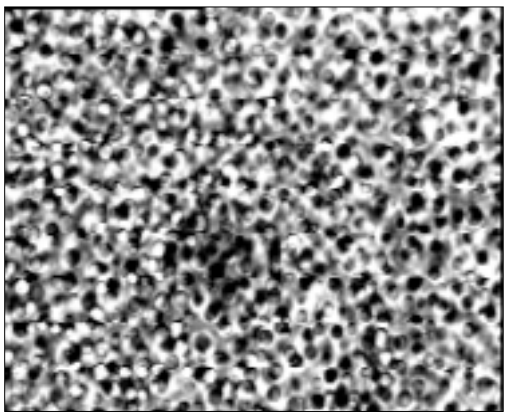

d

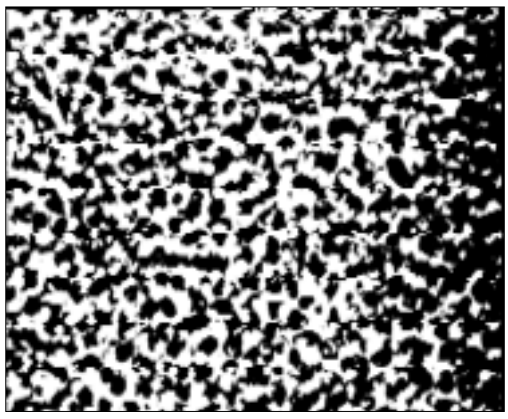

e

Fig 4: Optical micrographs of Epon 828- 10 volume % CTBN X31 formulations; Cooled from 180-30 ^{o}C at various rates (by varying the cooling time); 300X magnification. a: 1 hour; b: 2 hours; c: 4 hours; d: 6 hours; e: 8 hours;

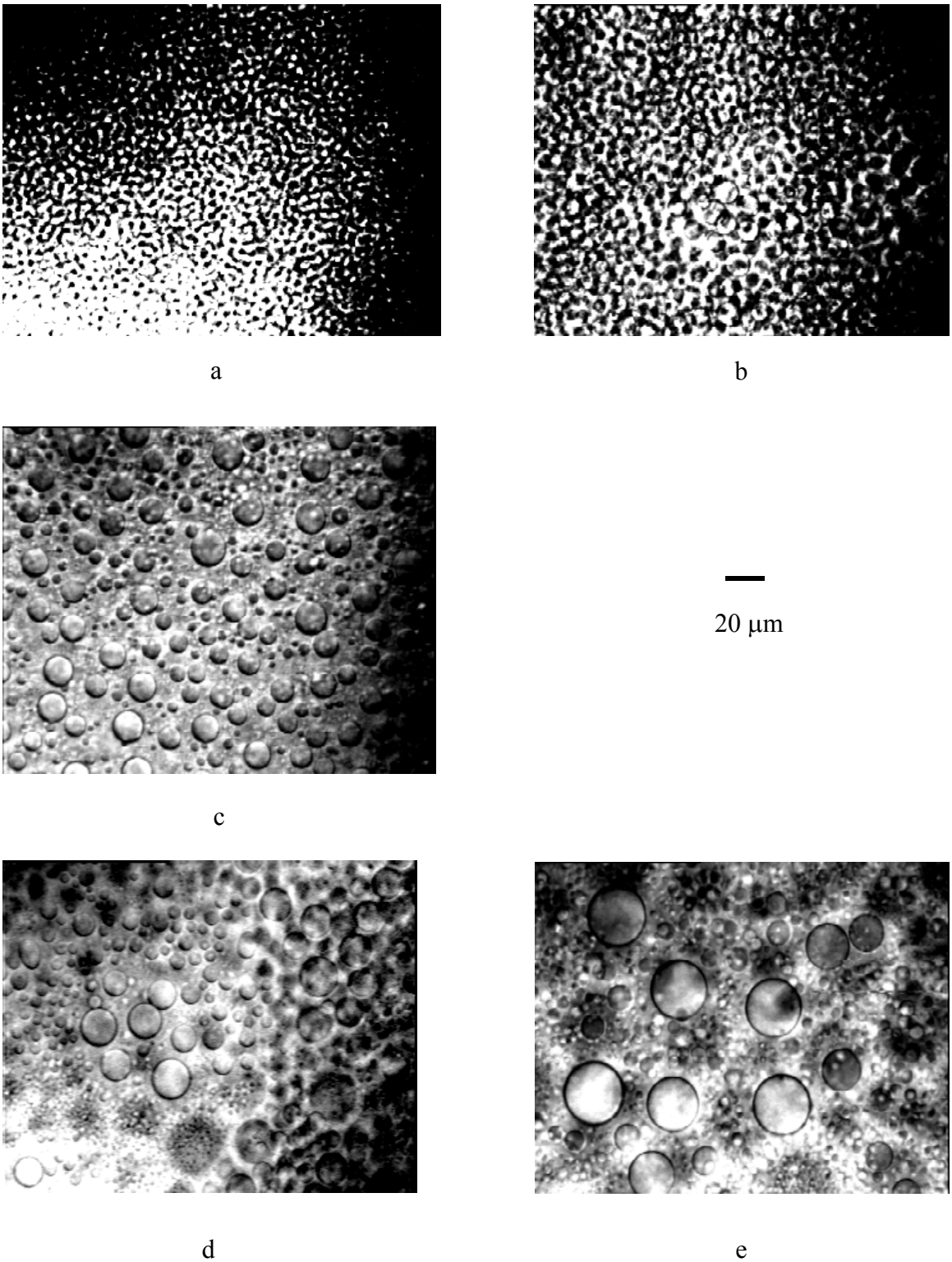

Fig 5: Optical micrographs of Epon 828- 15 volume % CTBN X31 formulations; Cooled from 180-30 ^{o}C at various rates (by varying the cooling time); 300X magnification. a: 1 hour; b: 2 hours; c: 4 hours; d: 6 hours; e: 8 hours;

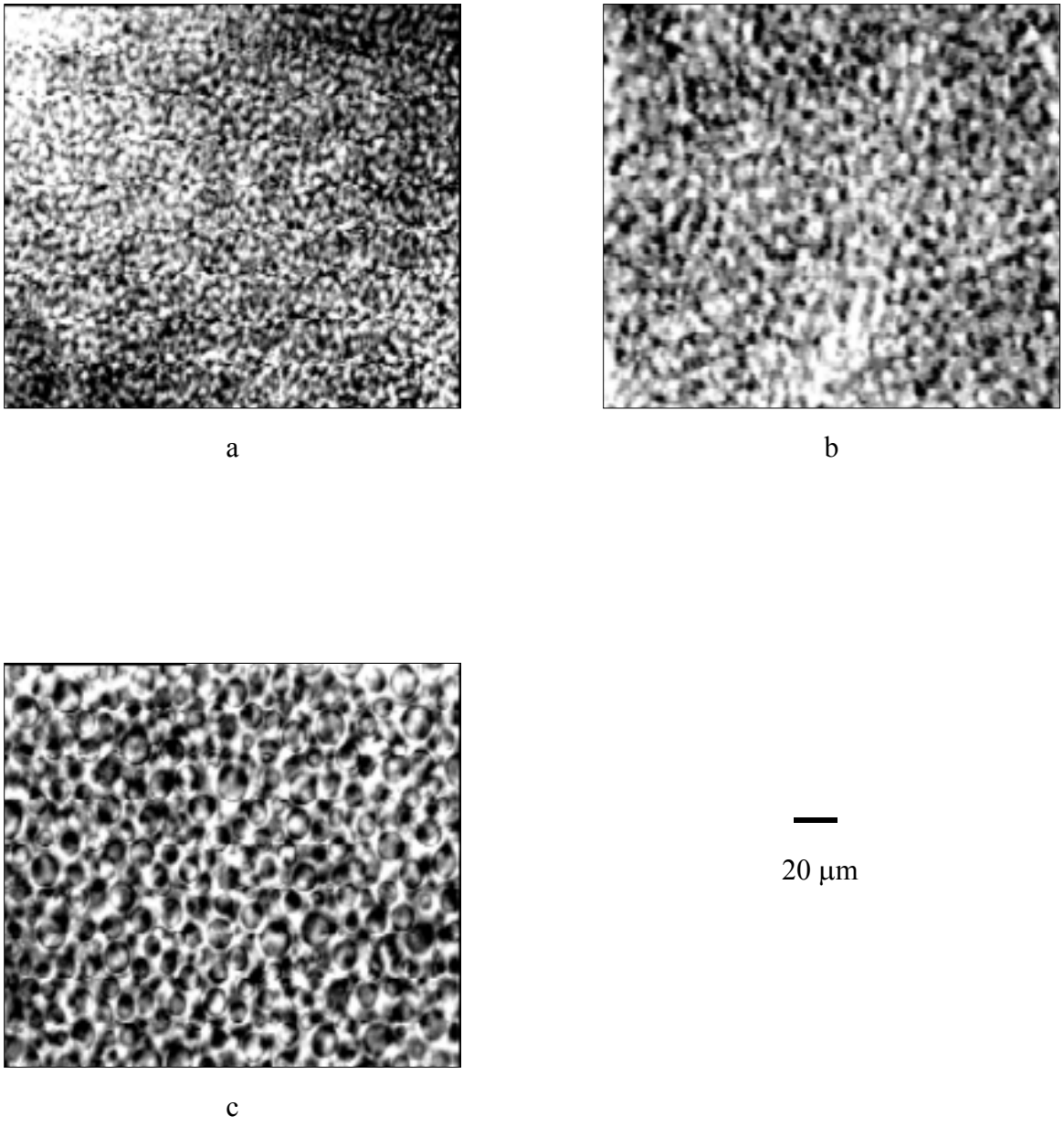

Fig 6: Optical micrographs of Epon 828- 20 volume % CTBN X31 formulations; Cooled from 180-30 ^{o}C at various rates (by varying the cooling time); 300X magnification. a: 1 hour; b: 2 hours; c: 8 hours;

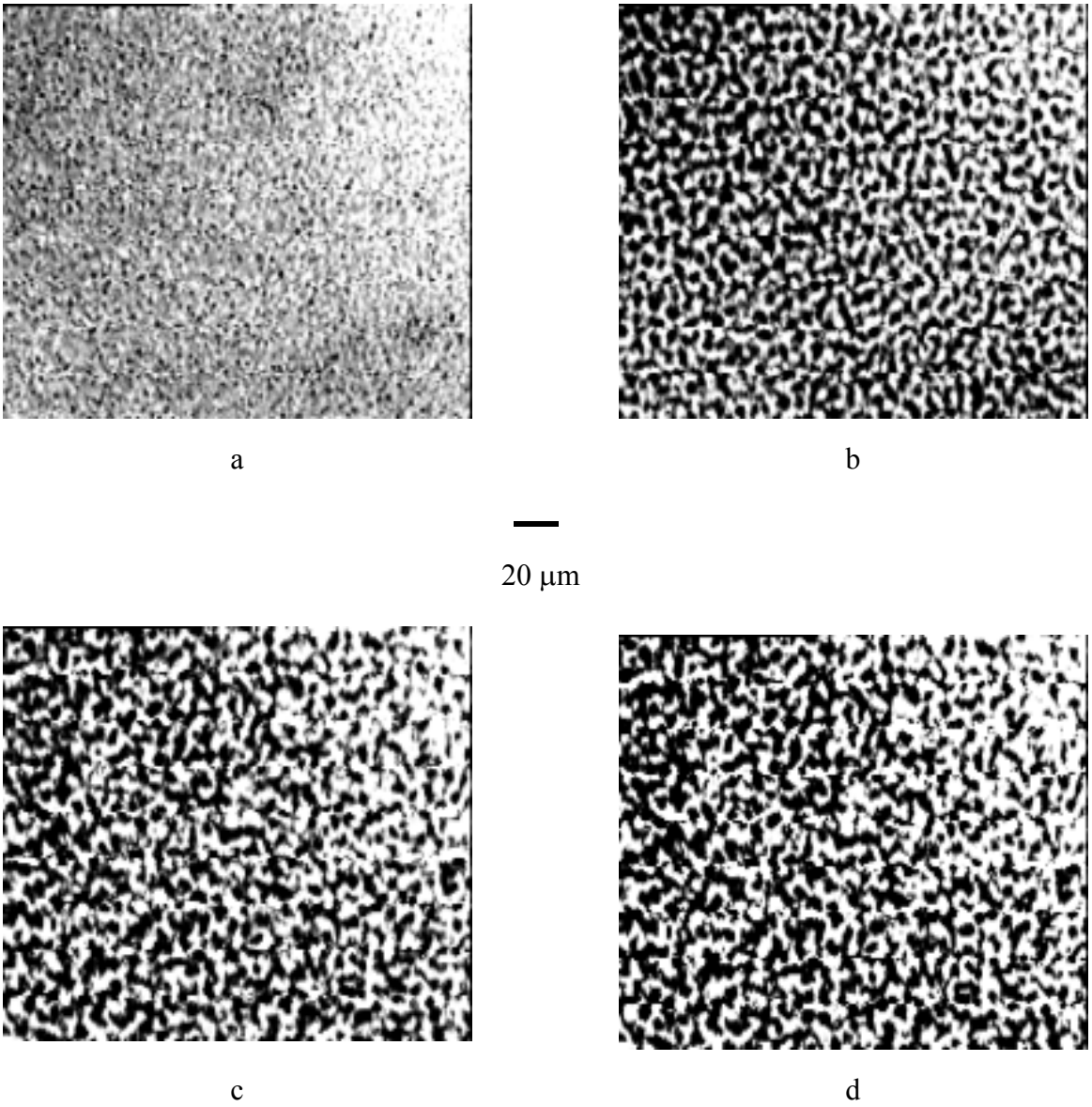

Fig 7: Optical micrographs of Epon 828- 15 volume % CTBN X31- 50 weight % Dimethacrylates (δ = 0.5) formulations; Cooled from 100-30 ^{o}C at various (but correspondingly same as compared to the two phase systems) rates (by varying the cooling time); 300X magnification. a: 1 hour; b: 2 hours; c: 3 hours; d: 4 hours;

monodisperse phase of smaller size. On the other hand, for lower quench rates, the homogenous solution is likely to phase-separate by nucleation and growth. Also, since the solution remains at high temperature for longer time, the phase-separated particles may agglomerate in some areas giving rise to the observed small number of large particles.

The particle size for 20 vol.% CTBNX31 for a particular quench rate is higher than that for 15 vol.% CTBNX31 which in turn is higher for that for 10 vol.% CTBNX31. This is due to a lowering of the cloud point with increased CTBN content (table 2).

Figure 8 represents the cloud point curves for formulations containing 10, 15 and 20-volume % each CTB/CTBN. The plots indicate that an increase in acrylonitrile content reduces the cloud point temperatures for all volume contents. Also, an increase in volume loading for any particular CTB/CTBN reduces the cloud point temperatures. Both these facts can be attributed to the increased content of polar acrylonitrile groups in the system, increasing the compatibility between Epon828 and CTB/CTBN. The anomalous behavior is seen for the 18-mol % acrylonitrile case where the cloud point temperatures are seen to be uncharacteristically higher. This cannot be explained.

Figure 9 shows the particle size plots for different cooling rates (continuous cooling). Plots for 10, 15 and 20-volume % CTBNX31 show that for faster cooling (higher cooling rates), the resulting particle sizes are smaller. This is because for faster cooling, the nucleated particles get very little time for particle growth. Also, for higher volume loadings, the particle size reduces. This is due to the reduced cloud point

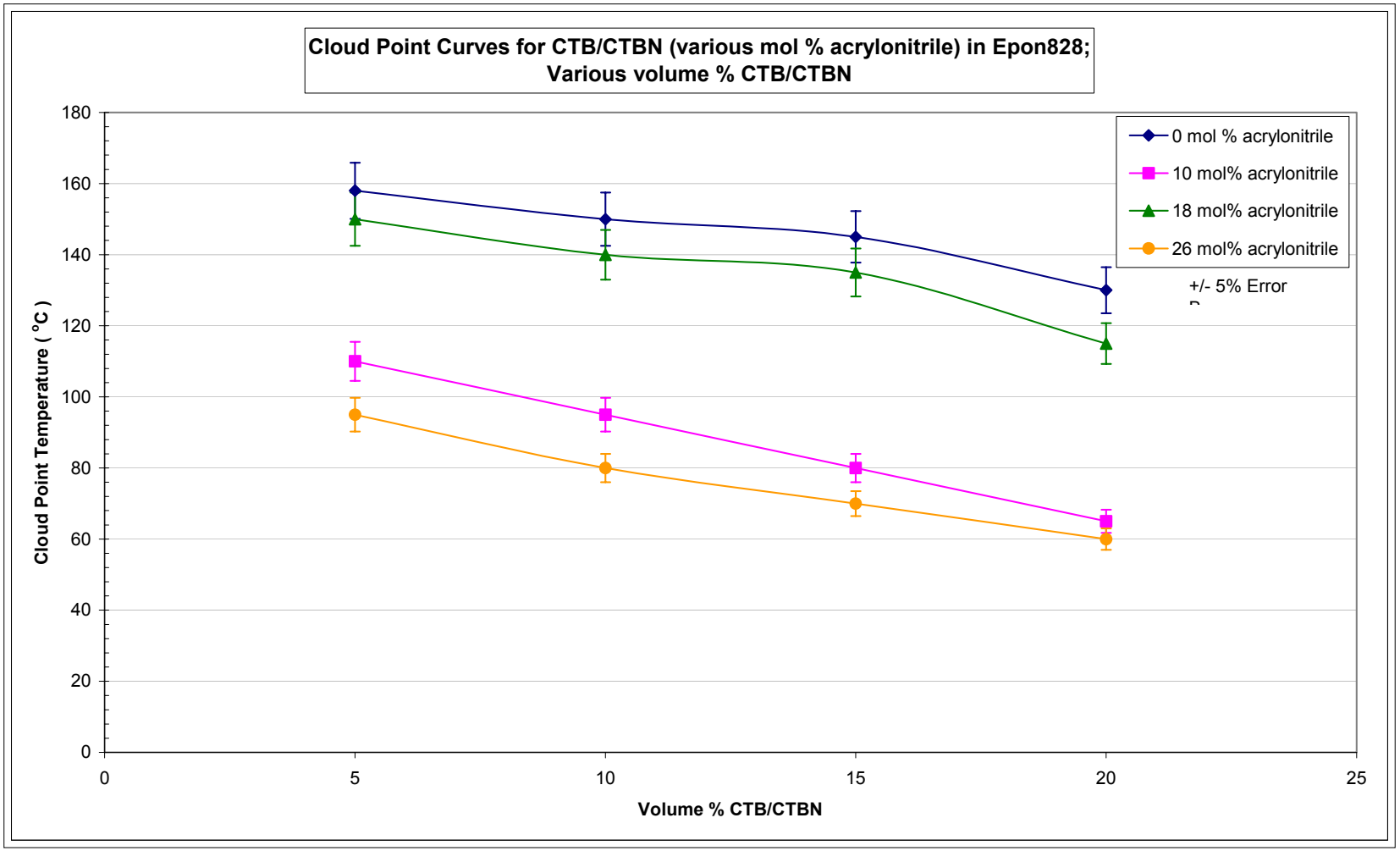

Fig. 8: Cloud Point Curves for CTBN (various mol % acrylonitrile) in Epon828

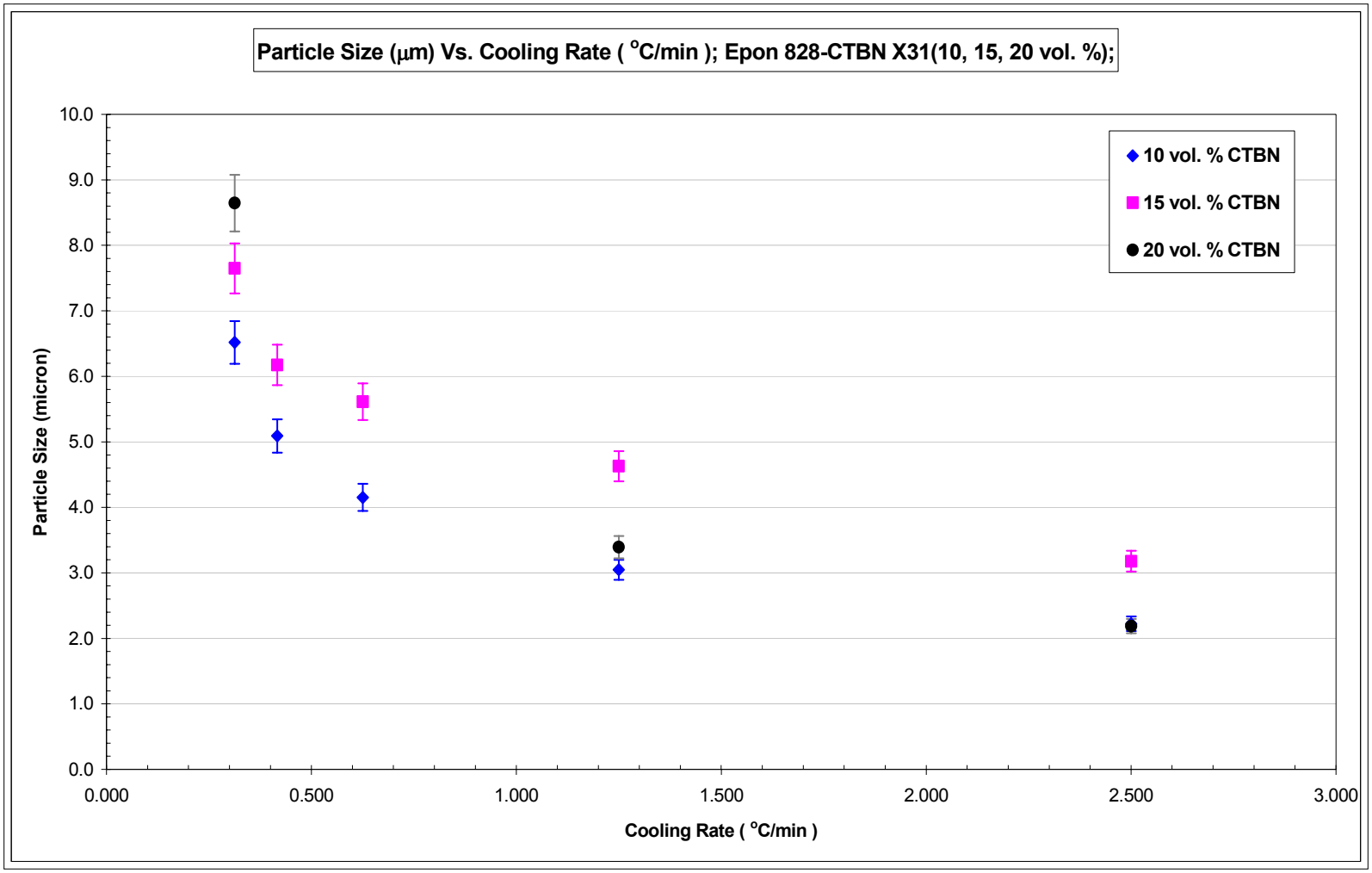

Fig. 9: Particle sizes for samples cooled at various rates; Epon828-CTBN X31 (10, 15 and 20 vol.%). Higher cooling rate results into a finer dispersion of CTBN. Also a higher volume loading results into larger sized particles for same cooling rates.

temperatures as a result of increased net acrylonitrile content in the system. Reduced cloud points give little time for the precipitated particles to grow.

Figure 10 is a plot of particle size against cooling rates for 15-volume % CTBNX31 in Epon828 for formulations with and without the dimethacrylates. It shows that in both cases, the particle size reduces with increasing cooling rates. Also, the particle size for formulations with dimethacrylates is lower. This is due to increased system polarity due to presence of the dimethacrylates, which dissolves more CTBN readily, reducing the cloud point and hence reducing the particle size.

Figure 11 represents the coarsening effect of the already precipitated particles. The precipitated particles of CTBN in the Epon828-5-volume% CTBNX31 grow almost 50% in a week while the particles in 20-volume % CTBN grow in size by over 300% in a week. However, the particles would grow only by about 2% in under an hour, which is the time between the quenching and the curing stages. So long as the quenched systems are cured in less than an hour, the precipitated particles are not likely to grow in size significantly and would not alter the morphology and hence the final mechanical properties of the cured systems.

4.2 Small Angle Laser Light Scattering Analysis (SALS):

SALS patterns for the 10 and 15 volume % CTBN samples, cooled at 5 different cooling rates, are shown in figure 12-13 respectively. The patterns do not seem to indicate a well-defined ring pattern as is observed generally in dispersion systems.

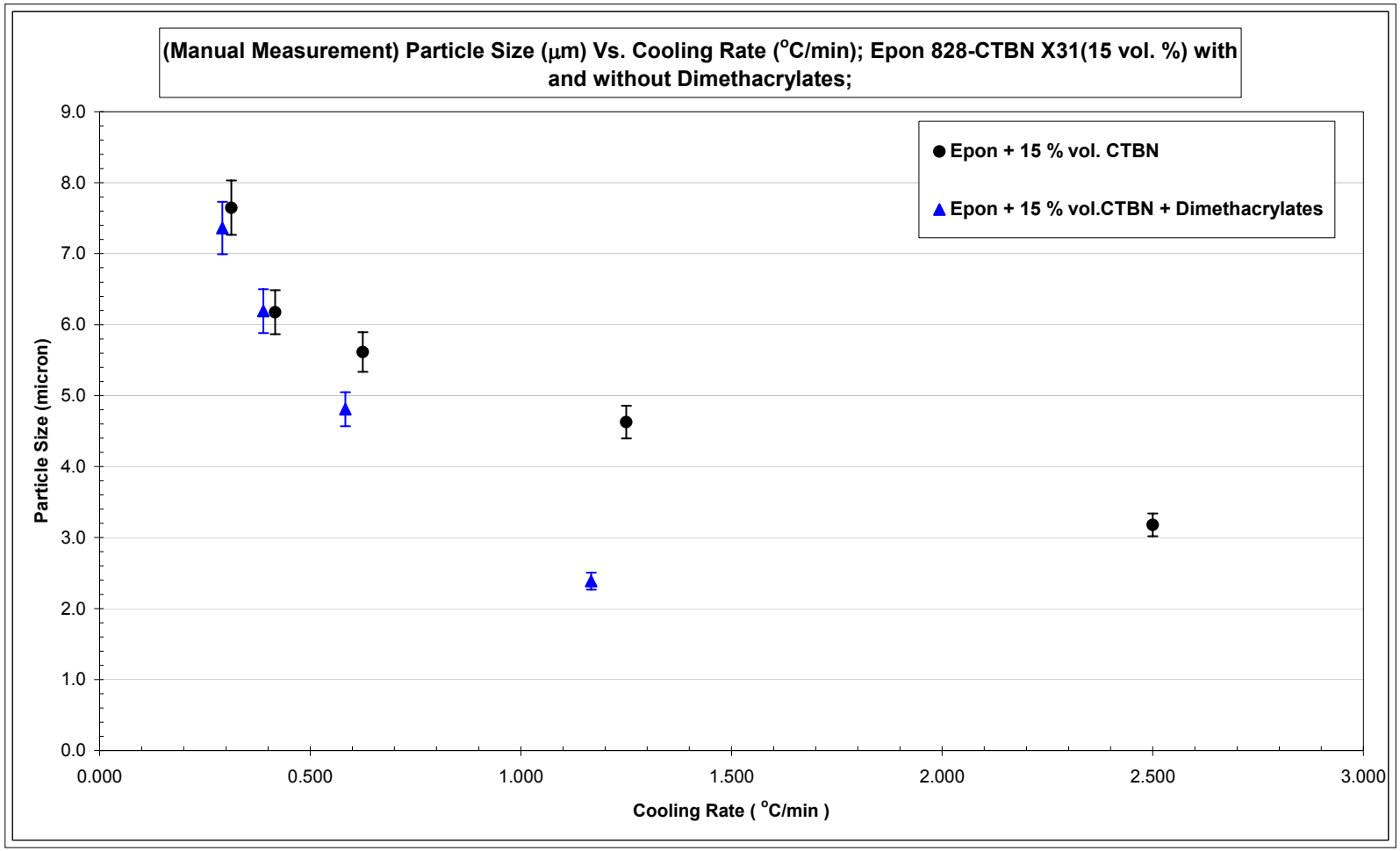

Fig. 10: Particle sizes for samples cooled at various rates; Epon828-CTBN X31 (15 vol.%) for formulations with and without Dimethacrylates. Higher cooling rate results into a finer dispersion of CTBN. Also the presence of Dimethacrylates reduces the particle size for same cooling rates.

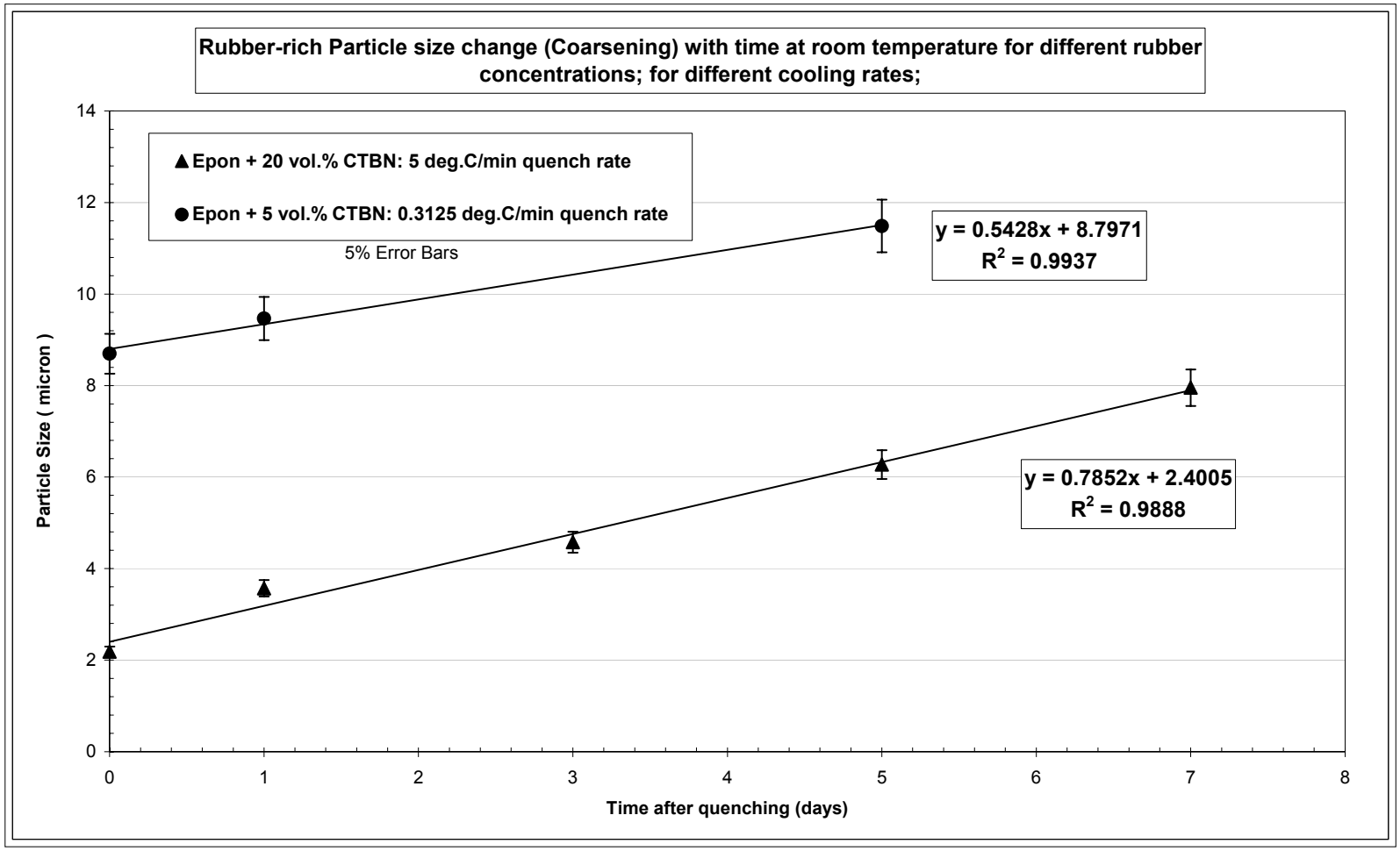

Fig. 11: Particle size change with time due to Ostwald Ripening for samples cooled at various rates; Epon828-CTBN X31. Particles coarsen by about 8% for the sample with 20 vol. % CTBN and 36% for the sample with 5 vol.% CTBN per day.

Figure 14 shows the SALS patterns for samples with dimethacrylates. SALS was carried out with monodisperse polystyrene latexes of well-defined particle sizes, covering a range from 0.5-6 micron. Even then, the SALS patterns did not show ring-like patterns. Various experimental settings were altered to see if a ring pattern was observed. The camera-screen distance, the camera settings, the sample-laser distance, sample-screen distance were readjusted so as to get a ring pattern, but to no avail. So, the best possible settings were chosen to capture images. The captured patterns were converted to Intensity versus q^2 plots, as mentioned in the earlier chapter. Matlab was used to fit sixth order polynomial to the plotted curves. This method was suggested by Effler et al. [42] to be valid for dilute systems, like the Guinier treatment, but is more accurate. Particle size of the dispersed light scattering particles was calculated from the first and zeroth order polynomial coefficients as mentioned earlier. The plots of the calculated particle sizes are plotted against cooling rate for the 10 and 15 volume % CTBN cases (figs. 15,16). These graphs show that the average particle size reduces to almost half the value for the fastest cooling rate employed (2.16 ^{o}C/min) as compared to the slowest cooling rate employed (0.3125 ^{o}C/min). This minimum average particle size is about 2 micron. This particle size is lower than that obtained from OM analysis. This is attributed to the fact that OM has a minimum resolution of 0.5 micron, while SALS is able to account for smaller particles. This accounting of the smaller particles, in addition to the larger particles, reduces the average of particle size, thus giving lower, but more accurate, values for SALS data.

It is worth mentioning here that Guinier's treatment is applicable only for very dilute dispersions with perfectly spherical or well-defined geometries of the dispersed

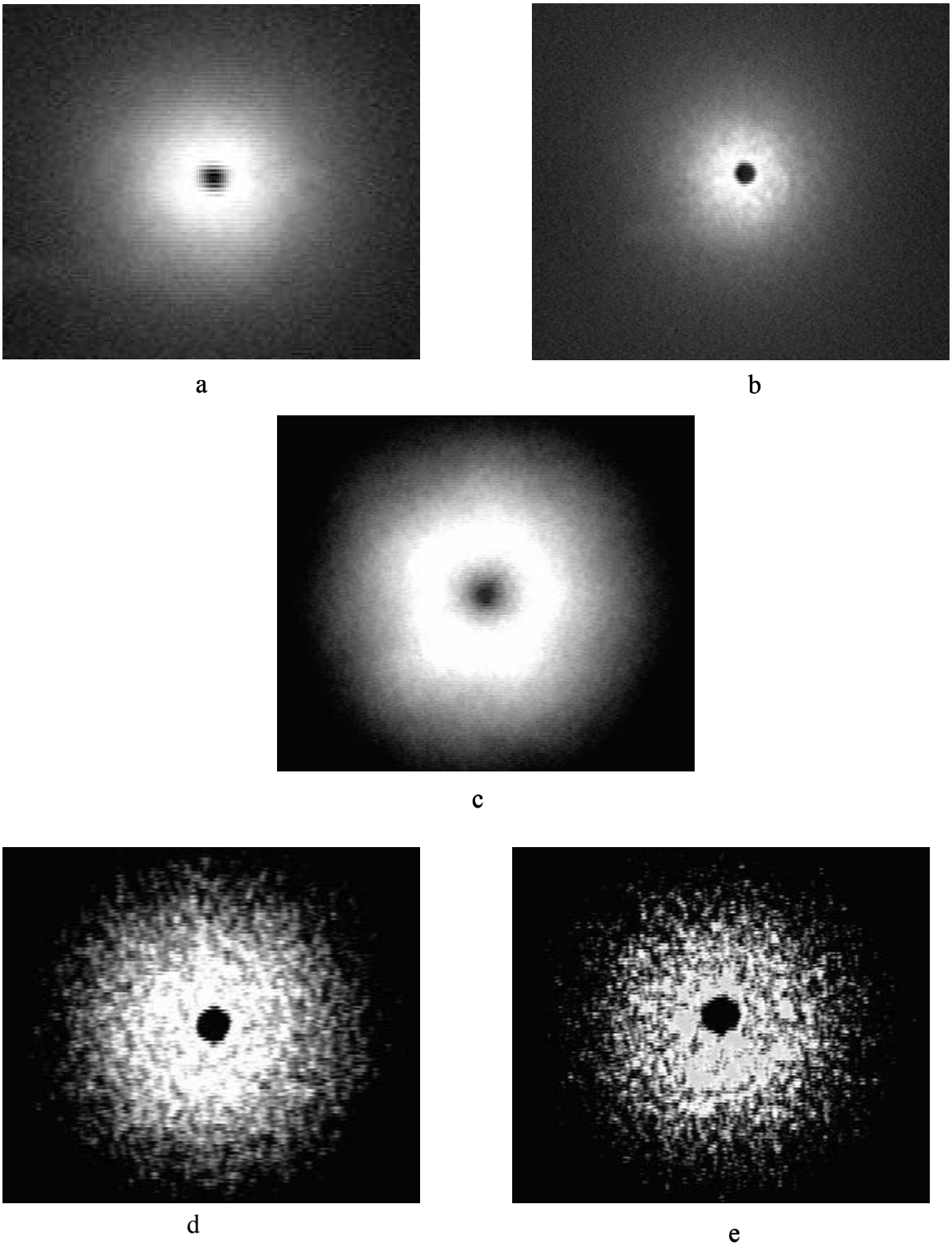

Fig. 12: Small Angle Light Scattering Patterns for Epon 828 / 10 volume % CTBN system. Solutions cooled from 180-30 ^{o}C in a: 1 hr., b: 2 hr., c: 4 hr., d: 6 hr., e: 8 hr.

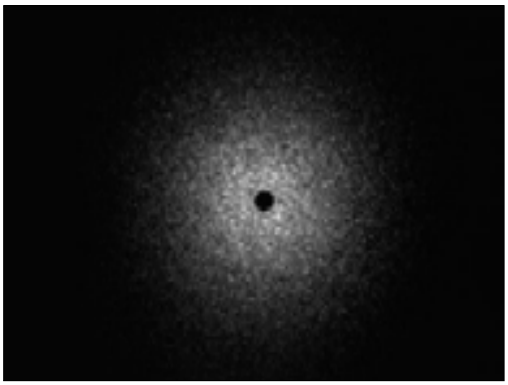

a

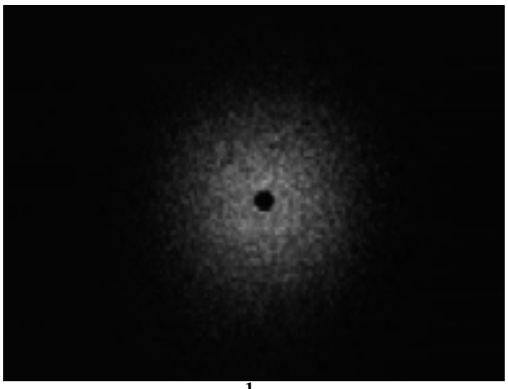

b

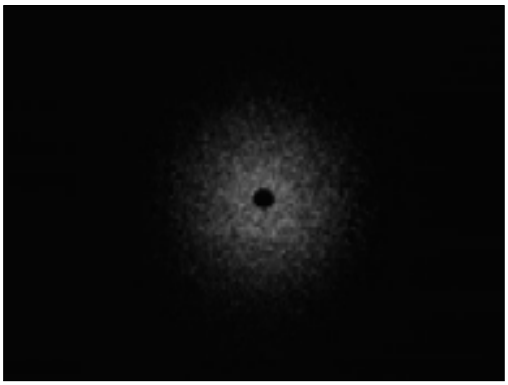

c

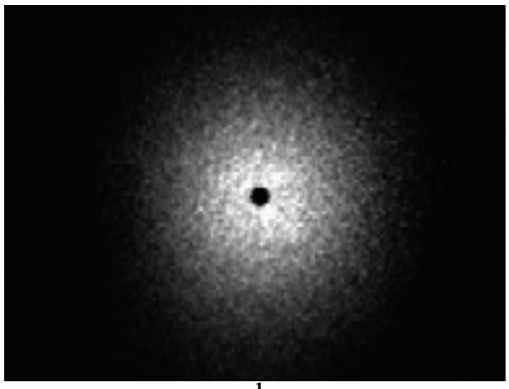

d

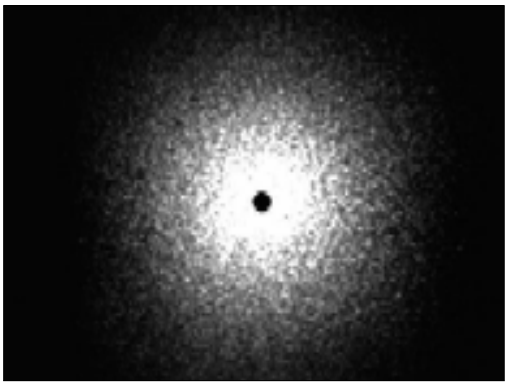

e

Fig. 13: Small Angle Light Scattering Patterns for Epon 828 / 15 volume % CTBN system. Solutions cooled from 180-30 ^{o}C in a: 1 hr., b: 2 hr., c: 4 hr., d: 6 hr., e: 8 hr.

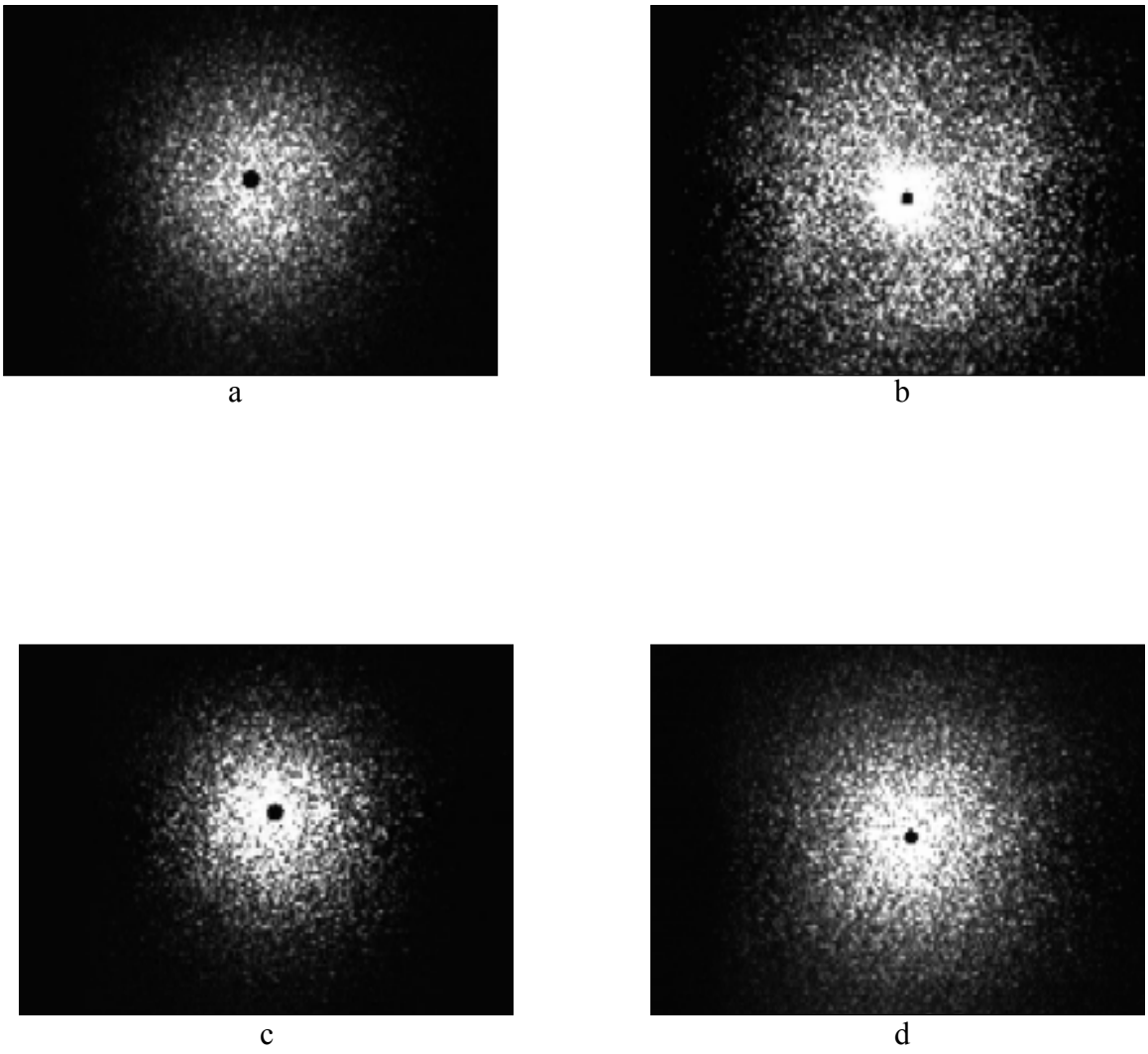

Fig. 14: Small Angle Light Scattering Patterns for Epon 828 / 100 phr Dimethacrylates (δ=0.5) / 15 volume % CTBN system. Solutions cooled from 100-30 ^{o}C in a: 1 hr., b: 2 hr., c: 3 hr., d: 4 hr.

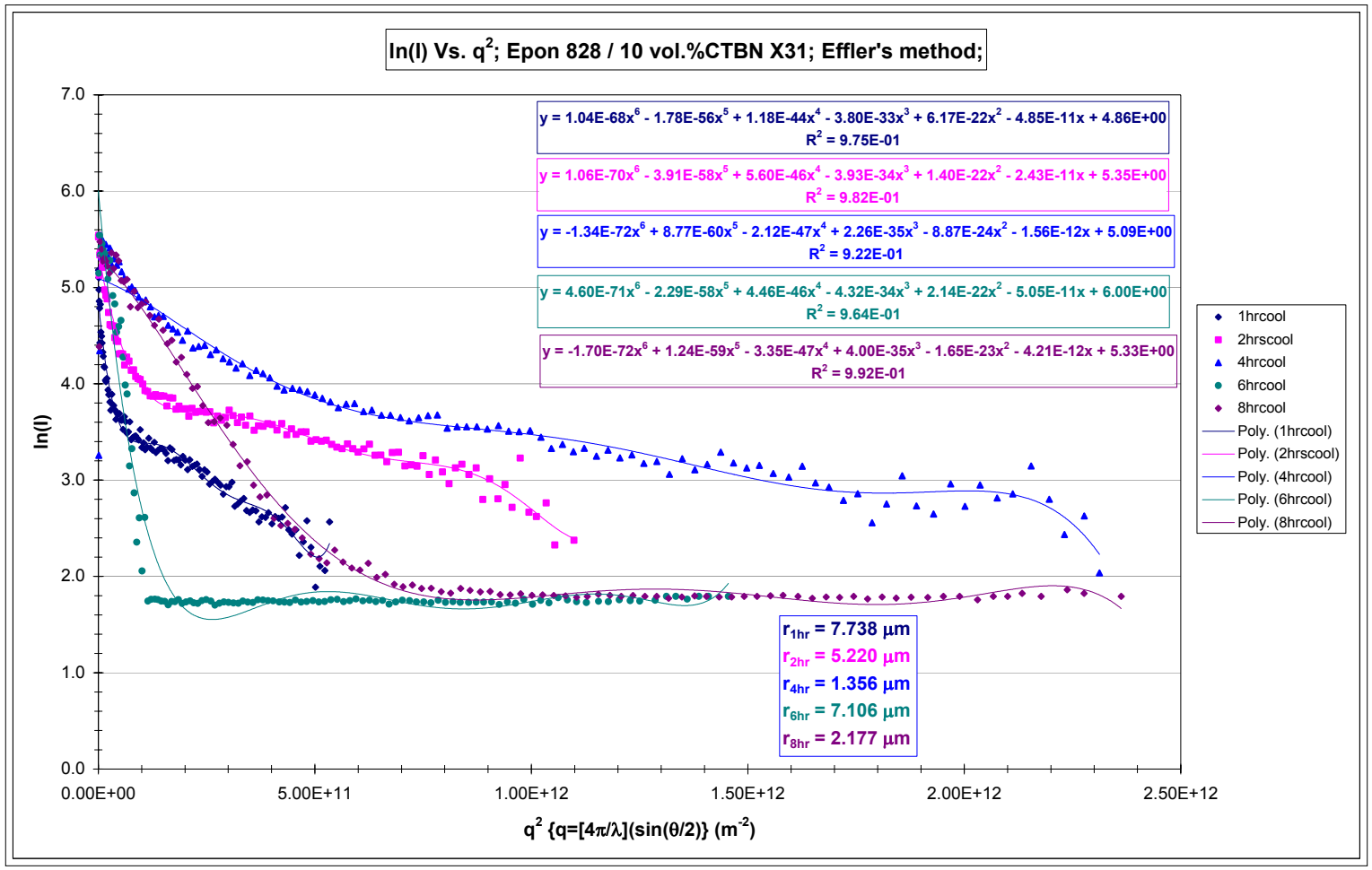

Fig. 15: SALS Data for samples cooled at various rates; Epon828-CTBN X31 (10 vol.%); Effler's method polynomial fits.

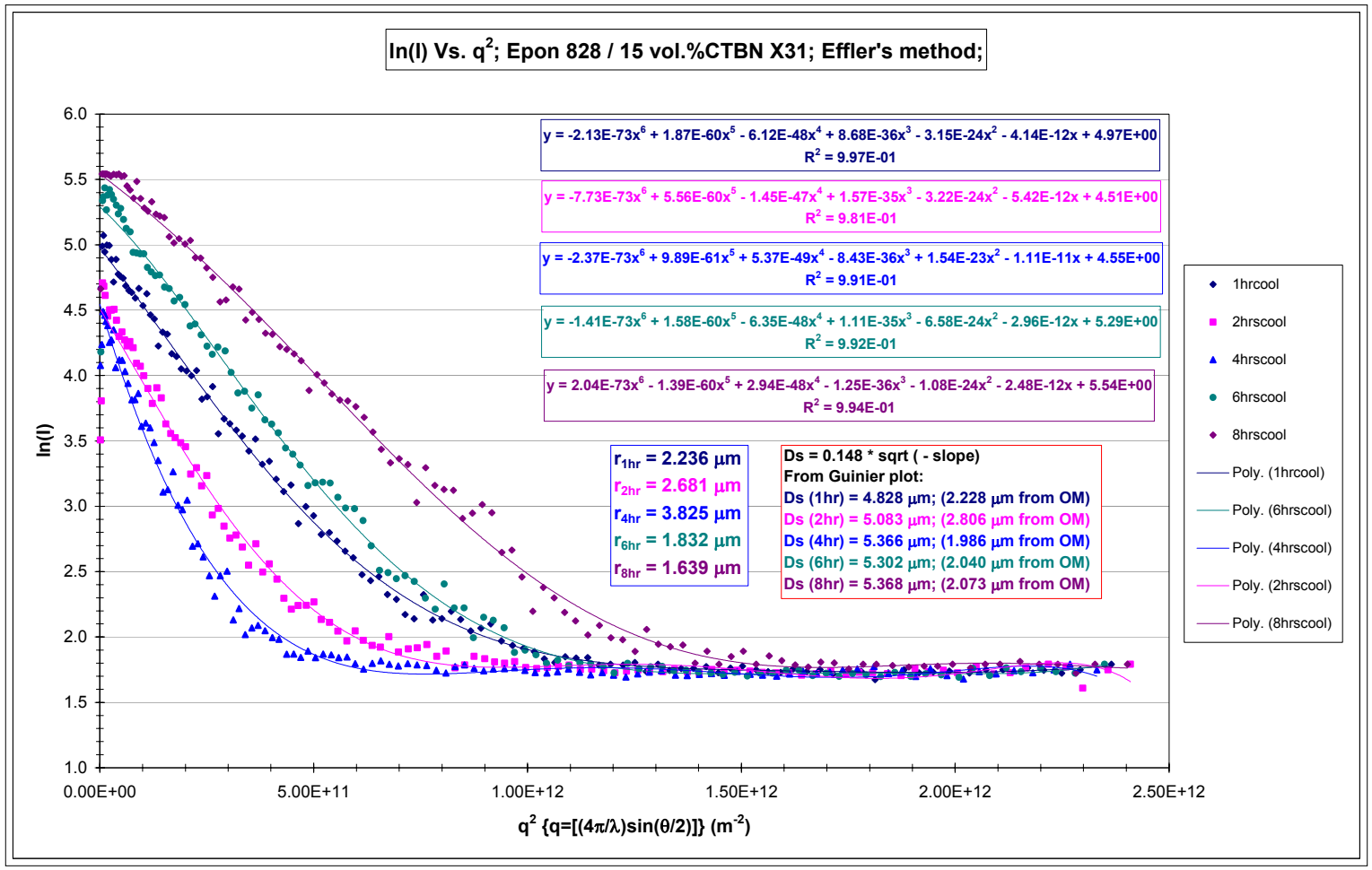

Fig. 16: SALS Data for samples cooled at various rates; Epon828-CTBN X31 (10 vol.%); Effler's method polynomial fits.

dilute dispersions with perfectly spherical or well-defined geometries of the dispersed particles. But it can be used for comparing similar systems differing only in particle sizes. Effler et al's method takes into account the smaller particles that scatter at larger angles, thus giving more accurate results. It is seen that Effler's method is giving lower values than Guinier's results for the above-mentioned reason. Table 3 gives a comparison of particle size calculations using all three methods. Calculations for 10 volume % CTBN samples were not consistent. Also, there is a large scatter in the particle sizes obtained. This is due to the bad polynomial fits obtained with low values of coefficients of determination (R^2 values). On the other hand, 15 volume % CTBN samples gave the most consistent results in both, OM and SALS. This fact is supported by the higher values of

Table 3: Table comparing the various dispersed phase particle sizes for compositions cooled at various rates. Comparison between Effler et al's method and Guinier treatment to results of Optical Microscopy. Epon828 / CTBN X31 (15 volume %).

Cooling Rate (^{o}C/min) (180 – 30^{o}C)	**Particle Size (micron)**		
	Guinier Treatment	**Effler et al.'s Treatment**	**Optical Microscopy**
0.312	5.368	1.639	7.648
0.416	5.302	1.832	6.175
0.625	5.366	3.825	5.614
1.250	5.083	2.681	4.628
2.500	4.828	2.236	3.179

coefficients of determination (R^2). Hence the 15 volume-% CTBN X31 samples were finally chosen for studying the other properties throughout.

4.3 Fourier Transform- Infrared Spectroscopy (FT-IR):

In order to understand the chemistry of possible reactions occurring in the formulations, the system was analyzed for possible reactive sites or functional groups. They were arranged in order of their priority for chemical reactions under the presence of the initiating UV radiation and the photoinitiator. The functional groups present are the epoxide ring (Epon828), the unsaturated >C=C< as chain ends (bisGMA), the main chain –CH=CH- of the butadiene section of CTBNX31 and the –COOH (CTBN) and –OH (bisGMA) (See figure 3).

Epon828 consists of the epoxide ring, which has one oxygen atom and two hydrogen atoms at the vertices of a triangle. Consideration of bond lengths leaves the included angle at the oxygen atom far less than the usual 108^o. This leaves the two –OC bonds (forming the included angle at –O-) very strained and susceptible for chemical attack. As such, the epoxide ring is the most reactive and is likely to react first.

The next possible reactive site is the >C=C< of bisGMA. This group is likely to react prior to that of CTBN because it is an end group in case of bisGMA. The unsaturation in CTBN is in the main chain. Also, the lower molecular weight of bisGMA (molecular weight = 552 g/mol) makes this group more mobile and reactive as compared to that in high molecular weight CTBN (molecular weight = 3800 g/mol) (From manufacturers data) main chain.

The next possible reactive group is the –CH=CH- of the CTBN main chain. This group is likely to undergo attack and subsequent crosslinking due to the generation of free radicals during the dissociation of the photoinitiator (See mechanism of dissociation in chapter 2).

FT-IR results are shown in the graph of normalized intensity versus wavenumber in figure 17. Table 4 shows the reactive bonds and functional groups and their corresponding characteristic IR absorption frequency range (in terms of wave number). A qualitative change in these intensities is also given for a basic understanding of the reactions. Results are compared for samples cured with only UV curing and UV and thermal curing to those of uncured samples.

Figure 18 indicates the reduction in peak intensity at 916 cm^{-1} of the absorptions for the epoxide ring stretching. A reduction in the normalized peak intensity at these two peak numbers (862 and 916 cm^{-1}) indicates a reduction of the concentration of the epoxide groups. This indicates that the epoxy groups are reacting as a result of the photoinitiator and the presence of UV and thermal energy. But the presence of some unreacted epoxide groups gives rise to the small peak at these locations on the plot. For the sample cured thermally in addition to UV curing, there are no visible peaks at these locations, indicating that additional thermal curing cures the unreacted epoxide groups completely.

Figure 19 show a peak at 1300 cm^{-1} representing the –CH=CH- stretching of the butadiene segment in CTBN. A very small decrease in the peak height may be indicating

Table 4: Important vibration bands, the functional groups and the qualitative changes in the intensities:

Bond/Vibration Type	Chemical Bond	Chemical Compound	Wave Number Range (cm^{-1})	Intensity Change
1] Single Bond				
a.	-O- (ether)	Epoxy & bisGMA	1060-1150	Moderate
b.	-OH (Hydroxyl)	BisGMA	1310-1410 1150	Reduces for q100
c.	-Δ (epoxide)	Epoxy	916 830	Reduces for q100 Reduces for q100
2] Double Bond				
a.	>C=CH_2	BisGMA & HDDMA	1620-1680	No change
b.	-COOH (>C=O stretching)	CTBN end group	1690-1730	
c.	-CH=CH-	CTBN diene group	1310	Reduces for q100

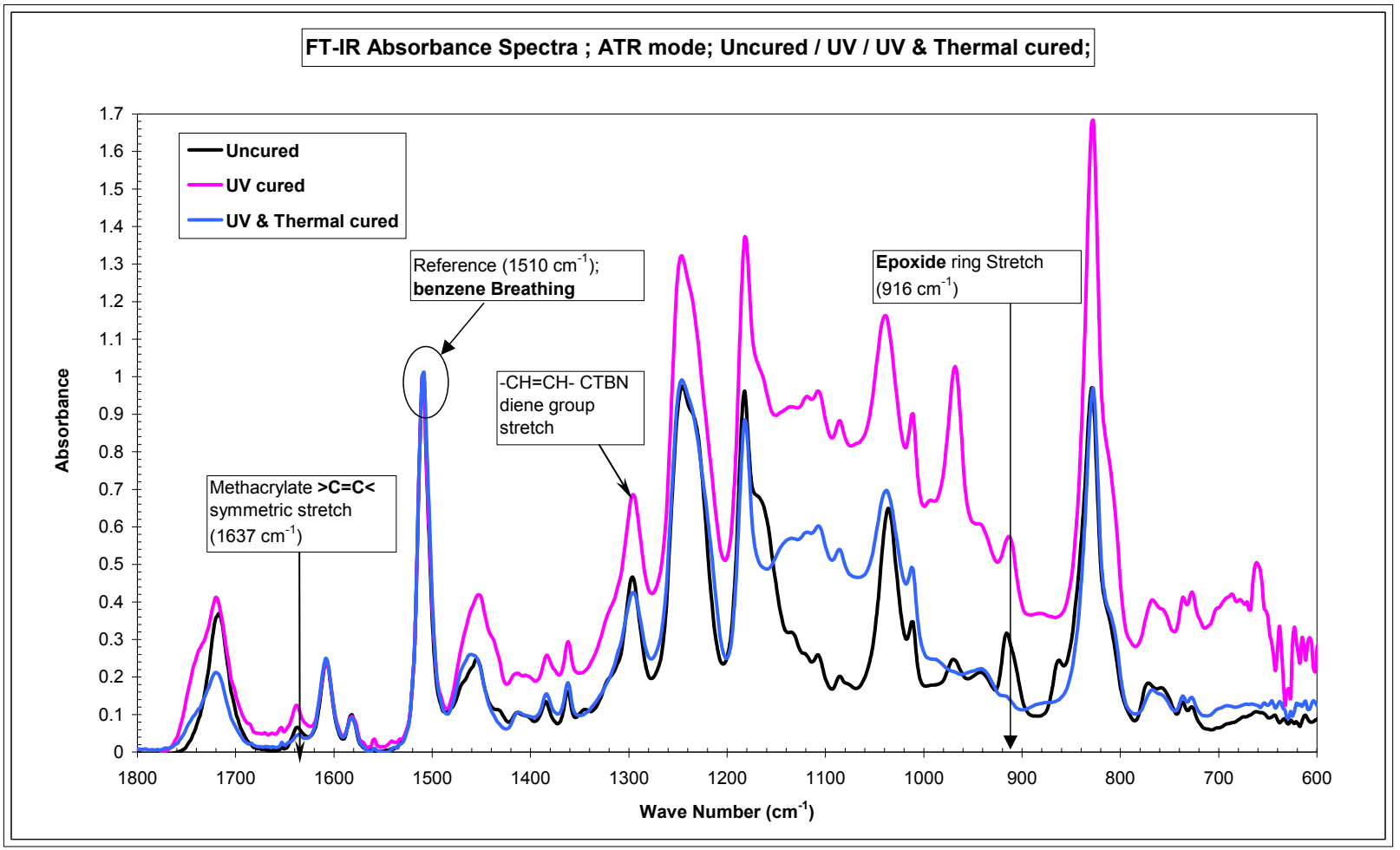

Fig. 17: FT-IR Data for samples with and without thermal curing (compared to the spectra for uncured formulation); Epon828-CTBN X31 (15 vol.%)- Dimethacrylates (100 phr; δ=0.5). The epoxide content reduces as seen from disappearance of the peak at 916 cm^{-1}. Also, the dimethacrylate C=C content reduces as seen from the reduction of the peak heights at 1637 cm^{-1}.

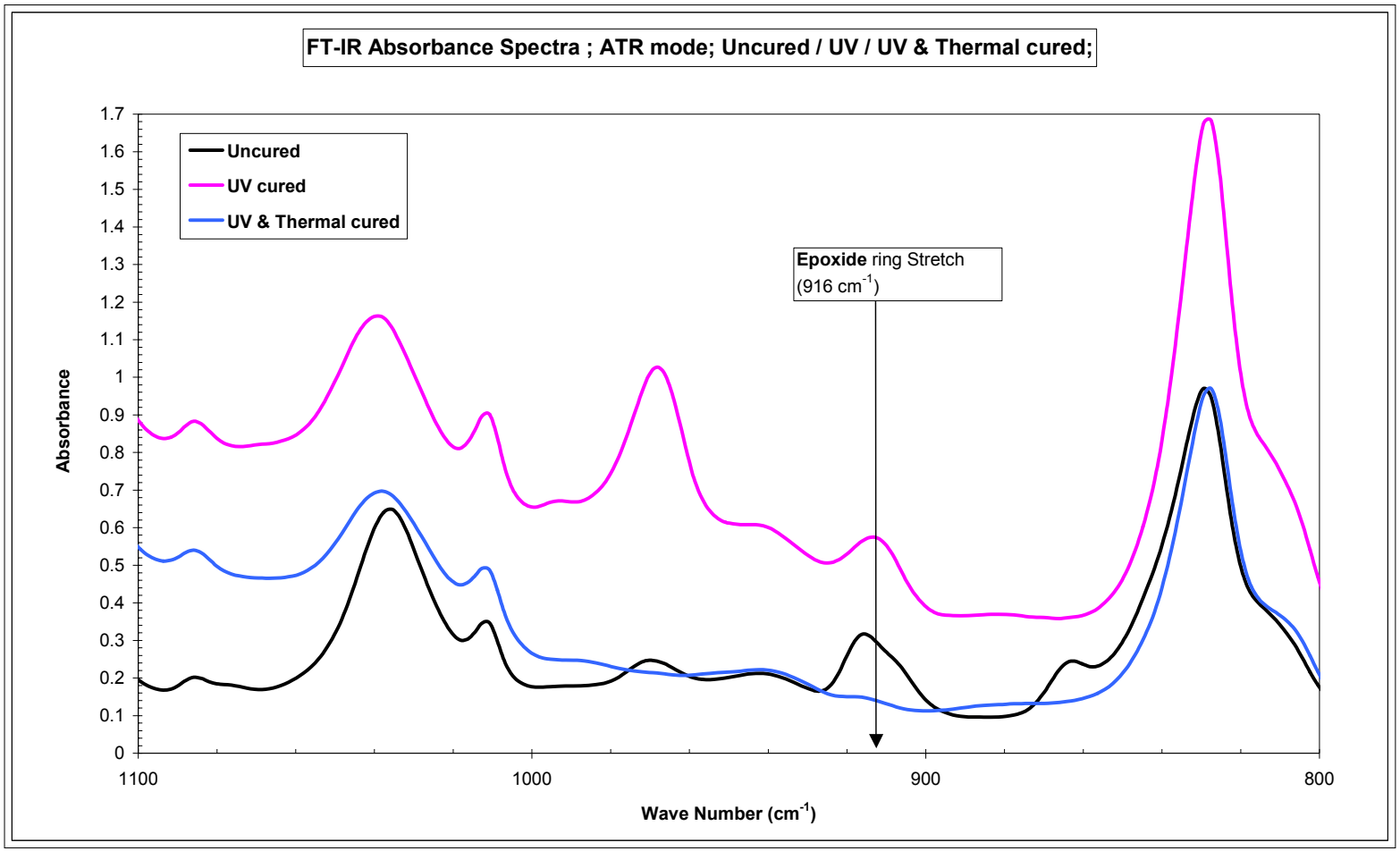

Fig. 18: FT-IR Data for samples with and without thermal curing (compared to the spectra for uncured formulation); Epon828-CTBN X31 (15 vol.%)- Dimethacrylates (100 phr; δ=0.5). The epoxide content reduces as seen from disappearance of the peak at 916 cm^{-1}. Also, the dimethacrylate C=C content reduces as seen from the reduction of the peak heights at 1637 cm^{-1}.

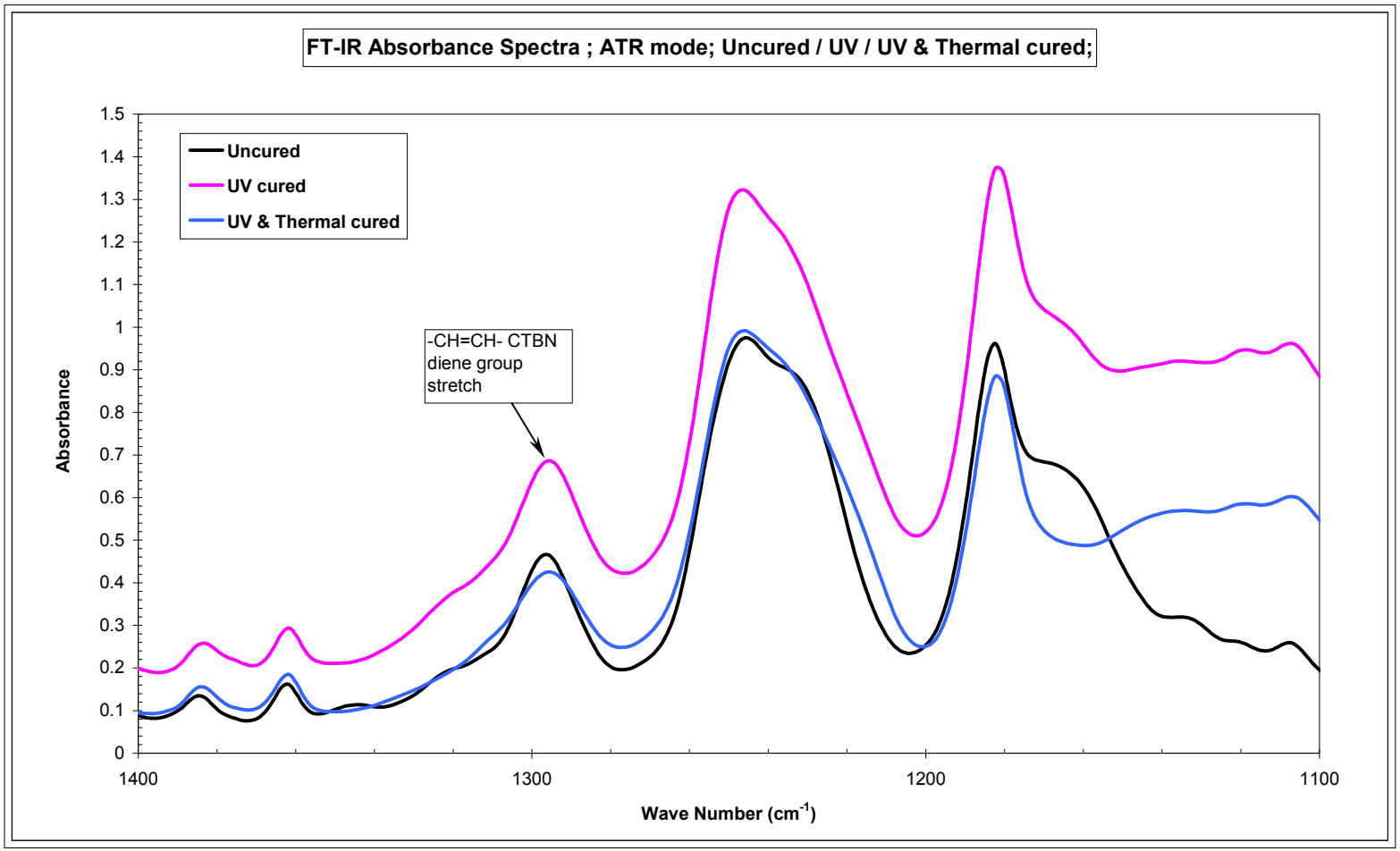

Fig. 19: FT-IR Data for samples with and without thermal curing (compared to the spectra for uncured formulation); Epon828-CTBN X31 (15 vol.%)- Dimethacrylates (100 phr; δ=0.5). The epoxide content reduces as seen from disappearance of the peak at 916 cm^{-1}. Also, the dimethacrylate C=C content reduces as seen from the reduction of the peak heights at 1637 cm^{-1}.

a small portion of the main chain double bonds getting cross linked by the free radicals generated. The possible mechanism is explained in the next section. Figure 20 showing the peak at 1637 cm-1 indicates the presence of double bonds in the HDDMA and bisGMA. A reduction in the normalized peak heights indicates that the double bonds of the HDDMA and bisGMA are reacting. This may be due to the presence of free radicals generated during the photoinitiator dissociation under UV light. This is likely to lead the simultaneous formation of the dimethacrylate network along with the growing epoxide network.

Hydroxyl groups absorb in the range 3400-3800 cm^{-1}. The absorption peak is as shown in figure 21. However, many impurities, including moisture, may contribute to this peak and may vary its intensity widely. Hence, this peak is not considered for further analysis.

From figures 17-21, it is seen that the epoxide concentration reduced after UV radiation and thermal curing. Also, the CTBN –CH=CH- concentration reduces by a very small amount. The concentration of >C=C< of bisGMA reduces upon UV curing and thermal curing step.

In order to check for the chemical nature of the samples quenched at different rates (quench depths), additional FTIR was done as shown in figs. 22-26. These spectra only prove that the samples quenched at different rates had got cured to varying extents. The concentration of epoxy groups (916 cm-1) is seen to be the least for the q100 sample (figure 23). The varying degrees of cure for the samples may be attributed to sample thickness variations. The q100 samples were half as thick as the other samples. The UV

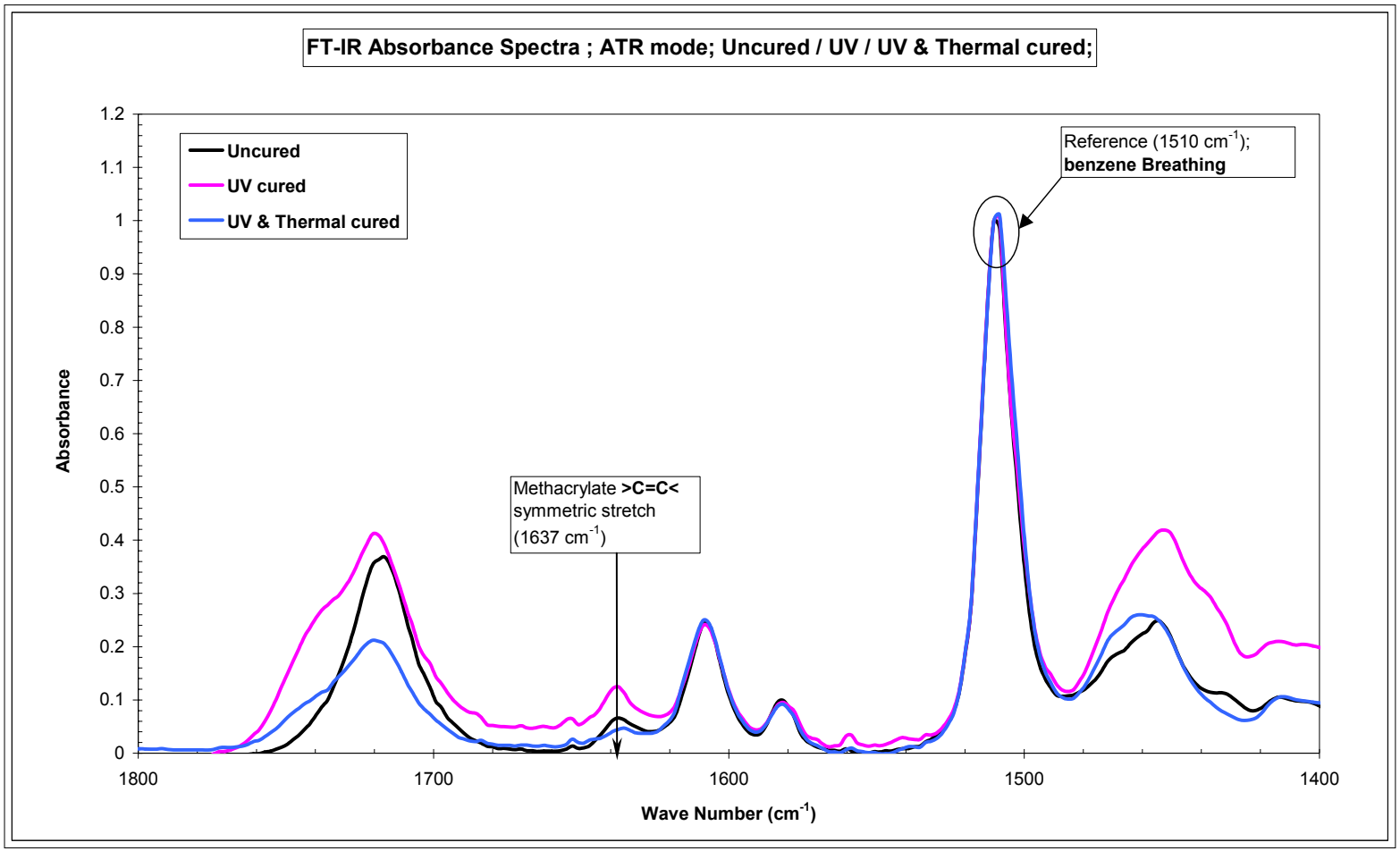

Fig. 20: FT-IR Data for samples with and without thermal curing (compared to the spectra for uncured formulation); Epon828-CTBN X31 (15 vol.%)- Dimethacrylates (100 phr; δ=0.5). The epoxide content reduces as seen from disappearance of the peak at 916 cm^{-1}. Also, the dimethacrylate C=C content reduces as seen from the reduction of the peak heights at 1637 cm^{-1}.

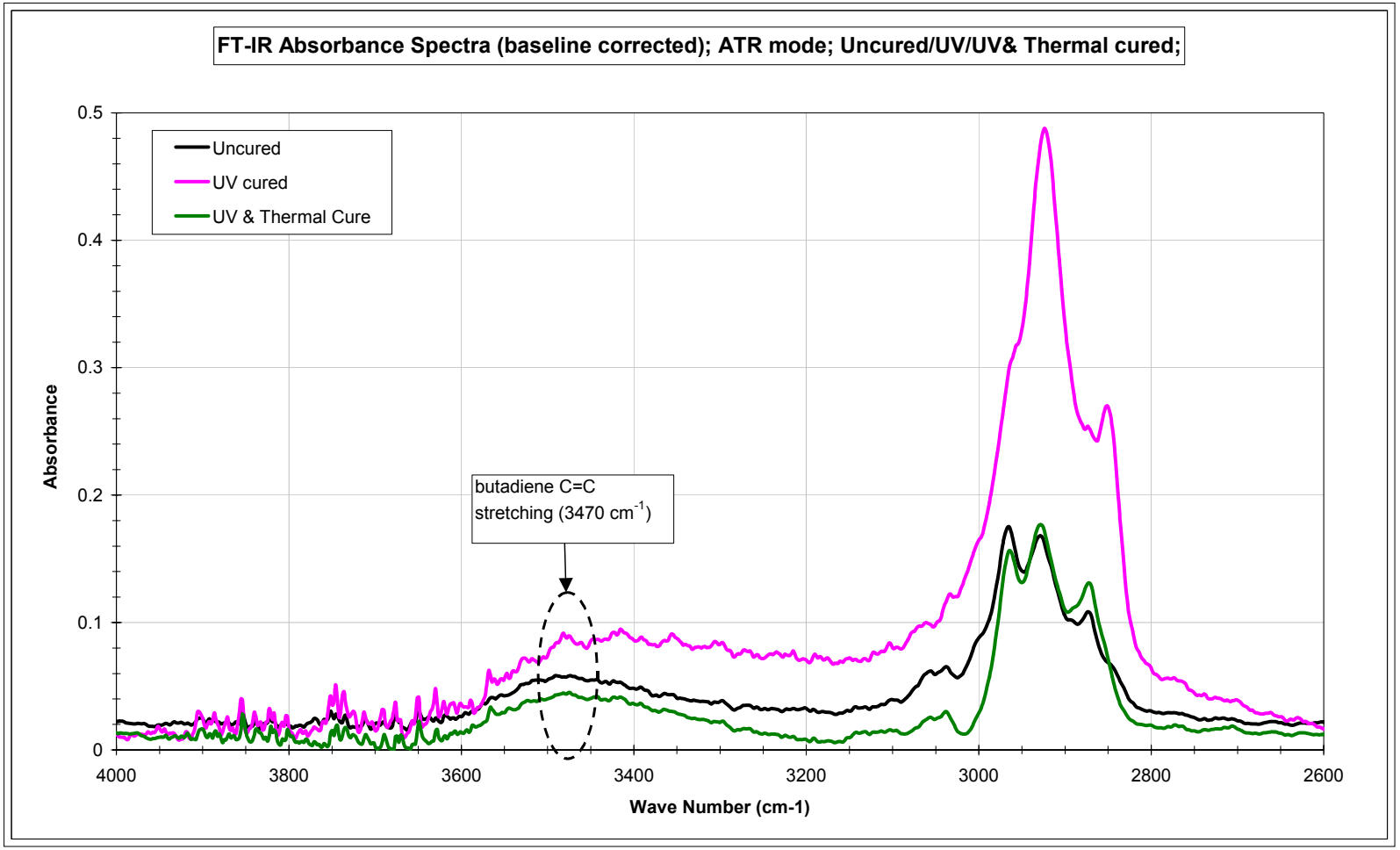

Fig. 21: FT-IR Data for samples with and without thermal curing (compared to the spectra for uncured formulation); Epon828-CTBN X31 (15 vol.%)- Dimethacrylates (100 phr; δ=0.5). The butadiene C=C content reduces slightly as seen from the reduction in peak height of the broad peak at 3470 cm^{-1}.

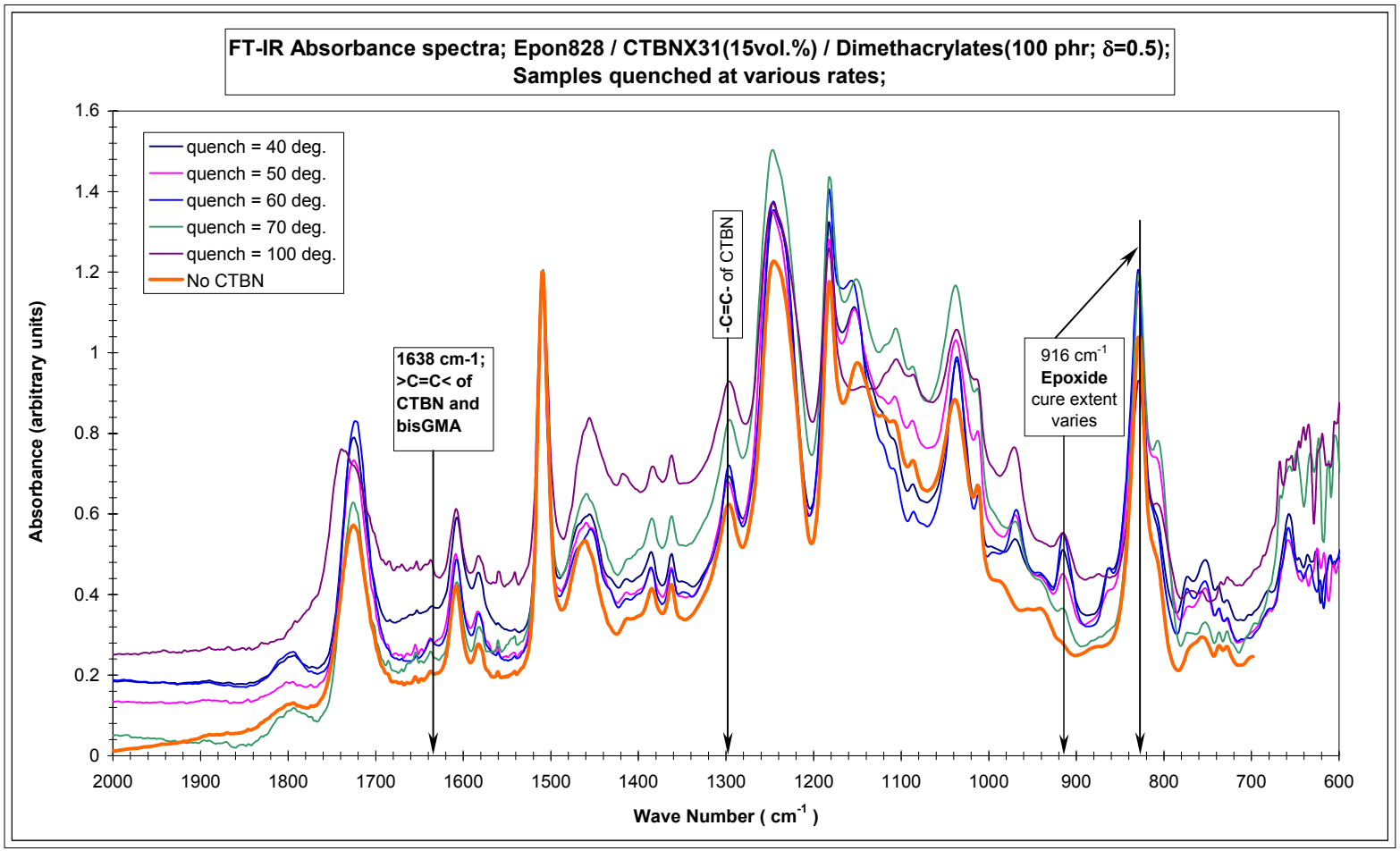

Fig. 22: FT-IR Data for samples with different quench depths; Epon828-CTBN X31 (15 vol.%)- Dimethacrylates (100 phr; δ=0.5).

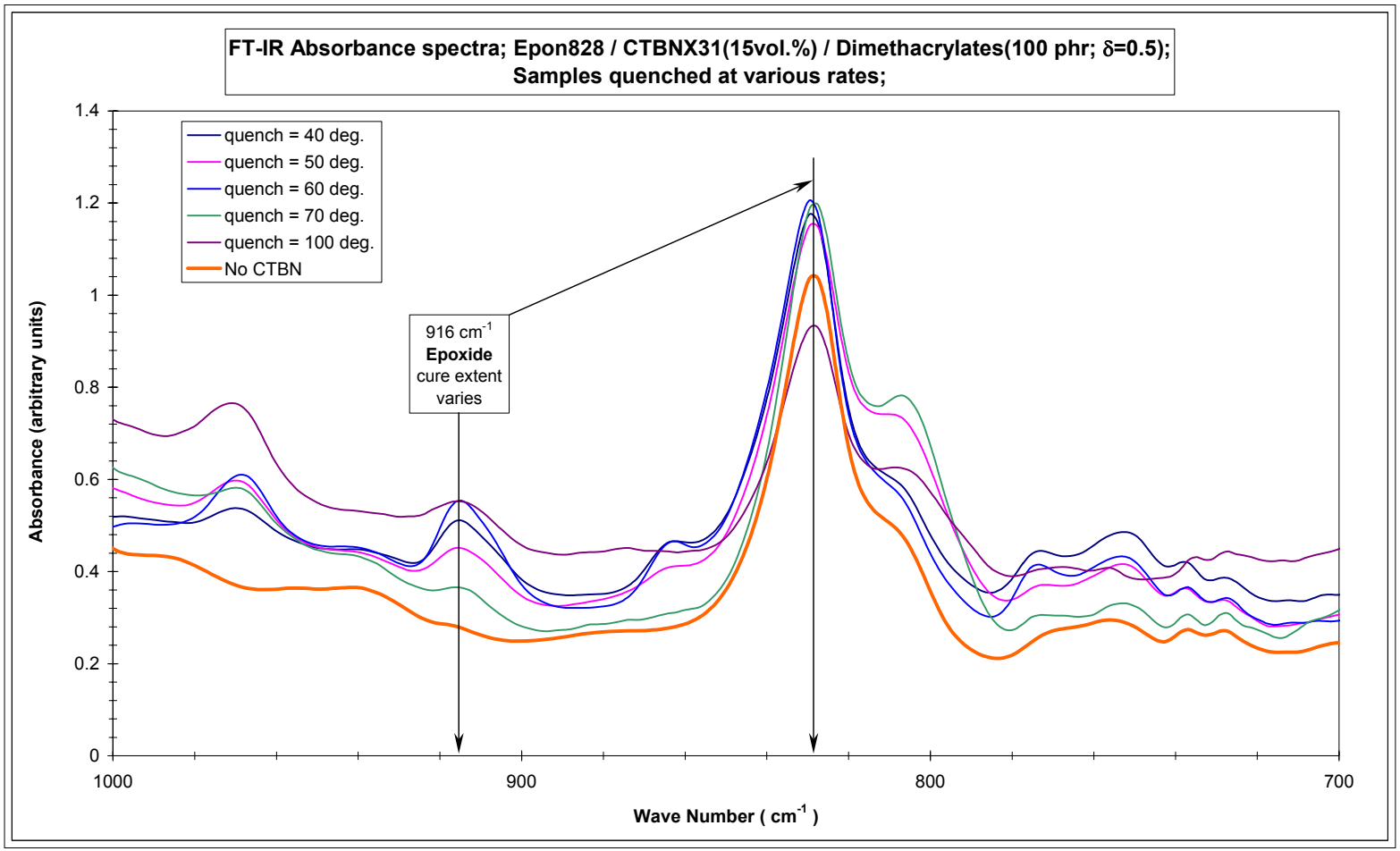

Fig. 23: FT-IR Data for samples with different quench depths; Epon828-CTBN X31 (15 vol.%)- Dimethacrylates (100 phr; δ=0.5).

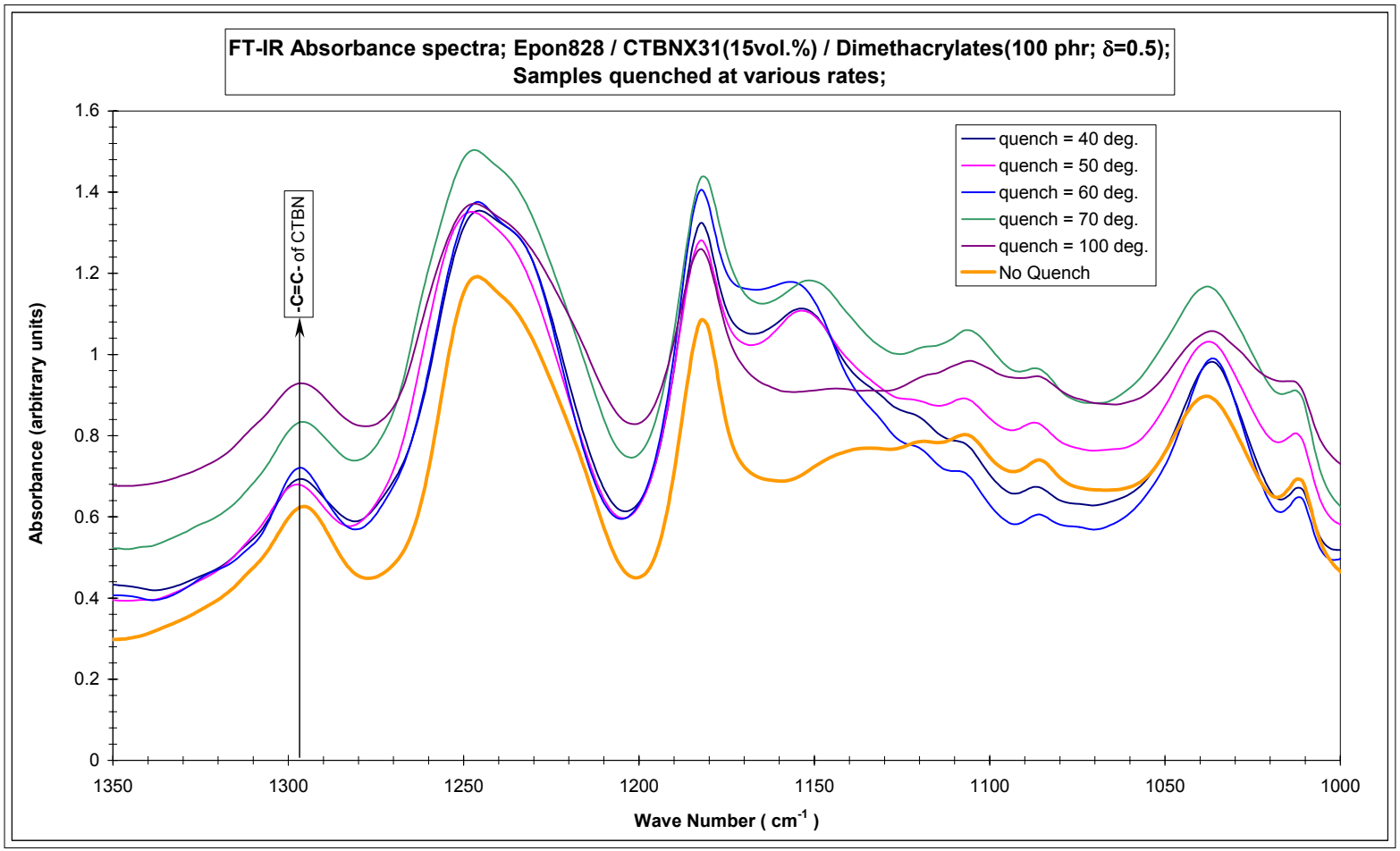

Fig. 24: FT-IR Data for samples with different quench depths; Epon828-CTBN X31 (15 vol.%)- Dimethacrylates (100 phr; δ=0.5).

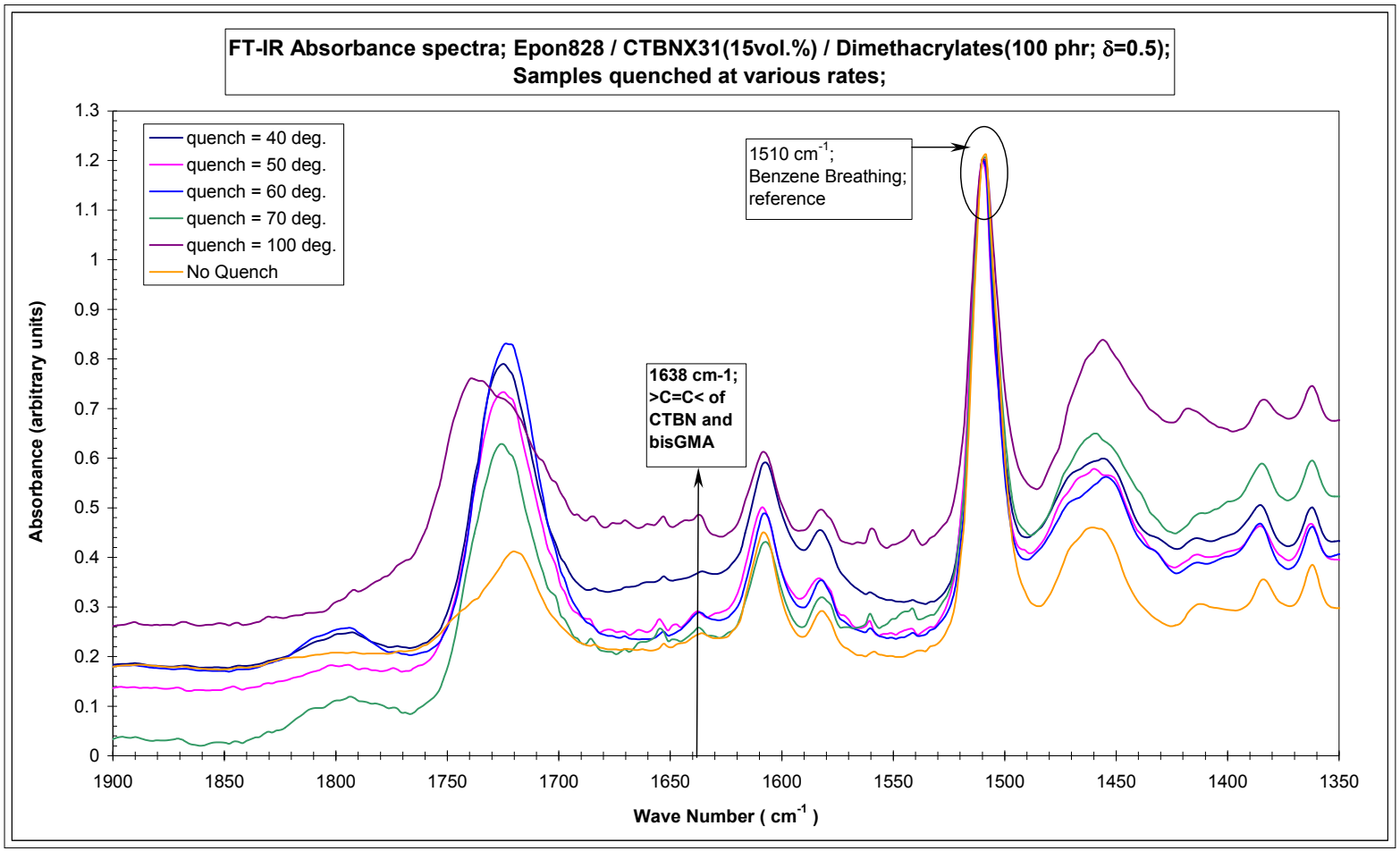

Fig. 25: FT-IR Data for samples with different quench depths; Epon828-CTBN X31 (15 vol.%)- Dimethacrylates (100 phr; δ=0.5).

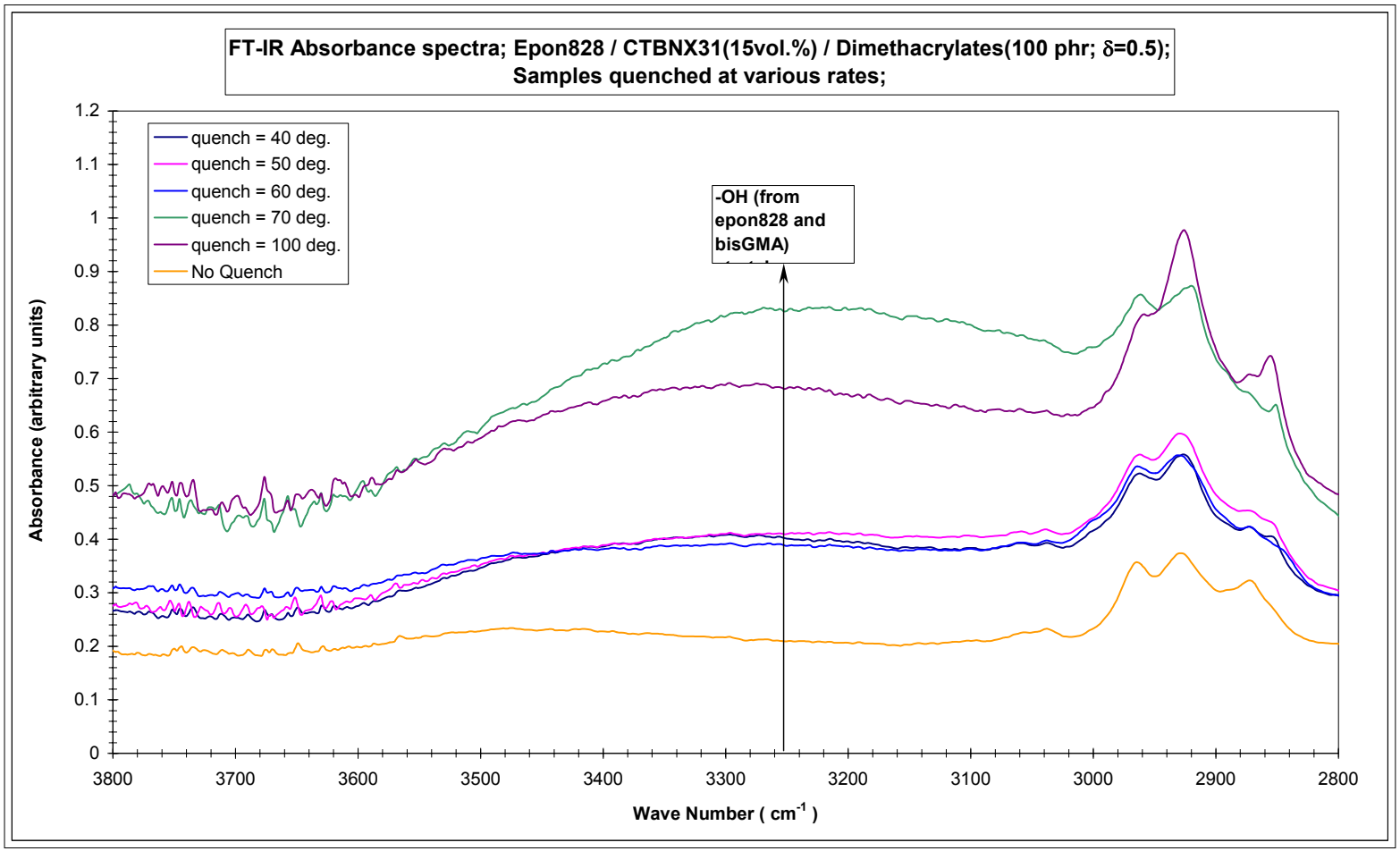

Fig. 26 FT-IR Data for samples with different quench depths; Epon828-CTBN X31 (15 vol.%)- Dimethacrylates (100 phr; δ=0.5).

radiation may have penetrated more deeply in the thin q100 samples than other samples, increasing the extent of initiation of the cure reaction.

4.4 Dynamic Mechanical Analysis (DMA):

The main purpose of DMA testing was to compare the mechanical properties of the samples quenched at various rates to that of samples without any CTBN. DMA results for samples for different amounts of quenches are shown in the form of tan δ curves for the various specimens. The sample designation is as given below in Table5.

Peak at @-50^{o}C:

CTBN loss peak is seen in all the cases at around –50 ^{o}C except for the pure epoxy (no CTBN) specimen and q100 (See figure 27). The absence of this peak in the q100 sample indicates that the CTBN present is still mostly trapped in the Epon828-dimethacrylate IPN matrix. The presence of low Tg CTBNX31 in the Epon828-dimethacrylates matrix phase is responsible for the reduction of the Tg of epoxy at +140^{o}C. The reduced Tg of epoxy is seen to be about +120^{o}C. Complementary to this, the Tg of the CTBNX31 is expected to increase correspondingly, if it is present as a single phase with the epon-dimethacrylates matrix phase. These Tg values are taken as the temperatures at the tan δ peaks (figure 27). As seen, the Tg of CTBNX31 is shifted up to –23^{o}C from –67^{o}C (Manufacturers MSDS) due to the dissolution effect.

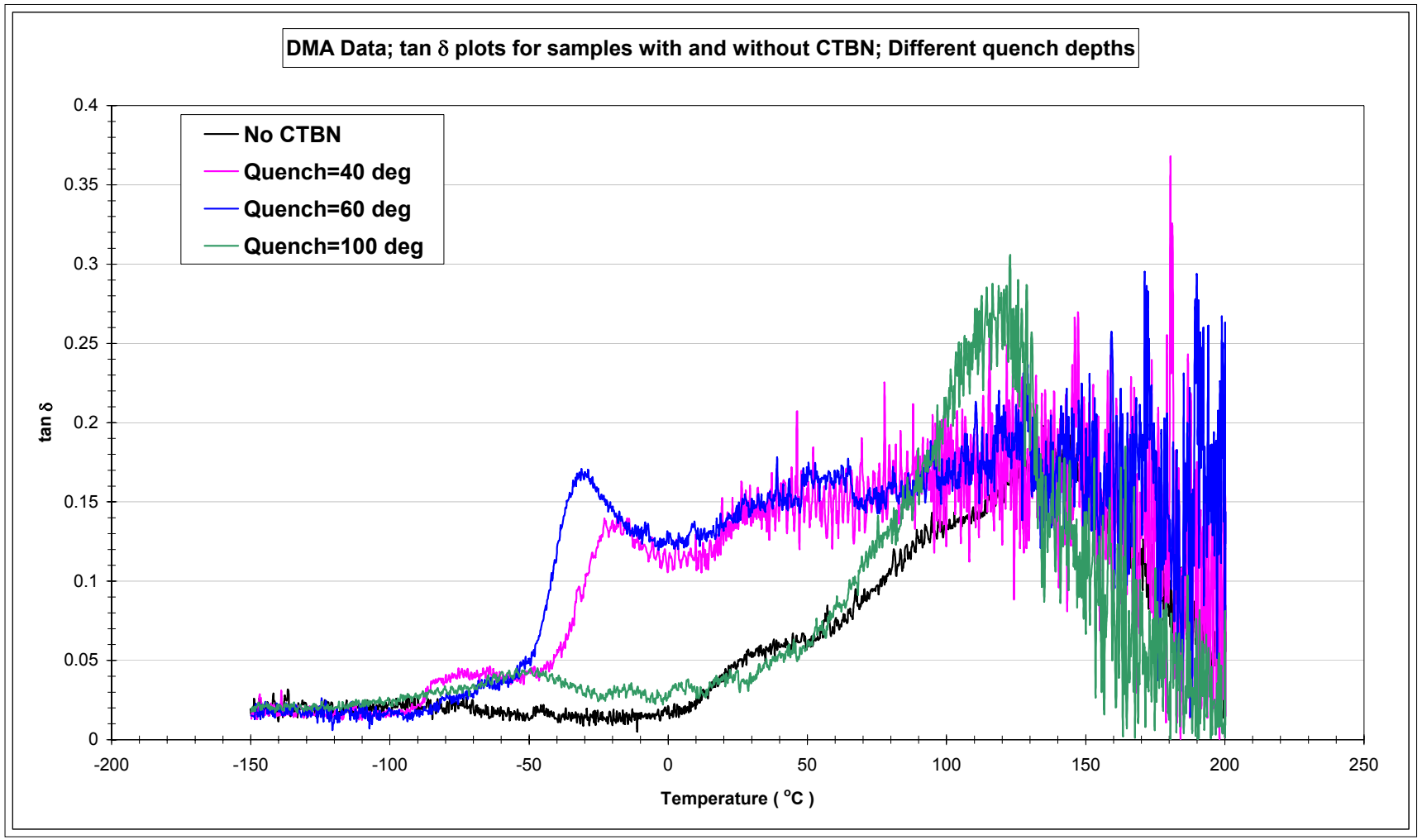

Fig. 27: Tan δ curves from DMA experiments for samples cooled at various rates; Epon828-CTBN X31 (15 vol.%)- Dimethacrylates (100 phr; δ=0.5).

Table 5: Table showing the degree of quench and corresponding sample designation used for the DMA test results.

Degree of Quench (^{o}C)	Sample Designation	Figure
Pure Epoxy-Dimethacrylates	edm	19 (No CTBN)
40	q40	19 (Quench=40 deg)
60	q60	19 (Quench=60 deg)
100	q100	19 (Quench=100 deg)

This means that for the q100 sample, most of the CTBN is trapped in the hard, cured epon828-dimethacrylates matrix IPN.

The q60 and q40 show similar tan δ peaks while q100 shows a quite different tan δ curve than q40 and q60 samples. This indicates that the q60 and the q40 samples have similar amounts of free CTBN (lowest modulus), followed by the q40 sample having intermediate CTBN level with higher modulus at 25^{o}C. The q100 sample has the lowest amount of free CTBN giving the highest modulus value at 25^{o}C. This also indicates that the thermal quenching step is reducing the amount of free CTBN, which is uncross-linked. Incidentally, the modulus of q100 sample at 25^{o}C is higher than that of the Epon828-dimethacrylates cured structure (no CTBN). Also, the presence of dissolved CTBN in the other samples in the IPN matrix phase is reducing the modulus from q60 to the q40 sample. But the observed higher modulus for the q100 sample may be attributed to the dissolved CTBN getting crosslinked to a higher extent.

Peak at +90°C:

The Dimethacrylates have a Tg close to +98 °C when cured. A tan δ peak at +90 °C in all the formulations is expected. However, since it is believed that the Dimethacrylates, owing to their structural similarity, are miscible with the Epon828 resin, forming an interpenetrating network (IPN) after curing, with the Epon828 matrix. Hence, due to the molecular level of mixing between the Dimethacrylates and Epon828, a single broad tan δ peak is to be expected. This is true as seen from the broad peak from +60 to about +140°C in all cases.

For the edm sample, a small shoulder is seen at about +90°C, which is that of the dimethacrylates [43]. All the other samples show a broad peak in this range, which makes it difficult to see the peak corresponding to Tg of the dimethacrylates. The storage modulus data is used to gain further insight into these details.

Peak at +120°C:

All the tested samples show a peak in the range +120 to +140°C. This peak is believed to be corresponding to the Tg of cured Epon828. Edm sample shows a broad peak at about +140°C. The broadness of this peak is attributed to the presence of a low Tg dimethacrylates (Tg of bisGMA is +68°C) forming an IPN with the Epon828 matrix. Since the mixing is on molecular level, there is only one observed Tg. However, the broadness of the peak indicates a spectrum of molecular motions. Some unreacted or uncrosslinked dimethacrylates or the epoxy could give rise to chains of varying molecular

weights. Samples q60 and q40 samples also have broad peaks at about +130^{o}C. These three samples had almost twice the thickness as the q100 sample. It is possible that the incident UV beam might not have penetrated through the thickness of the q60, q40 and the edm samples, resulting into incomplete curing particularly in the central portions. The q100 sample being relatively thin might be completely cured, resulting into molecular segments of the same order in molecular weight. Another thing that might be simultaneously causing the narrowing of the peak is that the dimethacrylates, either bisGMA or HDDMA or both, might be phase separating out of the generating matrix during curing [43]. This may be the reason the sample q100 shows a narrower peak in the DMA experiment. Interestingly, the peak for sample q100 is at around +120^{o}C. This shift in peak is a result of a higher content of the dissolved CTBN in the matrix phase. This shift in Tg due to presence or absence of CTBN in the matrix phase also explains the broadening of the epoxy Tg peak at 140^{o}C for the epoxy-dimethacrylates system (no CTBN), indicating a homogeneous single Epon828-dimethacrylates phase in this sample.

Figure 28 gives the corresponding storage modulus versus the temperature data. For the edm sample, modulus hardly decreases till about 50^{o}C. There is seen to be a gradual decrease in modulus by an order of magnitude from +50 to +150^{o}C. It is believed that the epon 828 and dimethacrylates form an IPN, leading to a uniform response to applied load in DMA testing. The samples q40 and q60 behave similarly with gradual decrease in modulus from +50 to +150^{o}C. However, the presence of distinct regions of decrease in modulus at the corresponding Tgs of the components seems to indicate that there is phase-separated morphology present in the sample. The presence of a gradual

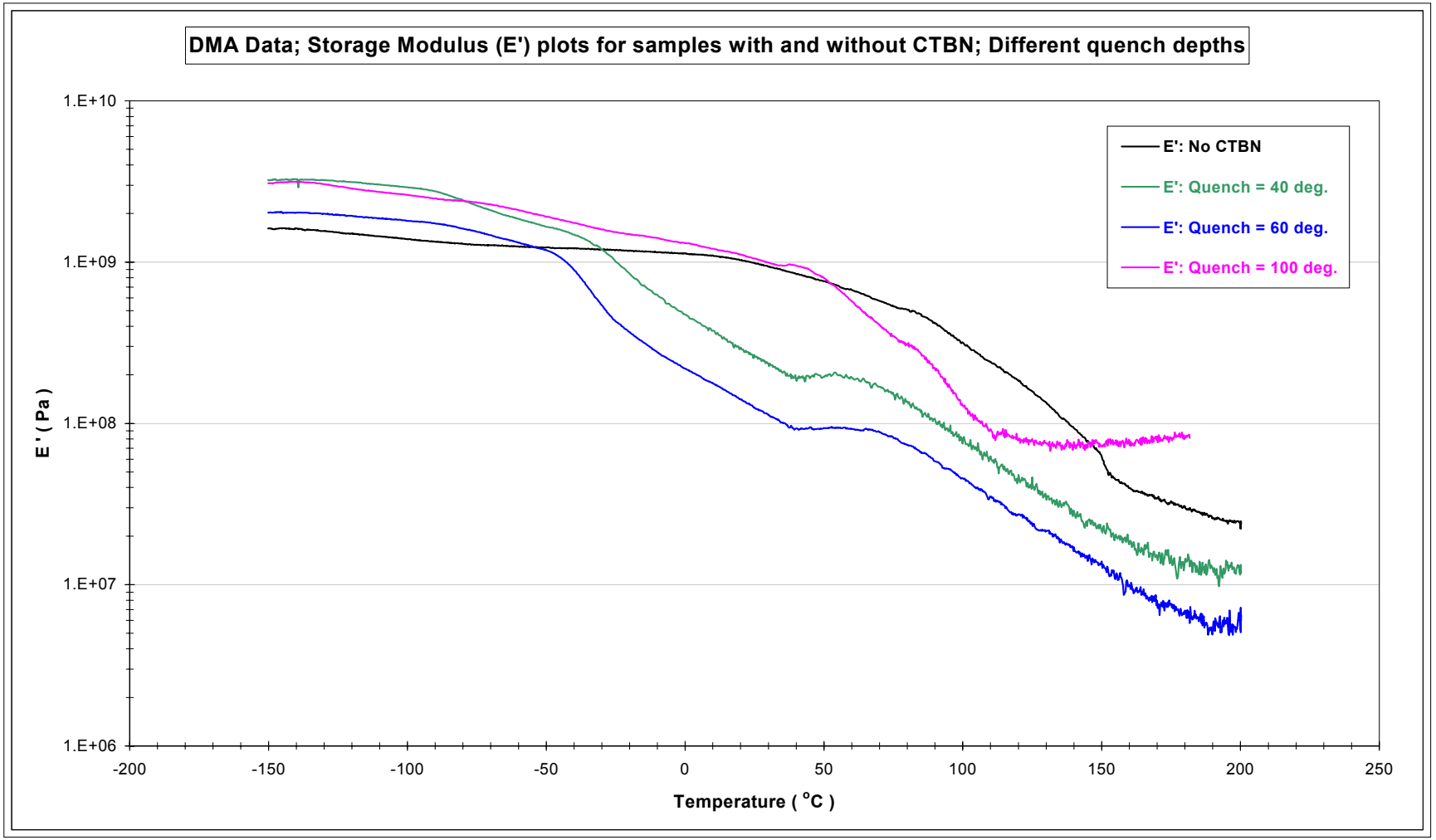

Fig. 28: Storage Modulus (E') curves from DMA experiments for samples cooled at various rates; Epon828-CTBN X31 (15 vol.%)-Dimethacrylates (100 phr; δ=0.5). The curves show the differing behavior of the q100 sample.

smooth decrease in modulus in case of sample q100 indicates an absence or very little presence of phase separated CTBN particles, as is consistent with the tan δ analysis above.

Figure 29 and figure 30 represent the storage modulus values for the three samples q40, q60 and q100 at the temperatures of –100^{o}C (below the Tg of CTBNX31) and +25^{o}C (Room temperature at which the material is going to be used). In both cases, the modulus decreases from q40 to q60. This is to be expected since more CTBNX31 is remaining back in the matrix phase, making the matrix more compliant, thus reducing the modulus. But the q100 sample has an unexpected higher values of moduli at both these temperatures. This is unexpected since the q100 sample also has the highest content of dissolved CTBNX31 in the matrix phase. This may be attributed to a higher degree of crosslinking of the butadiene links in the CTBNX31 in the matrix phase. Also, the dimethacrylates phase may be phase separating out due to rapid quenching and may be swelling the dispersed CTBNX31 particles. This dimethacrylate in the particulate phase may be crosslinking upon UV radiation, leading to hard CTBNX31 rich particles dispersed in the matrix.

4.5 Impact Testing Analysis (IT):

The main purpose of the work is to develop toughened epoxy systems having good impact toughness. As discussed previously, a finer dispersion of elastomer-rich phase in the cured morphologies result into higher toughness. In order to correlate the cured

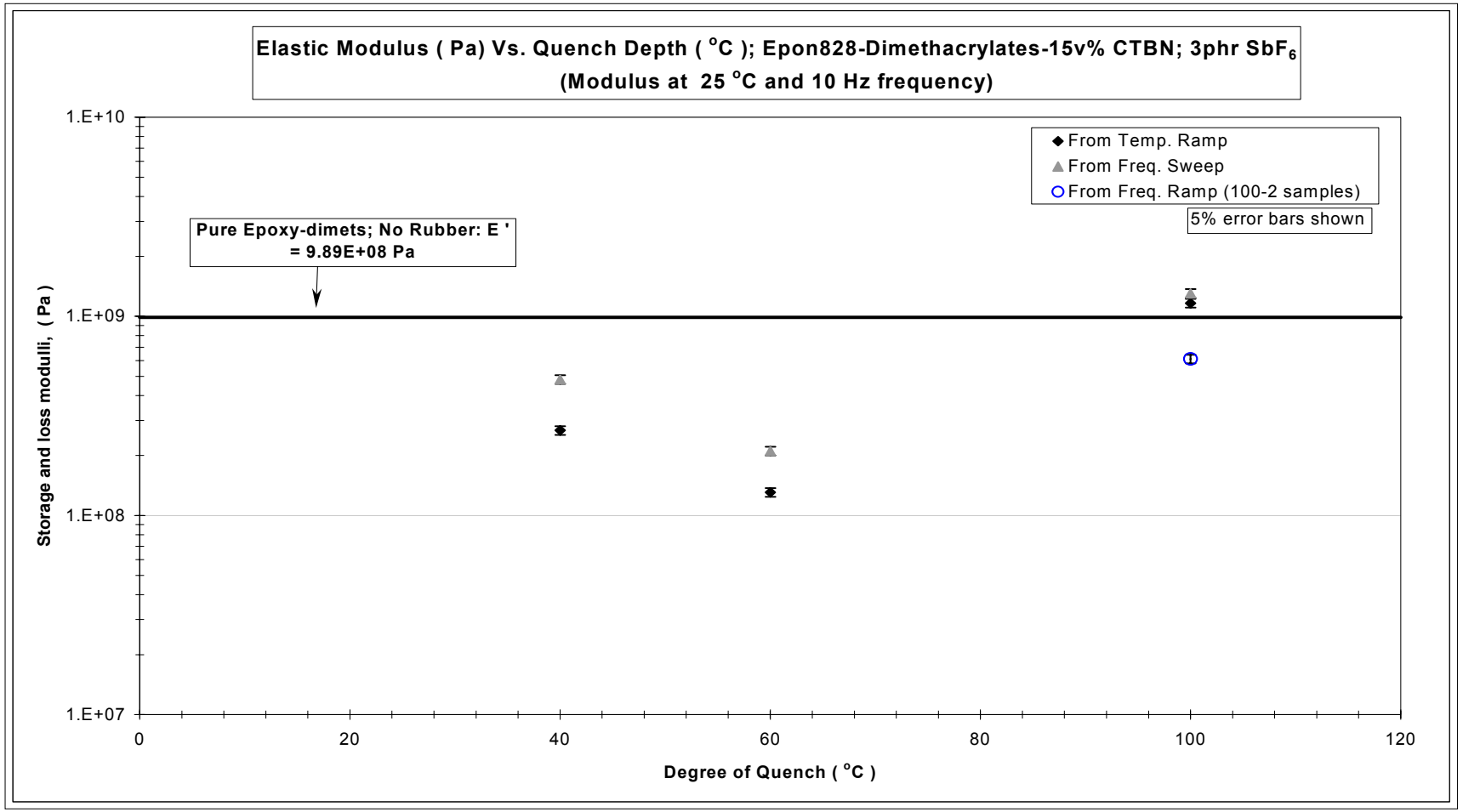

Fig. 29: Storage Modulus (E') values from DMA experiments for samples cooled at various rates; Epon828-CTBN X31 (15 vol.%)-Dimethacrylates (100 phr; δ=0.5). The values show the unexpected increase in modulus for the q100 sample.

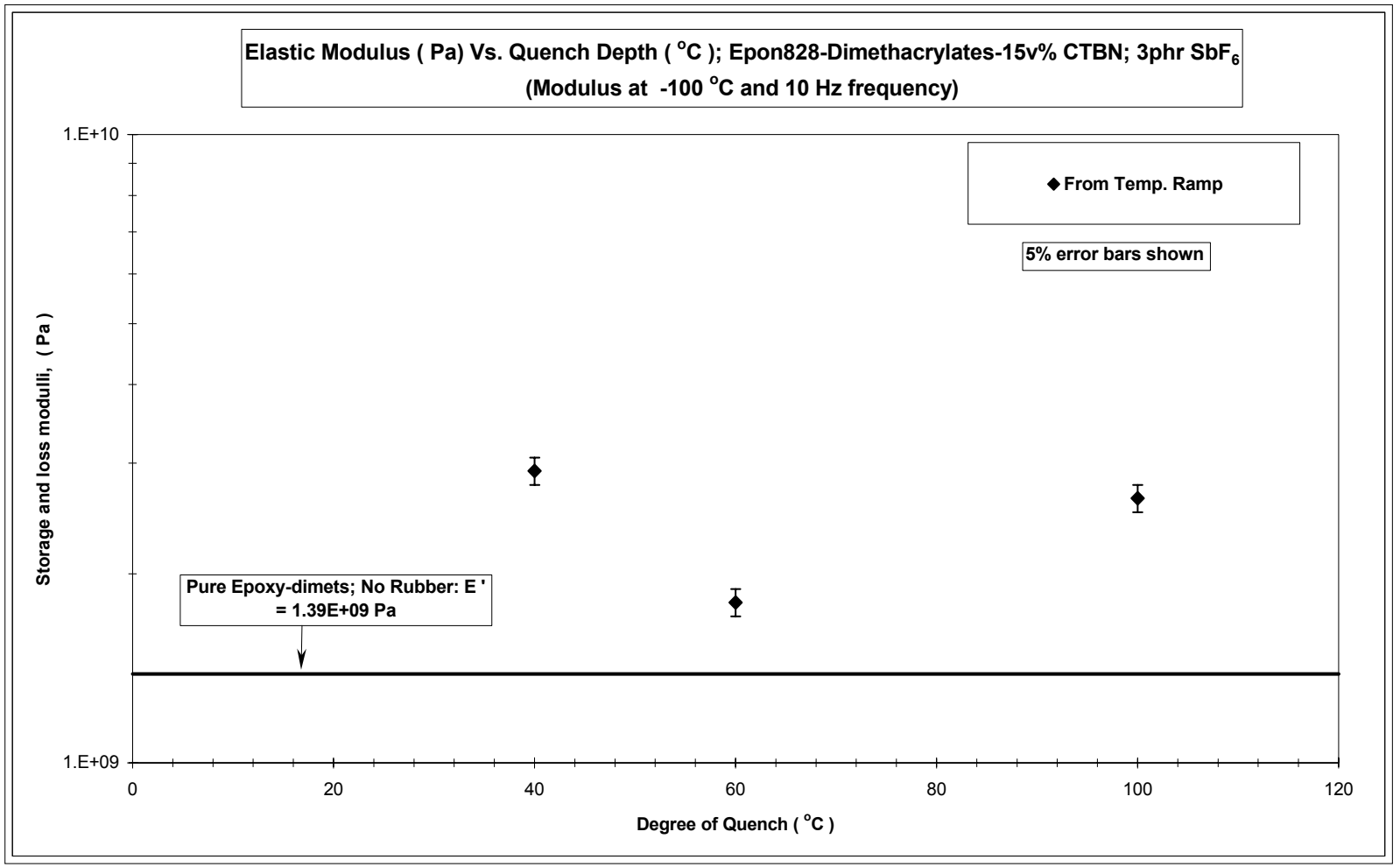

Fig. 30: Storage Modulus (E') values from DMA experiments for samples cooled at various rates; Epon828-CTBN X31 (15 vol.%)-Dimethacrylates (100 phr; δ=0.5). The values show the unexpected increase in modulus for the q100 sample.

toughness values to the dispersed elastomer-rich phase particle size, impact testing was carried out on the above-mentioned samples (as mentioned in section on DMA analysis).

Impact Testing results are shown in the graph of Impact energy (KJ/m^2) versus the degree of quench (Figure 31). Results clearly indicate an increase of about *150%* in the impact energy with the degree of quench for the fastest cooled samples (degree of quench=100). The highest depth of quench results in the smallest particle size of CTBN, resulting in higher values of impact toughness. Here, again, a higher degree of quench seems to disperse the dissolved rubber more favorably by spinodal decomposition than nucleation-growth mechanism, into a large number of small sized particles, consistent with the OM and SALS results. There is an increase in the effective surface area of the rubber particles offering resistance to the propagating crack, increasing the impact energy needed to break the specimen. In these toughened systems, impact toughness usually is inverse to the storage modulus. Materials with higher modulus usually have lower impact toughness. In this case, the q100 sample has both; highest impact toughness as well as highest modulus at room temperature. This may be due to the higher matrix flexibility due to higher dissolved CTBN in it. (higher impact toughness). But since the dissolved CTBN may crosslinked, the modulus may be higher. CTBN present has unsaturation in the butadiene segments. As mentioned in the scheme of uv-initiated dissociation of the TASHFA leads to formation of free radicals along with ions. These free radicals may be able to open up the butadiene double bonds, carrying out crosslinking to some extent. A possible crosslinking scheme may be as given below [44]. Figure 32 gives a quantative comparison of impact toughness ranges for various commercial impact resistant materials as obtained from Matweb.

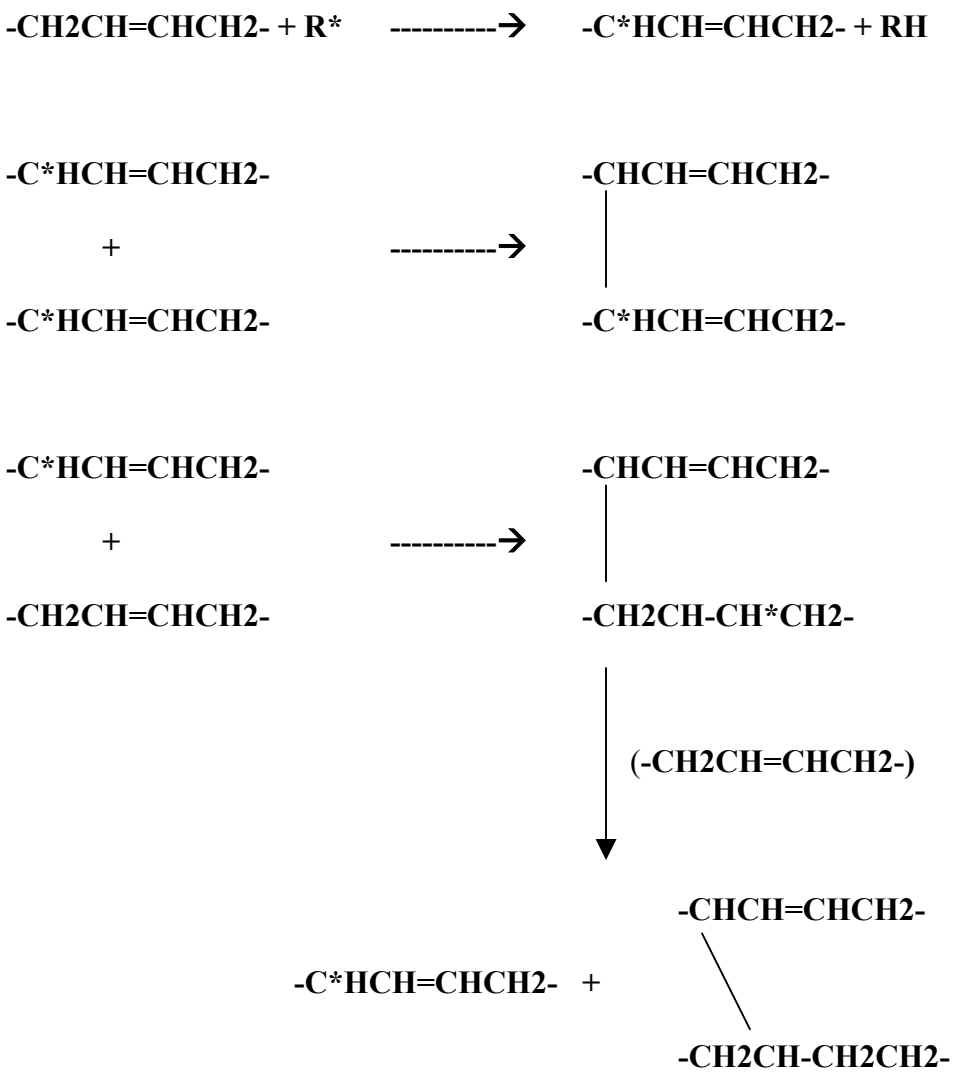

4.6 Scanning Electron Microscopy (SEM):

SEM photomicrographs for the Epon828-CTBN X31 (15 vol.%)-Dimethacrylates (100 phr; δ=0.5) system shows a uniform dispersion of particles in the epoxy matrix See figures 33-36, a and b). Even for the fastest cooled samples, the lower magnification micrographs show in addition some bigger sized particles (diameter greater than 30)

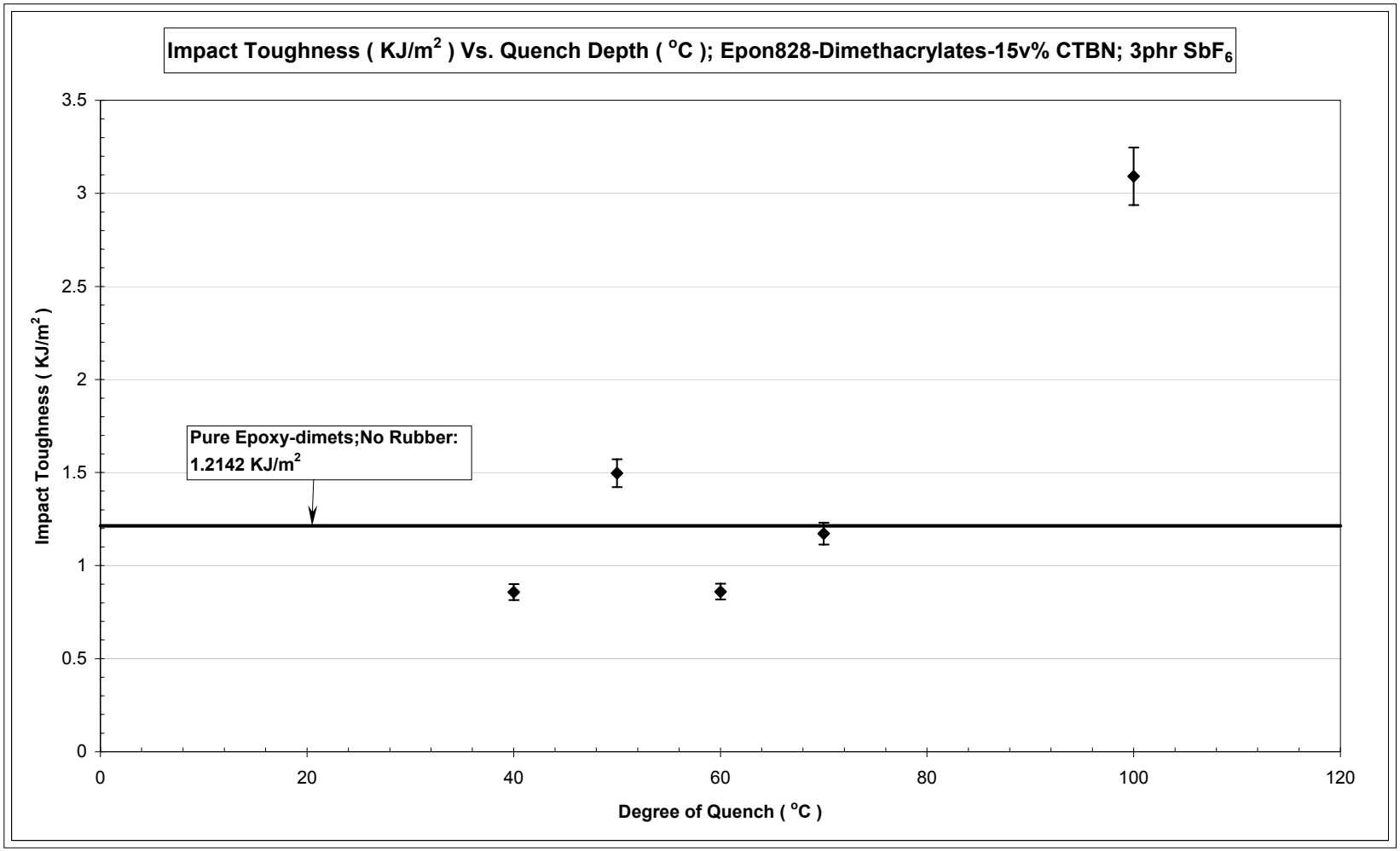

Fig. 31: Impact toughness for samples cooled at various rates; Epon828-CTBN X31 (15 vol.%)- Dimethacrylates (100 phr; δ=0.5).

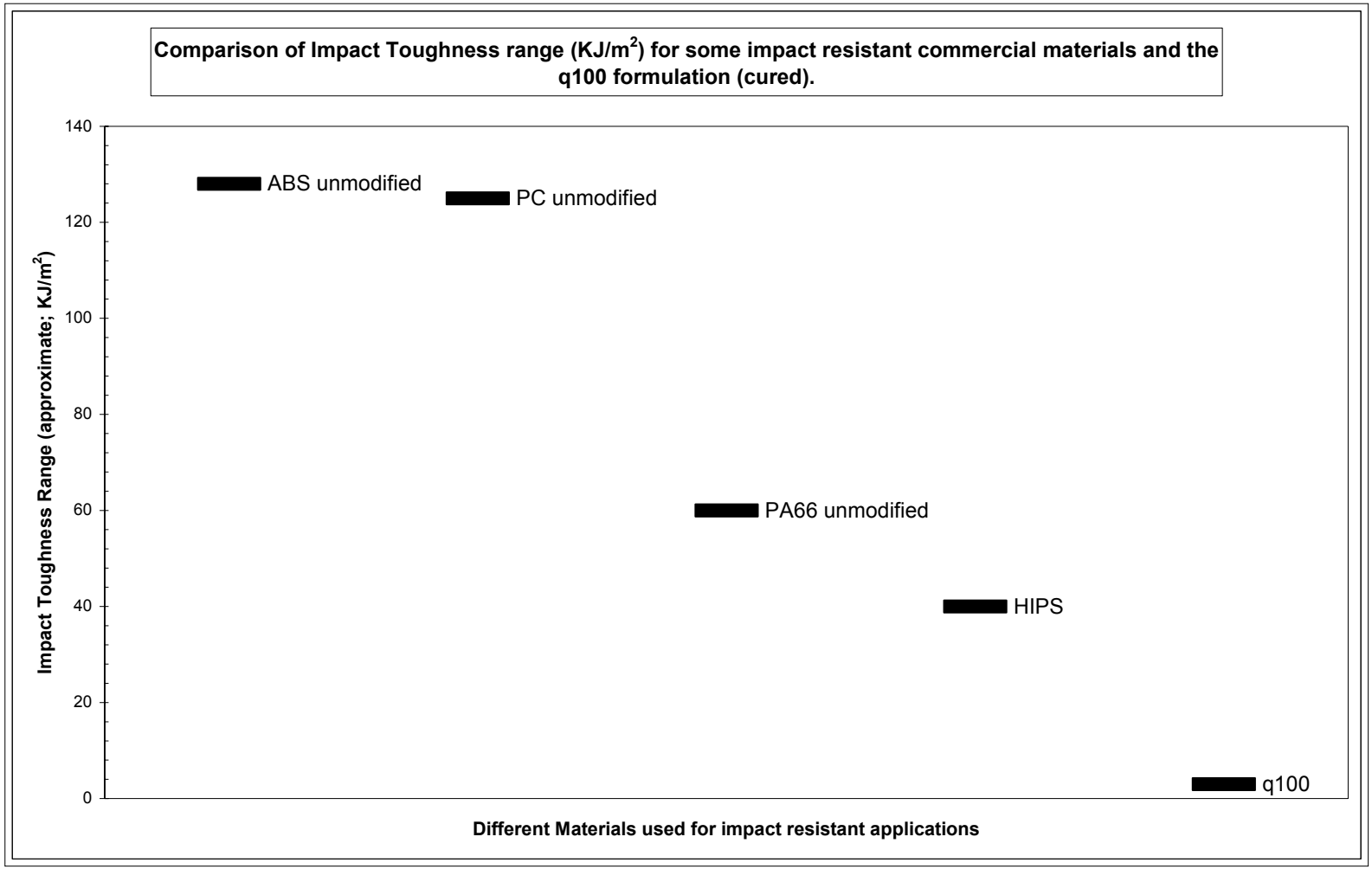

Fig. 32: Comparison of Impact Toughness Ranges for various impact-resistant materials with the q100 sample.

micron). Since the CTBN is fully dissolved initially at higher temperatures (120 ^{o}C), and since it is cooled at a fast rate, the rubber is unlikely to get sufficient time to precipitate and grow into such large sized particles. Sands et al. [43] have reported that the dimethacrylates phase separate from epoxy-dimethacrylates-CTBN dispersions during epoxy curing. During the amine-initiated curing of epoxies, the epoxy molecular weight increases with the curing time, leading to the rubber phase separation. In addition to the rubber phase, the dimethacrylates may phase separate as well. The phase-separated dimethacrylates might be the ones showing up as submicron sized particles in the SEM. So, some dimethacrylates remain phase separated in the matrix phase during the curing stage. This is evident from the SEM micrographs of the same specimen after etching with 10% by weight chromic acid. The unetched samples had a smooth surface while the etched samples had an uneven surface. This is because the dissolved dimethacrylates in the final system also gets attacked by the etchant.

In case of q100 sample, some very large sized particles were seen in SEM (size greater than 50 micron) (Figure 37; a and b). They were first thought to be coarsened CTBN particles. To check this, a microhardness test was done at points on the large particle and the hardness value compared with that at a point outside the particle (in the matrix). Vickers hardness standard was used and the values of microhardness in the particle and matrix region were 524.5 HV. The hardness values were seen to be similar and also high, corresponding to those of matrix phase. To ascertain this assumption, more readings were taken at various locations in the matrix phase. This proved that the large particles were either separated dimethacrylates or epoxy matrix phase.

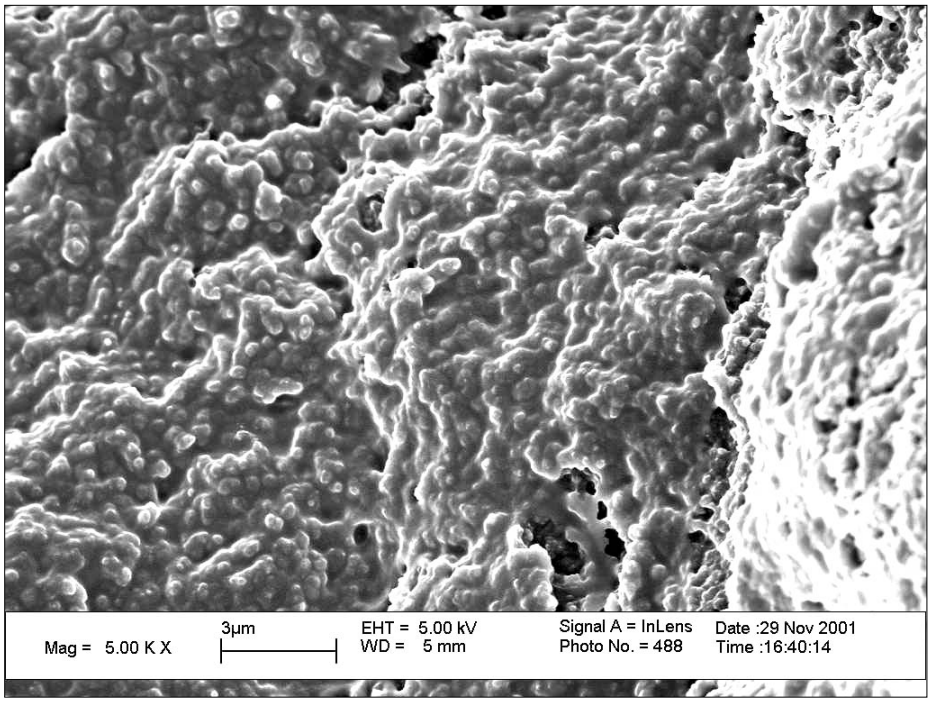

a

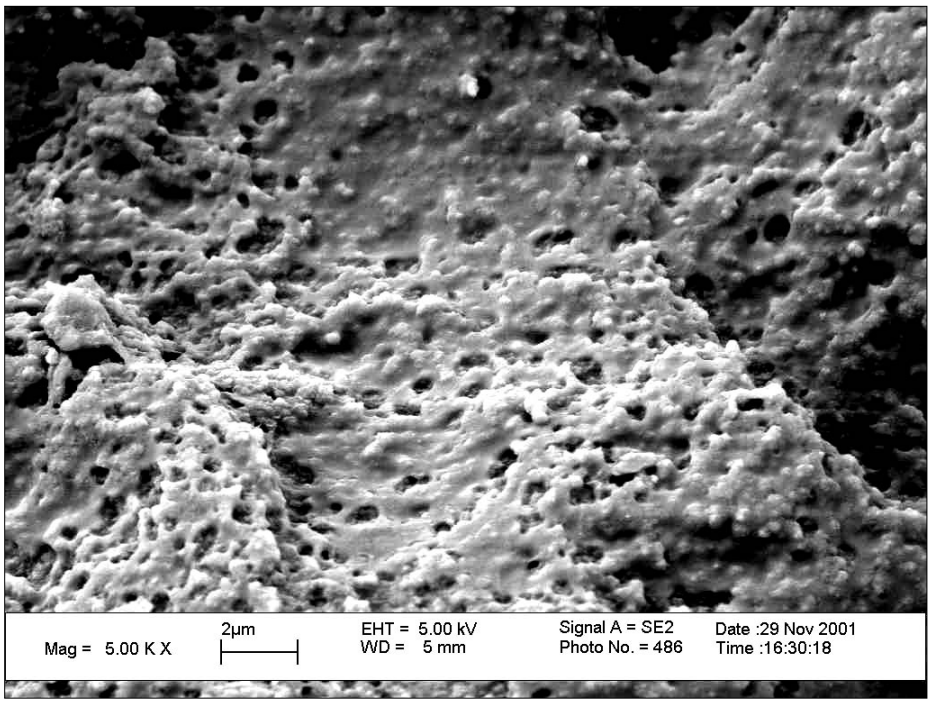

b

Fig. 33: SEM micrograph; Epon828-CTBN X31 (15 vol.%)-Dimethacrylates; quench=100 ^{o}C; a: Unetched and gold coated; b: Etched and gold coated

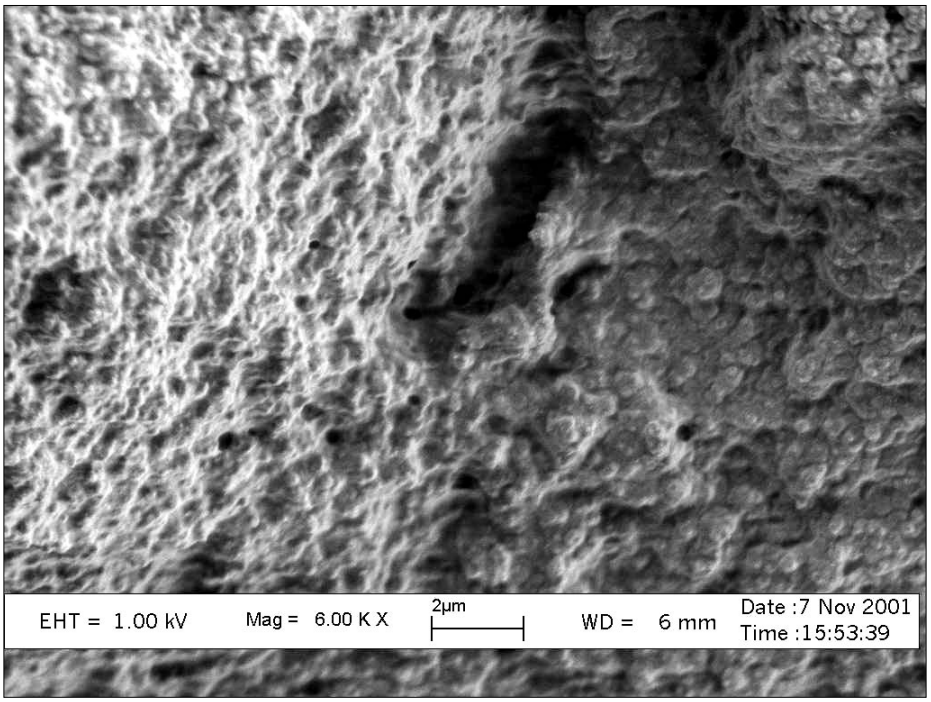

a

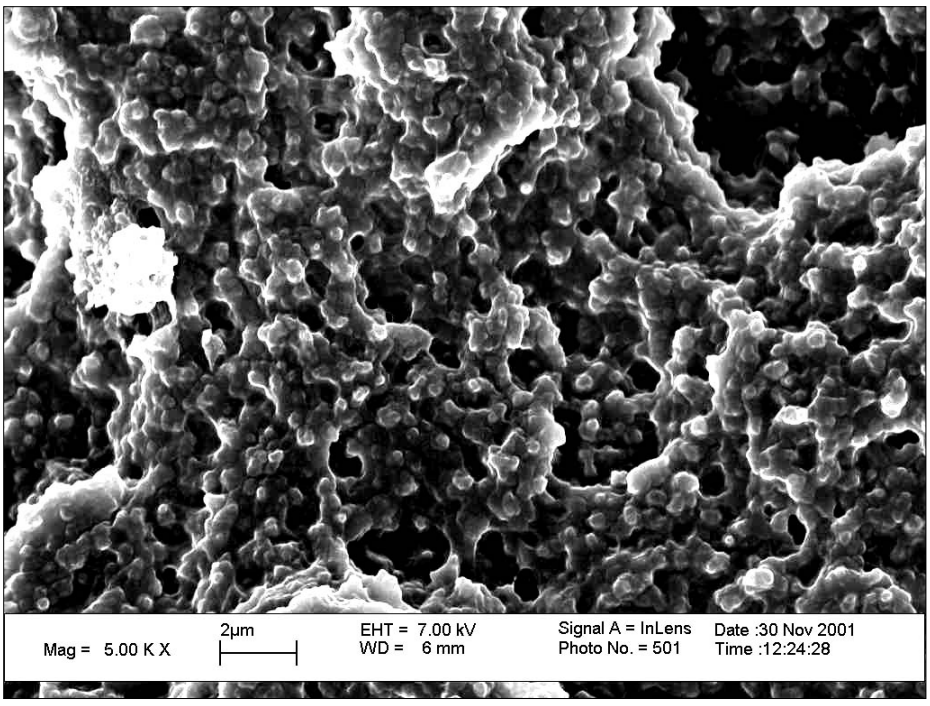

b

Fig. 34: SEM micrograph; Epon828-CTBN X31 (15 vol.%)-Dimethacrylates; quench=70 ^{o}C; a: Unetched and gold coated; b: Etched and gold coated.

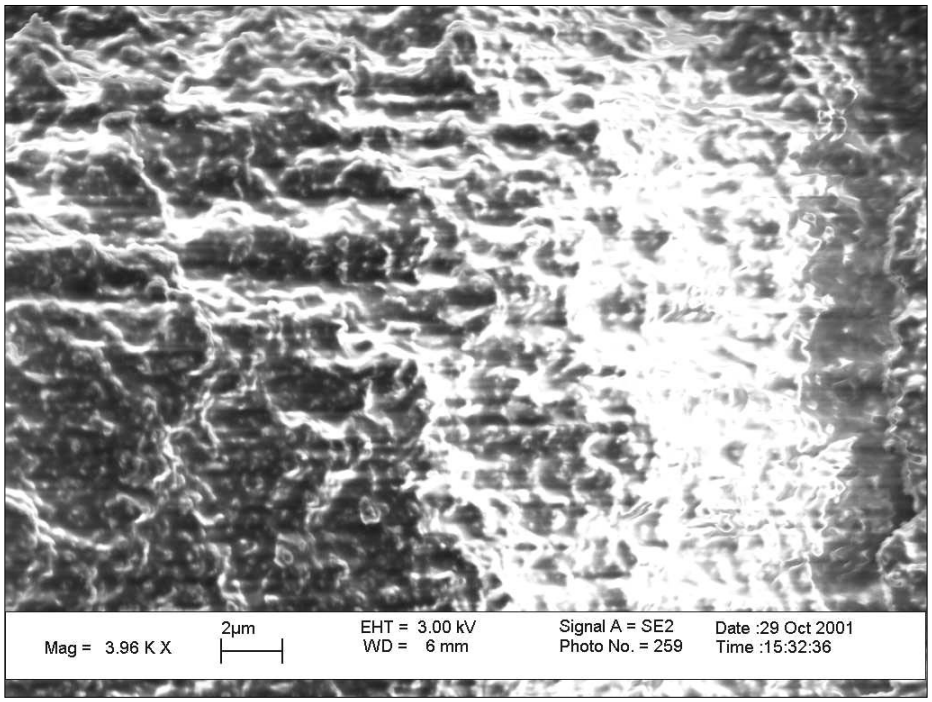

a

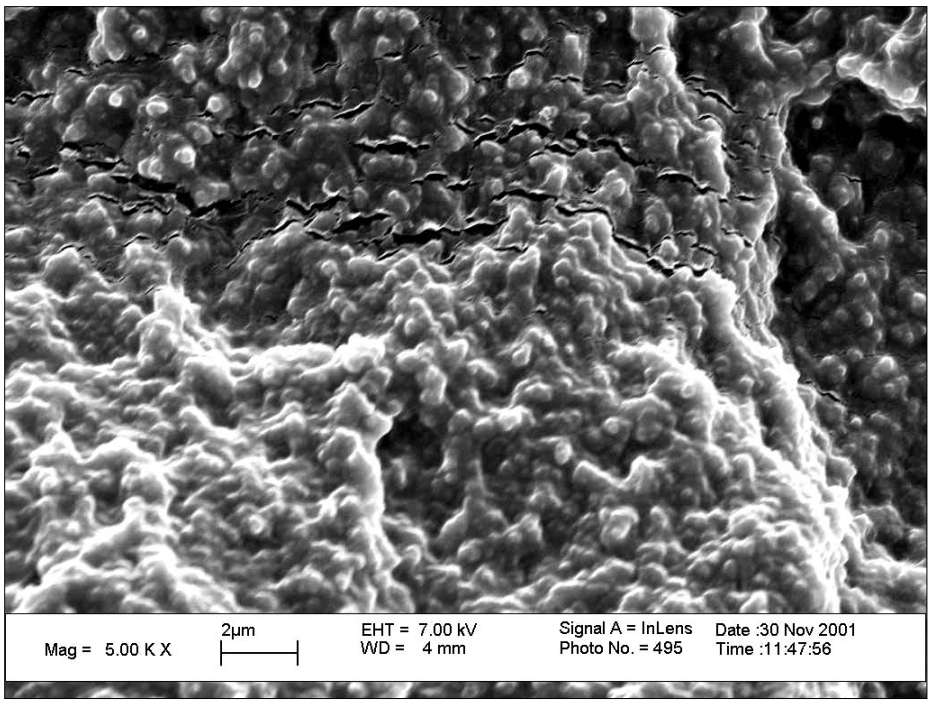

b

Fig. 35: SEM micrograph; Epon828-CTBN X31 (15 vol.%)-Dimethacrylates; quench=60 ^{o}C; a: Unetched and gold coated; b: Etched and gold coated.

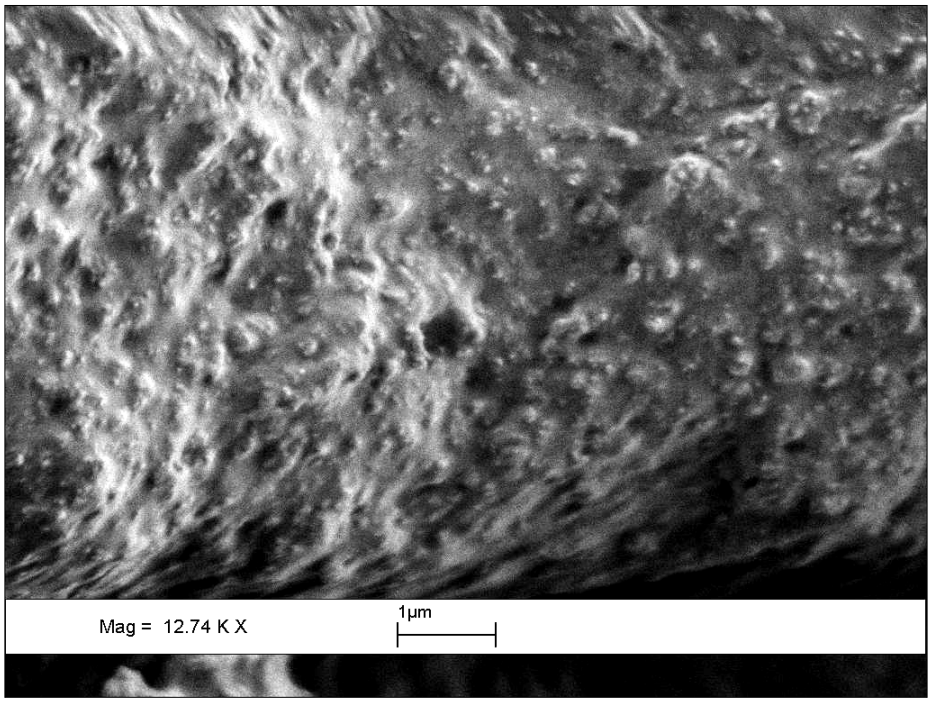

a

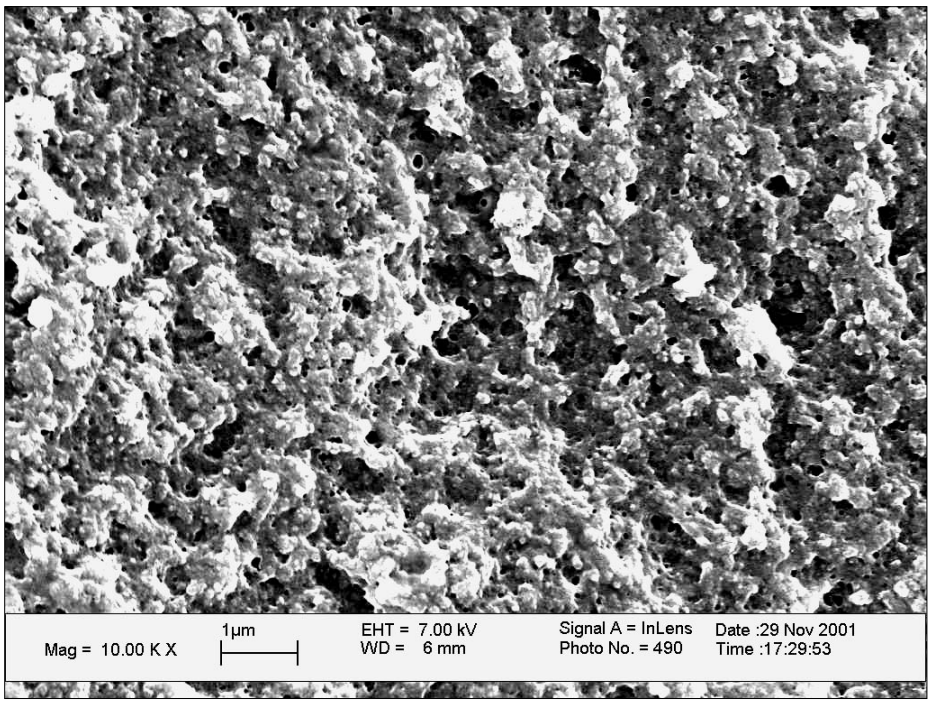

b

Fig. 36: SEM micrograph; Epon828-CTBN X31 (15 vol.%)-Dimethacrylates; quench=50 ^{o}C; a: Unetched and gold coated; b: Etched and gold coated.

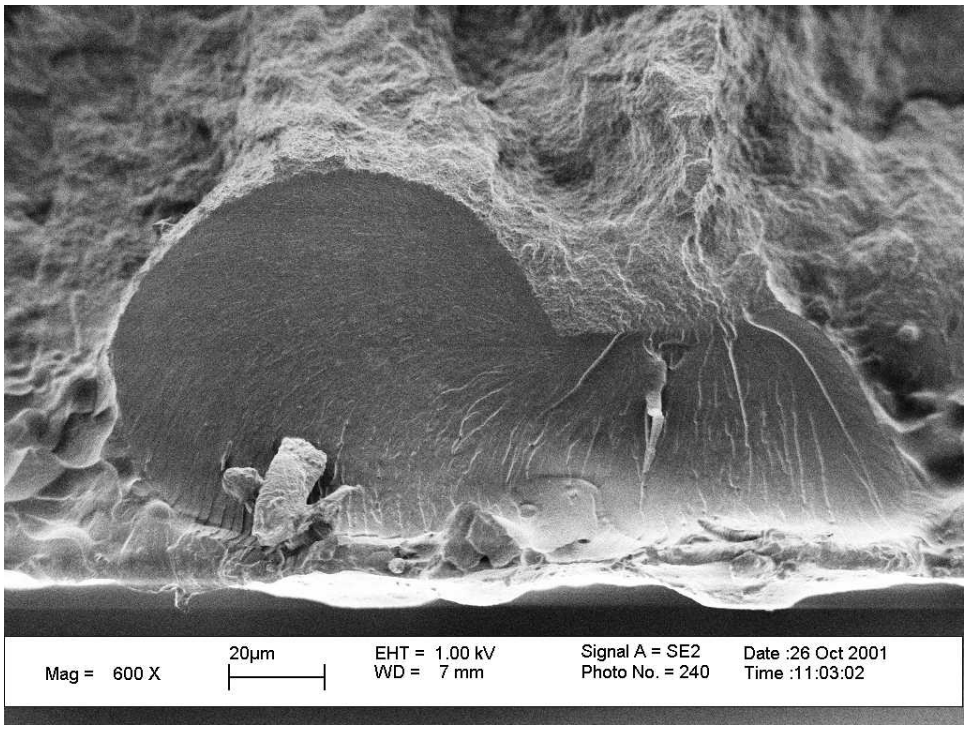

a

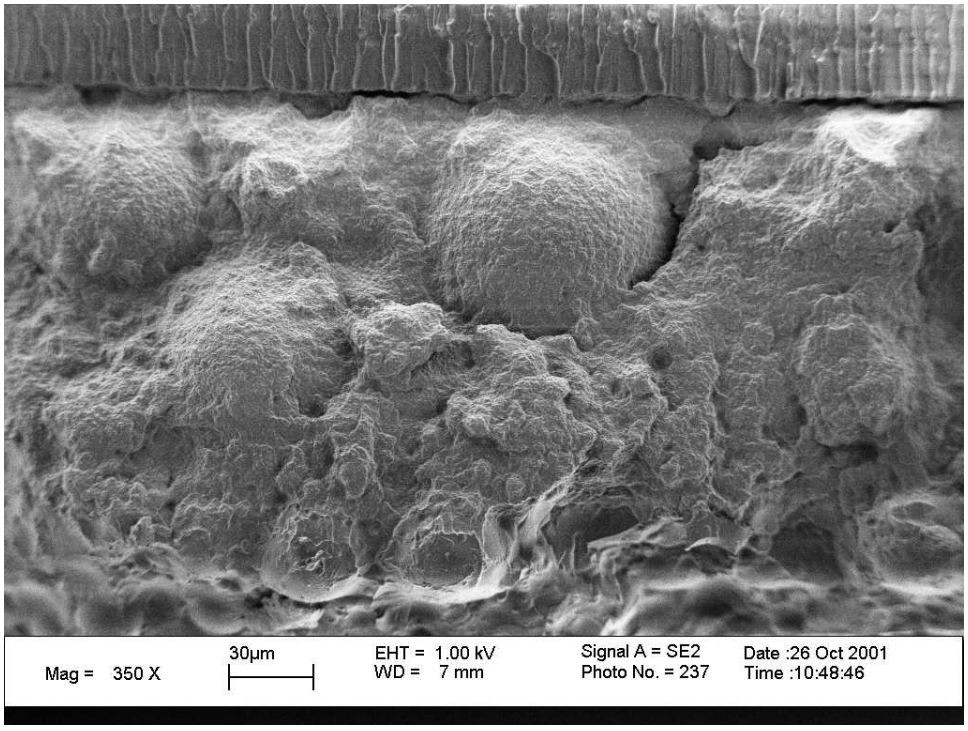

b

Fig. 37: Q100 sample with large particles (size > 50 micron); a and b represent 2 different areas of the sample.

CHAPTER 5- CONCLUSIONS AND RECOMMENDED FUTURE WORK

Reactive elastomers like carboxyl-terminated butadiene acrylonitrile dissolve in diglycidyl ether of bisphenol-A type epoxy resins to an extent depending upon the accrylonitrile content in them. Greater the acrylonitrile content, easier do the CTBNs get dissolved and consequently, lower is the phase separation temperature or the cloud point of such dispersions.

Small angle laser light scattering can be used to compare the particle sizes of the phase-separated elastomers-rich domains with those from optical microscopy. The treatment suggested by Effler et al. [42] is useful for this purpose.

Dimethacrylates added as reactive diluents form an interpenetrating network (IPN) with the epoxy matrix of Epon-828. Upon thermal quenching, some amount of the dimethacrylates phase-separates from the IPN structure and swells the phase-separated elastomeric particles, giving rise to large domains (sizes greater than 30 micron). These domains are predominant in the fastest cooled samples. Upon UV curing and subsequent thermal cure, the dimethacrylates swelling the elastomeric particles cure and make these domains hard, giving hardness values comparable to that of the matrix IPN structure.

The thermal quenching process forces the elastomer to phase-separate as small particles in the matrix phase. The size of dispersed particles and their distribution depends on the degree of quench (rate of quenching). Faster cooling rates result in the formation of smaller-sized dispersed particles.

The impact toughness is affected by the particle size of the phase-separated elastomeric particles. The impact toughness (KJ/m^2) is almost twice for the fastest cooled sample as compared to that of a similar sample containing no elastomer in it. This increase is significant. Lower cooling rates (lower quench depths) result in samples with impact energies lower than that of a similar sample containing no elastomer.

It is recommended that further experimentation using more powerful UV source be carried out to see if the extent of curing is enhanced. This will help determine if the thermal step can be eliminated or not and also whether thicker UV cured sections are possible.

Also, a similar study on other three CTBNs mentioned earlier can be carried out to see if the acrylonitrile content affects the cure characteristics and the impact toughness of the cured resins.

A similar study by varying the HDDMA content (viscosity modifier) can be carried out to study the kinetic aspects of the system. It will give both qualitatively and quantitatively, the degree to which the phase separation process of the elastomer in the matrix phase depends on the thermal quenching step as compared to the curing step.

A detailed analysis of the fracture mechanics can be done to determine the fracture mechanisms responsible for the observed higher toughness for the fastest cooled resin formulations. This will help to better control the particle size and achieve a particular fracture mode depending on the application.

BIBLIOGRAPHY

1. McGarry, F. J.; Willner, A. M., research report, School of Engineering, Massachusetts Institute of Technology: Cambridge, MA, (1966).
2. Drake, R. S.; McCarthy, W. J. Rubber World October (1968), 159.
3. Sultan, J. N.; McGarry, F. J. Polym. Eng. Sci. (1973), 13, 29.
4. Rowe, E. H.; Riew, C. K. Plast. Eng. (1975), 45.
5. Rowe, E. A.; Siebert, A. R.; Drake, R. S. Mod. Plast. (1970), 47, 110.
6. Lee, W. H; Hodd, K. A.; Wright, W. W, Rubber-Toughened Plastics, American Chemical Society, Advances in Chemistry Series 222, (1987), 263-288.
7. Sayre, J. A; Assink, R. A; Lagasse, R. R, Polymer (1981), 22, 87.
8. Lee, W. H; Hodd, K. A.; Wright, W. W, Rubber-Toughened Plastics, American Chemical Society, Advances in Chemistry Series 222, (1987), 67.
9. Wang, T. T; Zupko, H. M, J. Appl. Polym. Sci. (1981), 26, 2391.
10. Hsieh, H. S. Y; Polym. Eng. Sci. (1990), 30, 493.
11. Verchere, D; Sautereau, H; Pascault, J, P; Moschiar, S. M; Riccardi, C. C; Williams, R. J. J, Toughened Plastics I, American Chemical Society, Advances in Chemistry Series 233, (1993), 339.
12. Langhammer, G; Nester, L. Makromol. Chem. (1965), 88, 179.
13. Lee, H. S; Kyu, T. Macromolecules (1990), 23, 459.
14. McGarry, F. J.; Willner, A. M., Amer. Chem. Soc. Div. Org. Coating Plast. Chem., Pap., 28, (1), 512 (1968).
15. Meeks, A. C., Polymer, 15, (1974), 675.
16. Kinloch A. J., Shaw S. J., Tod D. A., Hunston D. L., Polymer, 24, (1983), 1341.

17. Riew C. K., Gillham J., Ed., Rubber Modified Thermosets Resins, American Chemical Society, Advances in Chemistry Series 208, (1984).
18. Riew C. K., Kinloch A. J., Toughened Plastics I, Science and Engineering, American Chemical Society, Advances in Chemistry Series 233, (1993).
19. Leonard L., Advanced Composites, 6, n4, (1991), 35.
20. Mika T. F., Bauer R. S., Epoxy Resins- Chemistry and Technology, Second Ed., C. May, Ed., Marcel Dekker, (1988), 506.
21. Almen G. R., Mackenzie P, Malhotra V., Maskell R. K., McGrail, P. T., Sefton, M. S., SAMPE International Technical Conference, 20, (1988), 46.
22. Bauer R. S., SAMPE International Symposium, 34, (1989), 899.
23. Bucknall C. B., Gilbert A. H., Polymer, 30, (1989), 213.
24. Bauer R. S., Stenzenberger H. D., Romer W., SAMPE International Symposium, 35, (1990), 395.
25. Hendrick J. L., Yilgor I., Hendrik J. C., Wilkes G. L., McGrath J. E., SAMPE International Symposium, 30, (1985), 947.
26. Cecere J. A., Hendrick J. L., McGrath J. E., SAMPE International Symposium, 31, (1986), 580.
27. Bauer R. S., SAMPE International Technical Conference, 18, (1986), 510.
28. Hendrick J. C., Hendrik J. L., Cecere J. A., Liptak S.C., McGrath J. E., Polym. Mater. Sci. Eng., 63, (1990), 190.
29. Crivello J. V., Nucl. Instr. And Meth. In Phys. Res., B 151, (1999), 8-21.
30. Garg A. C., Mai Y. W., Compos. Sci. Technol., 31, (1988), 179.
31. Pearson R. A., Yee A. F., J. Mater. Sci., 24, (1989), 2571.

32. McGarry F. J., Proc. R. Soc. London A, 319, (1970), 59.

33. Bucknall C. B., Toughened Plastics, Applied Science Publishers Ltd. London, (1977), 182-211.

34. Argon A. S., Phil. Mag., 28, (1973), 839.

35. Sue H. J., Garcia-Meitin E. I., Yang P. C., Bishop M. T., J. Mater. Sci. Letters, 12, (1993), 1463.

36. Jang B. Z., Pater R. H., Soucek M. D., Hinkley J. A., J. Polym. Sci.-Part-B: Polym. Phy., 30, (1992), 643.

37. Kinloch A. J., Adv. Polym. Sci., 72(Epoxy Resins Compos. 1), (1985), 45.

38. Pearson R. A., Yee A. F., J. Mater. Sci., 24, 7, (1989), 2571.

39. Finch C. A., Hashemi S., Kinloch A. J., J. Polym. Commun., 28, (1987), 322.

40. Kinloch A. J., Rubber-Toughened Plastics, American Chemical Society, Advances in Chemistry Series 222, (1987), 67-90.

41. Lohse F., Zweifel H., Epoxy Resins And Composites III, Springer-Verlag publ., Advances in Polymer Science 78, (1986), 61-81.

42. Effler L. J., Lewis D. N., Fellers J. F., American Chemical Society Symposium, SER, 384, (1989), 225-253.

43. Sands J. M., Jensen R. E., Fink B. K., McKnight S. H., J. Appl. Poly. Sci., 81, (2001), 530-545.

44. Malcom Stevens, Polymer Chemistry- An Introduction, 2nd Ed., 1990.

45. Wu Jingshen and Mai Yiu-Wing, Materials Forum, 19, (1995), 181-199.

VITA

Abhijeet Godbole was born on March 16, 1976 in Pune, India. He received his Bachelor of Engineering (Polymer Engineering) in June 1997 from Maharashtra Institute of Technology, Pune. He then worked for two years at the National Chemical Laboratory (NCL), Pune, India as a Project Assistant. He joined The University of Tennessee, Knoxville in fall 1999 for his Master of Science degree in Polymer Engineering.